TURUN
YLIOPISTO
UNIVERSITY
OF TURKU

TARGETING SOMATOSTATIN RECEPTORS WITH PEPTIDE-FUNCTIONALIZED SILICA NANOPARTICLES

Valeriy M Paramonov

TURUN YLIOPISTON JULKAISUJA – ANNALES UNIVERSITATIS TURKUENSIS
SARJA – SER. D OSA – TOM. 1563 | MEDICA – ODONTOLOGICA | TURKU 2021

TURUN
YLIOPISTO
UNIVERSITY
OF TURKU

TARGETING SOMATOSTATIN RECEPTORS WITH PEPTIDE-FUNCTIONALIZED SILICA NANOPARTICLES

Valeriy M Paramonov

TURUN YLIOPISTON JULKAISUJA – ANNALES UNIVERSITATIS TURKUENSIS
SARJA – SER. D OSA – TOM. 1563 | MEDICA – ODONTOLOGICA | TURKU 2021

University of Turku

Faculty of Medicine
Institute of Biomedicine
Physiology
Turku Doctoral Programme of Molecular Medicine (TuDMM)

Supervised by

Professor Adolfo Rivero-Müller
Research Centre for Integrative Physiology and Pharmacology, University of Turku, Finland;
Department of Biochemistry and Molecular Biology, Medical University of Lublin, Poland

Professor Cecilia Sahlgren
Cell Biology, Åbo Akademi University, Turku, Finland;
Institute for Complex Molecular Systems, Eindhoven University of Technology, The Netherlands

Veronika Mamaeva†, PhD
Cell Biology, Åbo Akademi University, Turku, Finland (†deceased 06 January 2018)

Reviewed by

Professor Hélder A. Santos
Drug Research Program, Faculty of Pharmacy, and Helsinki Institute of Life Science (HiLIFE),
University of Helsinki, Helsinki, Finland

Professor Paweł Piotr Jagodziński
Department of Biochemistry and Molecular Biology,
Poznan University of Medical Sciences, Poznan, Poland

Opponent

Professor Arto Urtti
Drug Research Program,
Faculty of Pharmacy,
University of Helsinki, Helsinki, Finland

The originality of this publication has been checked in accordance with the University of Turku quality assurance system using the Turnitin OriginalityCheck service.

ISBN 978-951-29-8516-6 (PRINT)
ISBN 978-951-29-8517-3 (PDF)
ISSN 0355-9483 (Print)
ISSN 2343-3213 (Online)
Painosalama, Turku, Finland 2021

to Veronika

UNIVERSITY OF TURKU
Faculty of Medicine
Institute of Biomedicine
Physiology
Turku Doctoral Programme of Molecular Medicine (TuDMM)
Research Centre for Integrative Physiology and Pharmacology
VALERIY M PARAMONOV: Targeting Somatostatin Receptors with Peptide-functionalized Silica Nanoparticles
Doctoral Dissertation, 278 pp.
June 2021

ABSTRACT

Nano-sized synthetic drug carriers comprise a valuable addition to oncology armaments, opening new avenues for improved delivery of anticancer therapies. Nanocarriers designed to bind surface receptors of tumor cells by virtue of bearing cognate high affinity ligands, also called as actively-targeted nanocarriers, have drawn a lot of attention during the last decade, promising to enable selective tumor accumulation via ligand-receptor interactions. The present work encompasses development and early *in vitro* evaluation efforts with a particular type of such a targeted nanocarrier [nanoparticles of mesoporous silica (SiO_2), MSN], functionalized with short peptide ligands of somatostatin receptors (SSTR), frequently abundant in tumors. The synthesized targeted MSN, as well as control inactive peptide–functionalized counterparts, were characterized by physicochemical means and evaluated for their ability to bind to SSTR and enter living cells *in vitro*. We sequentially studied MSN in protein-depleted and serum-enriched media – the latter condition involved adsorption of proteins to MSN surface (formation of the so-called protein *corona*), which invariably happens *in vivo* and affects cellular interactions of nanomaterials. We demonstrate that the targeted MSN can bind SSTR not only under the rectified conditions, but also in the presence of protein adsorption. Ultimately, we show that SSTR targeting leads to a decreased cellular accumulation of MSN with protein corona, which highlights the complexity of nanobiointeractions and urges to re-consider the applicability of the conventional model of tumor receptor targeting with nanocarriers to somatostatin receptors.

The work covers a number of chemical (MSN design, synthesis and surface functionalization) and molecular biology (*in vitro* targetability evaluation and generation of relevant tools, receptor signaling, endocytosis) aspects of high relevance for development and characterization of targeted nanocarriers and as such should be of interest to the broad community working with nanomedicines and targeted delivery. The discussion of the original experimental evidence is preceded by a critical literature review, introducing the current concepts of nanocarrier-mediated delivery in oncology.

KEYWORDS: nanocarrier, tumor receptor targeting, ligand-receptor interaction, nanoparticle corona, mesoporous silica nanoparticle, somatostatin receptor, cAMP.

TURUN YLIOPISTO
Lääketieteellinen tiedekunta
Biolääketieteen laitos
Fysiologia
Molekyylilääketieteen tohtoriohjelma (TuDMM)
Integratiivisen fysiologian ja farmakologian tutkimuskeskus
VALERIY M PARAMONOV: Somatostatiinireseptorien kohdentaminen peptidi-funktionaalisilla piioksidi-nanohiukkasilla
Väitöskirja, 278 s.
Kesäkuu 2021

TIIVISTELMÄ

Nanokokoiset lääkkeiden kantajat avaavat uusia keinoja syöpähoitojen parantamiseksi. Nanokantajat, joiden pinnalla olevat korkean affiniteetin ligandit ovat suunniteltu sitomaan tuumorisolujen pintareseptoreita (ns. aktiivisesti kohdennetut nanokantajat), mahdollistavat nanohiukkasten selektiivisen kertymisen syöpäkasvaimeen ligandi-reseptori-vuorovaikutusten kautta. Tämä työ kattaa kehityksen ja varhaiset *in vitro*-kokeet kohdennetulla nanokantajahiukkasella [mesohuokoisen piidioksidin (SiO_2) nanohiukkaset, MSN], jotka on funktionalisoitu somatostatiinireseptorien lyhyillä peptidiligandeilla (SSTR), joita esiintyy usein runsaasti kasvaimissa. Syntetisoidut kohdennetut MSN-hiukkaset sekä kontrollina käytetyt inaktiiviset peptidifunktionaaliset vastineet karakterisoitiin fysikaalis-kemiallisilla menetelmillä sekä arvioitiin niiden kykyä sitoutua SSTR:ään ja päästä eläviin soluihin *in vitr*o. Tutkimus suoritettiin MSN-hiukkasilla sekä proteiinipitoisessa että seerumilla rikastetussa ravintoliuoksessa – jälkimmäisessä tapauksessa proteiinit kiinnittyivät MSN:n pinnalle (ns. proteiinikoronan muodostuminen), joka tapahtuu *in vivo* ja vaikuttaa nanomateriaalin ja solun väliseen vuorovaikutukseen. Osoitamme, että kohdennettu MSN voi sitoa SSTR:ää paitsi puhdistetuissa olosuhteissa, myös proteiinikoronan läsnäollessa. Lopuksi osoitamme, että SSTR-kohdennuksessa proteiinikorona vähentää MSN:n kertymistä soluihin, mikä korostaa nanobiovuorovaikutusten monimutkaisuutta, ja kyseenalaistaa nanokantajien kanssa käytetyn tavanomaisen kasvainreseptorikohdennusmallin soveltuvuutta somatostatiinireseptoreihin.

Työssä käytettiin kemiallisia (MSN-suunnittelu, synteesi ja pinnan funktionalisointi) ja molekyylibiologisia (kohdennettavuuden arviointi *in vitro*, työkalujen luominen, reseptorisignalointi ja endosytoosi) menetelmiä, jotka ovat olennaisia kohdennettujen nanokantajien kehitykselle ja karakterisoinnille. Tulosten oletetaan kiinnostavan laajaa yhteisöä, joka työskentelee nanolääkkeiden ja niiden kohdentamisen parissa. Kokeellista osuutta edeltää kirjallisuuskatsaus, jossa esitellään nanokantaja-välitteisen kuljetuksen nykyiset käsitteet syöpäbiologiassa.

AVAINSANAT: nanokantaja, kasvainreseptorikohdistus, ligandi-reseptorivuorovaikutus, nanohiukkasen korona, mesohuokoinen piidioksidi-nanopartikkeli, somatostatiinireseptori, cAMP.

Table of Contents

Abbreviations

(m/p)Ab/Abs	(monoclonal/polyclonal) antibody/ies
AC/ACs	adenylyl cyclase/s
AFC	autofluorescence control
AGE	agarose gel electrophoresis
ART	active receptor targeting
AU	arbitrary units
AUC	area under curve
bp/bps	base pair/s
BSA	bovine serum albumin
cAMP	3′-5′-cyclic adenosine monophosphate
CavDE	caveolin-dependent endocytosis
CCK-8	cell counting kit-8 (*in vitro* assay for cell viability)
CDS	coding sequence
CI	confidence interval
ClaDE	clathrin-dependent endocytosis
COR	corona (a layer of adsorbates on a surface of a nanoparticle)
DLS	dynamic light scattering
DMEM	Dulbecco's modified Eagle's medium
DMF	dimethylformamide
EDC	N-(3-dimethylaminopropyl)-N-ethylcarbodiimide
EPR	enhanced permeability and retention
EtBr	ethidium bromide
EtOH	ethanol
IBMX	3-isobutyl-1-methylxanthine
IndMed	inducing medium
FACS	fluorescence-activated cell sorting
FC	flow cytometry
FI	fluorescence intensity
FoV	field of view
FSK	forskolin
GRK	G protein-coupled receptor kinase
gNP	a generic nanoparticle
GPCR/GPCRs	G protein-coupled receptor/s
GS22/cAMP	GloSensor-22F, luminescent cAMP probe
HA	human influenza hemagglutinin epitope

IC_{50}	concentration of a compound triggering half of the maximum inhibitory effect
(i)FBS	(heat-inactivated) foetal bovine serum
KO	knockout (a stable disruption of a gene with loss of its protein product)
LB	Luria-Bertani medium
MALDI-TOF MS	matrix-assisted laser desorption ionization – time of flight mass spectrometry
MetOH	methanol
MSN/MSNs	mesoporous silica nanoparticle/s
NHS	N-hydroxysuccinimide
non-CCE	clathrin/caveolin–independent endocytosis
n/r	not reported
ns	non-significant
OC	octreotide
ON	overnight
PB	permeabilization buffer
PDE/PDEs	phosphodiesterase/s
PEI	poly(ethylenimine)
PEG	poly(ethylene glycol)
PFA	paraformaldehyde
PRRT	peptide receptor radionuclide therapy
qRT-PCR	quantitative (real-time) reverse transcription polymerase chain reaction
RES	reticuloendothelial system
RT	room temperature
SangerSeq	Sanger sequencing
SB	stain buffer
SDS-PAGE	sodium dodecyl sulfate – polyacrylamide gel electrophoresis
SD	standard deviation
SEM	standard error of the mean
SN/SNs	supernatant/s
SP	scrambled peptide
Sst14/28	somatostatin-14/somatostatin-28
SSTR/SSTRs	somatostatin receptor/s
TEM	transmission electron microscopy
TFA	trifluoroacetic acid
WB	western blotting
WT	wild type

List of Original Publications

This dissertation is based on the following original publications, which are referred to in the text by their Roman numerals (I–III):

I **Paramonov, V. M.**, Desai, D., Kettiger, H., Mamaeva, V., Rosenholm, J. M., Sahlgren, C., and Rivero-Müller, A. Targeting somatostatin receptors by functionalized mesoporous silica nanoparticles – are we striking home? *Nanotheranostics,* 2018; 2, 320–346.

II **Paramonov, V. M.,*** Gerstenberg, M.,* Sahlgren, C., Lindén, M., and Rivero-Müller, A. *In vitro* targetability validation of peptide-functionalized mesoporous silica nanoparticles in the presence of serum proteins. *Front. Chem.,* 2020; 8, 1048.

III **Paramonov, V. M.,** Gerstenberg, M., Sahlgren, C., Lindén, M., and Rivero-Müller, A. SSTR5/2 targeting downregulates *in vitro* cellular uptake of silica nanoparticles with protein corona. *Manuscript*.

* Equal contribution

1 Introduction

The present works pursuits one major aim – to evaluate how custom-designed nanoparticles of mesoporous silica (MSN), functionalized with short peptides of high affinity to somatostatin receptors (SSTRs), would be accumulating in SSTR-positive cells under biologically-relevant conditions *in vitro*. In depth understanding of ligand-receptor interactions in the context of nanocarrier-mediated drug delivery, specifically of the functional outcomes of ligand-receptor coupling in terms of nanocarrier tissue accumulation and associated effects, is of enormous relevance for applied nanomedicine and, most notably, its oncology domain. The latter should come as no surprise, assuming the renowned dysregulation of the receptome in many cancers, frequently characterized by overexpression of plasma membrane receptors, which naturally makes them attractive targets for therapeutic and diagnostic purposes[1,2]. SSTRs make an excellent example of such a target, for these receptors are frequently upregulated in neoplasias of endocrine glands (pituitary, adrenals, thyroid and parathyroids), as well as in tumors of so-called neuroendocrine differentiation, collectively comprising a significant fraction of malignancies of the digestive tract, pancreas, lungs, and prostate[3,4].

In the following sections, I would introduce the major models of nanocarrier-mediated delivery to solid malignancies, while considering the models in a broader context of a typical *in vivo* life cycle of a nanocarrier. We would go through the main steps that a typical nanocarrier traverses *en route* to a solid tumor *in vivo*, with putting special emphasis on selected aspects, known to be of paramount importance for tissue accumulation of nanoparticles, for the latter represents one of the most critical determinants of how treatment with a nanoformulation affects tumor growth. Ultimately, the Literature Review chapter provides a focused perspective on nanocarrier-mediated delivery in oncology, which should facilitate interpretation of the experimental approach, the derived data and conclusions on SSTR targeting with MSN, presented in the thesis.

2 Review of the Literature

The explosive growth of the nanoscience in the late 20th century yielded an extensive repertoire of biocompatible nanocarriers[5,6]. The basic nanoplatforms, such as metal nanoparticles, liposomes, nanoparticles of branched polymers and silica nanoparticles, not only enabled progress in the field and our current understanding of how nanomaterials interact with the living matter, but served as templates for a host of derivatives. The latter feature a general trend towards evolving design complexity and exemplify not only incremental optimization efforts (such as "tinkering" with size, shape and basic surface functionalization of a nanocarrier), but also ingenious feats of functional design (*e.g.,* multilayer nanocarriers with external stimuli-controlled cargo release or ordered assemblies of several distinct nanocarriers)[7,8]. As the result, hundreds of nanoformulations have been published in the literature over the last three decades and this influx does seem to ebb. With this, a reasonably detailed literature survey even of the basic nanocarriers becomes a very challenging task.

However, despite a host of approaches to chemical design and dissimilar final appearance, all the nanocarriers share one cardinal feature – a size at the nanoscale (*i.e.,* dimensions within 1–1000 nm range). This dimensional similarity in effect underlines all the principal functional traits of nanocarriers that are of relevance for biomedical applications – specifically, enormous surface to volume ratio and distinct pharmacokinetics, collectively endowing nanoparticles with an outstanding capacity to serve as delivery vehicles[9–11]. On the other facet of this dimensional similarity, however, lie the common issues inherent to *in vivo* administration of the majority of nanocarriers, such as distinct toxicity and clearance profiles, propensity to accumulate in phagocytic cells, underlying off-target nanocarrier deposition in liver, spleen and lungs, as well as poorly predicted interactions with immune system.

Thereby, to introduce the reader to the main models of nanocarrier-mediated delivery (a.k.a passive and active targeting models), important in the context of the present work, I would depict a typical *in vivo* life cycle of a nanocarrier, utilizing a prototypic nanocarrier of extremely simplified design. Such a generic nanoparticle, that could be thought of as a monocomponent sub-micrometer sphere devoid of any surface decorations, would travel about the same *in vivo* journey upon systemic

administration as the vast majority of hitherto described nanocarriers. Yet, the utmost design simplicity of our prototypic particle should facilitate focus placement on the general phenomena inherent to *in vivo* administration of nanocarriers, avoiding the proverbial "can't see the wood for the trees" problem, frequently following generalization attempts with diverse nanoparticles of varying inner core and surface functionalization.

2.1.1 A typical life cycle of a nanocarrier *in vivo*

In this section, I would concisely review the main events along the *in vivo* journey of our prototypic nanocarrier, administered to a human or a small rodent (a standard animal model) with a solid malignancy for a purpose of tumor accumulation, enabling diagnostics/treatment. I will explicitly focus on intravenous (i.v.) injection, by far the most frequently used and most comprehensively characterized administration route, typically allowing for both the fastest and widest possible tissue distribution of the administered agent. Other routes of systemic (*e.g.,* enteral or via inhalation) and topical administration (*e.g.,* transcutaneous absorption) of nanoparticles are much less studied and converge with the i.v. route from the moment nanoparticles enter systemic circulation. Furthermore, the current models of nanocarrier-mediated delivery principally stem from experimental evidence with administration of nanocarriers in systemic circulation and as such could be best explicated within the context of i.v. injection of the generic nanocarrier.

Consider the i.v. injection of the generic nanocarrier suspended in isotonic saline (Table 1). Upon entry into the bloodstream, the nanoparticles instantaneously get in contact with a host of blood solutes (proteins, sugars, vitamins, lipids, collectively comprising blood plasma) and start encountering blood cells (*i.e.,* erythrocytes and immune cells). The consequences of these interactions are extremely diverse[12–14]. In the first place, the contact with the plasma enables adsorption of blood solutes (most notably, proteins) onto the originally bare surface of the generic nanocarrier, leading to formation of a so-called biocorona. The biocorona drastically alters the functional surface and the associated physicochemical features (*e.g.,* surface charge, roughness) of a nanocarrier, in effect endowing it with a novel biological interface. Most importantly, the novel biointerface affects the way a nanoparticle is recognized and "approached" by cells, including signaling and endocytosis, which establishes biocorona as one of the principal determinants of the functional performance of nanocarriers *in vivo*[14,15]. Biocoronas are covered in more detail in section 2.1.4.

Table 1. A journey to a tumor lesion of a generic nanocarrier after i.v. administration and the current models of passive and active uptake of nanoparticles in solid malignancies.

MAIN JOURNEY PHASES *IN VIVO*	**PASSIVE UPTAKE (EPR) MODEL**	**ACTIVE UPTAKE (ART) MODEL**
Entry to the blood and systemic circulation:		
• biocorona build-up and maturation	(-)	(-)
• interactions with blood cells and plasma	(-)	(-)
• clearance:		
○ clearance by RES	(-/+)	(-/+)
○ evasion of renal clearance	(+)	(+)
Interaction with vascular endothelium and extravasation:		
• specific mechanism of endothelial homing, uptake and transcytosis, (collectively, ***active transport***)	(-)	(-/+)[A]
• extravasation via filtration (through abnormal gaps between endothelial cells) and transendothelial diffusion (collectively, ***passive transport***)	(+)	(+)
• biocorona evolution during endothelial transcytosis and extravasation	(-)	(-)
Entry into and retention within tumor matrix:		
• uptake by tumor cells *vs.* non-malignant parenchymal cells		
○ interaction with cellular membranes and endocytosis	(-)	(+/-)[B]
○ intracellular trafficking, exocytosis and degradation	(-)	(-)
• biocorona evolution within tumor matrix	(-)	(-)
○ (for cases of exocytosis or nanocarrier release upon cellular death): biocorona evolution during cellular uptake, trafficking and release	(-)	(-)
Tumor tissue clearance via lymphatics and re-entry into systemic circulation:	(-)	(-)
• biocorona evolution	(-)	(-)

[A] Concerns cases of endothelial targeting, where nanocarriers are functionalized with ligands to endothelial receptors.

[B] Typically limited to a targeted receptor–specific internalization.

Listed are the principal phases of *in vivo* journey of a typical nanocarrier after its i.v. administration for the purpose of accumulation in a solid malignancy. Whether the given phases are fully acknowledged, recognized up to some degree, or predominantly disregarded by the tumor uptake models in question, are indicated with (+), (+/-), or (-), respectively. EPR – enhanced permeability and retention model; ART – active receptor targeting model. Further explanations are in the main text (refer also to sections 2.1.2 – 2.1.3, and Fig. 1-2).

Interactions with blood cells tend to be very complex and to a high degree depend on both the physical properties (*i.e.,* size, shape and surface features) and biocoronas of nanocarriers[12,16]. However, several common aspects could be highlighted. Firstly, a fraction of the administered nanocarriers is likely to get sequestered by the blood cells (through internalization and/or association)[17–19], which in effect removes it from the pool of free circulating particles. Secondly, nanoparticles are subjected to surveillance by immune cells. To a significant extent, interactions with leucocytes are mediated by antibodies and complement proteins, adhering to nanocarriers as a part of the biocorona. Collectively called opsonins, these moieties spark up heterogeneous defence responses, including phagocytosis, generation of nanocarrier epitope-specific antibodies and priming of cellular immunity[13,20–22]. These responses in turn underline a good deal of adverse immune reactions to nanocarriers and tend to promote their clearance, negatively impinging on pharmacokinetics and bioavailability.

Next comes the actual circulation phase of the nanocarrier in blood, which typically spans the period from several hours to several days. Importantly, nanocarriers tend to stay in systemic circulation on average up to several fold longer as compared to conventional small-molecule drugs[23–25]. This extended retention in the circulation is believed to represent one of the cardinal features of nanocarriers and, again, is principally attributed to their size. More specifically, when the size of a nanocarrier exceeds *ca* 5–6 nm, which is the dimensional threshold for renal filtration in humans, it avoids renal clearance[26–28], which is the main excretory route for hydrophilic low molecular compounds[29,30]. Besides, the dimensional factor strongly disfavours transendothelial diffusion of nanoparticles (for diffusion flux is inversely proportional to a solute's radius times 6, as stipulated by Fick's first law and Stokes-Einstein equation for spherical particles in liquids with low Reynolds number), which is believed to heavily contribute to extravasation of small-molecule pharmaceuticals[31,32]. And though other factors, such as shape, elasticity and surface charge, are also known to affect the half-life of nanocarriers in circulation[16,33], the described nanocarrier size-dependent effects on renal clearance and transendothelial diffusion are still considered to be the main determinants of the extended retention of nanoparticles in blood.

After staying in the circulation for a period of time, the nanocarriers eventually either leave the vasculature and enter surrounding tissues, or are subjected to clearance. In the absence of efficient renal filtration, the latter is predominantly mediated by 1) hepatic elimination (hepatocytes actively take up nanoparticles from blood and excrete them with bile)[13,34] and 2) specialized endotheliocytes (a.k.a scavenger endothelial cells) and professional phagocytes (tissue-residing macrophages) of liver, spleen and lymph nodes, collectively comprising a reticuloendothelial system (RES)[13,35,36]. Renal clearance could also aid the above

processes, provided the nanocarrier is degradable *in vivo* and stays in the circulation sufficiently long to erode/disintegrate into components small enough to pass through the renal filter.

Transport from the vascular bed to the parenchyma of perfused organs (extravasation) is another critical phase in the life cycle of the prototypic nanocarrier. Indeed, the maximal theoretically achievable tissue accumulation of a nanocarrier after its systemic administration is a function of its blood concentration, tissue extravasation and tissue clearance. However, the accumulated evidence indicates that the contribution of lymphatic drainage, which is the major physiologic mode of tissue clearance, tends to be rather limited in case of the nanoparticles in solid tumors[37,38]. Besides, it appears that the bulk of the extravasated nanoparticles is either internalized by the parenchymal cells (discussed below) or *trapped* in the extracellular matrix in the vicinity of the vessels. The latter scenario is especially valid for nanocarriers bigger than 50 nm – smaller particles are less diffusion-limited and typically can penetrate deeper into tumor parenchyma[39–41]. As a result, just a modest fraction of the extravasated nanoparticles could eventually re-enter systemic circulation via lymphatics. This further highlights extravasation as one of the main determinants of tissue accumulation of nanocarriers.

Surprisingly, specific molecular mechanisms governing passage of synthetic nanoparticles through vascular barrier *in vivo* have not received much of attention thus far and remain rather poorly understood[42–44]. Early studies with nanocarriers frequently disregarded active functions of the endothelium and considered the microvascular bed rather as "*a system of interconnected semipermeable pipes*", allowing for pressure gradient-driven filtration and concentration gradient-dependent diffusion of solutes across the vascular wall. In other words, extravasation of nanoparticles was mainly thought of in terms of physical laws of hemodynamics and diffusion at the level of microvessels, with the only principal difference from the established models of *in vivo* pharmacokinetics for molecular drugs being adjustment for the size of the agent[31,45,46].

On the verge of 1990s, such a standpoint was integrated with the insights from tumor vasculature studies, yielding a refined model of *in vivo* nanocarrier uptake by solid cancers, named *Enhanced Permeability and Retention* (EPR, discussed in detail in 2.1.2; Fig. 1). The EPR model recognizes profound structural abnormalities of the vasculature in solid malignancies, such as appearance of pathologically dilated vessels with excessive tortuosity and irregular branching, yielding distorted microvascular bed with impaired hemodynamics. Combined with dramatically enhanced permeability of tumor microvessels due to appearance of gaps between endothelial cells, thinning and disintegration of basal membrane, as well as failing pericyte support, this allows for increased tumor extravasation (a.k.a increased vessel leakiness) of both small molecules and bigger agents up to few micrometers in

size[23,24,47]. Furthermore, extravasated agents face difficulties with tissue clearance in view of depleted and malfunctioning lymphatics, which underlies the enhanced retention facet of the model[37,38,48]. Thereby, the EPR model principally attributes increased accumulation of nanocarriers in solid tumors to concerted effects of distorted hemodynamics, elevated vascular permeability and impaired lymphatic drainage at the microcirculatory level. As the interactions of nanoparticles with endothelial and tumor cells, including transcytosis and endocytosis, are globally disregarded by the model, the EPR is also frequently referred to as the model of passive tumor uptake. Despite such a reductionistic perspective, the EPR quickly established itself as the governing model for nanocarrier-mediated drug delivery and to the present moment continues to instruct development of nanoparticles for solid malignancies[42,49].

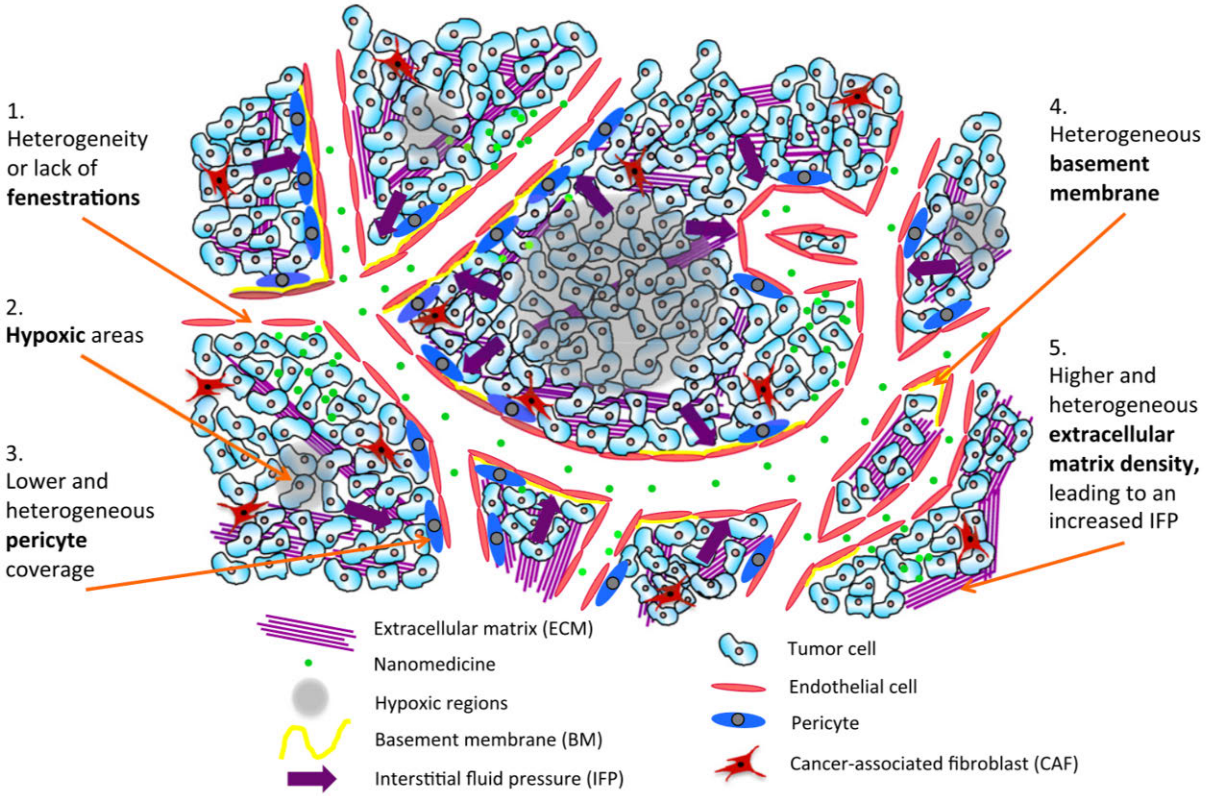

Figure 1. The EPR model. Nanocarriers extravasate through corrupted tumor microvasculature, characterized by abnormal endothelium (pathological fenestrae between endotheliocytes), attenuated basal membrane and inadequate pericyte support, and gradually accumulate in tumour parenchyma due to reduced lymphatic clearance and dense extracellular matrix. Further details are in the main text. (Reprinted from ref[50], page 113; © 2016, with permission from Elsevier).

However, as already pointed out, the EPR model overlooks cellular interactions of nanocarriers within the tumor matrix. Arguably, the most important aspect at this stage is nanoparticle endocytosis by tumor cells. As would be discussed later (section 2.1.5), nanoparticles could traverse cellular membranes and enter cytoplasm via a number of internalization mechanisms, with the predominant endocytosis mode being strongly depended on the size and functional surface of a nanocarrier, aligned with availability of relevant endocytosis machinery in a given cell.

The surface receptors on tumor cells have received specific attention in this regard. Dwelling in plasma membranes and coupled to distinct internalization pathways, surface receptors not only act as natural sensors for external cues, but enable specific and efficient entry routes for numerous ligands, including peptides and hormones. Overexpression of certain receptors, such as G protein-coupled receptors (GPCR) and integrins, in selected solid malignancies, as well as examples of successful clinical translation of cognate ligands and antibodies for tumor-specific diagnostics and treatment[1,51], inspired similar attempts to nanocarrier-mediated drug delivery. The ensuing efforts with nanoparticles could be collectively thought of within a model of active receptor targeting (ART, detailed in section 2.1.3; Fig. 2), which implies surface decoration of nanocarriers with ligands to receptors of high abundance in diseased tissues (a.k.a targeted sites), in anticipation that ligand-functionalized (targeted) nanocarriers would feature enhanced accumulation in targeted sites by virtue of ligand-receptor binding and associated effects on cellular endocytosis and/or tissue retention of nanoparticles[2,23,52]. Noteworthy, the ART model is broadly applicable to multiple classes of receptors and ligands, with the sole cardinal requirement being the high affinity and specificity of expected ligand-receptor interactions. However, with the exclusion of a special case of vascular targeting, when nanocarriers are functionalized with ligands to endothelial receptors and thus are more likely to engage into specific interactions with vascular endothelium[53,54], targeted nanoparticles travel the same journey to tumor parenchyma after systemic administration *in vivo* as their non-targeted counterparts. Thereby, the ART model in effect represents an improved extension of the EPR model, which pays extra attention to how nanocarriers interact with surface receptors of tumor cells.

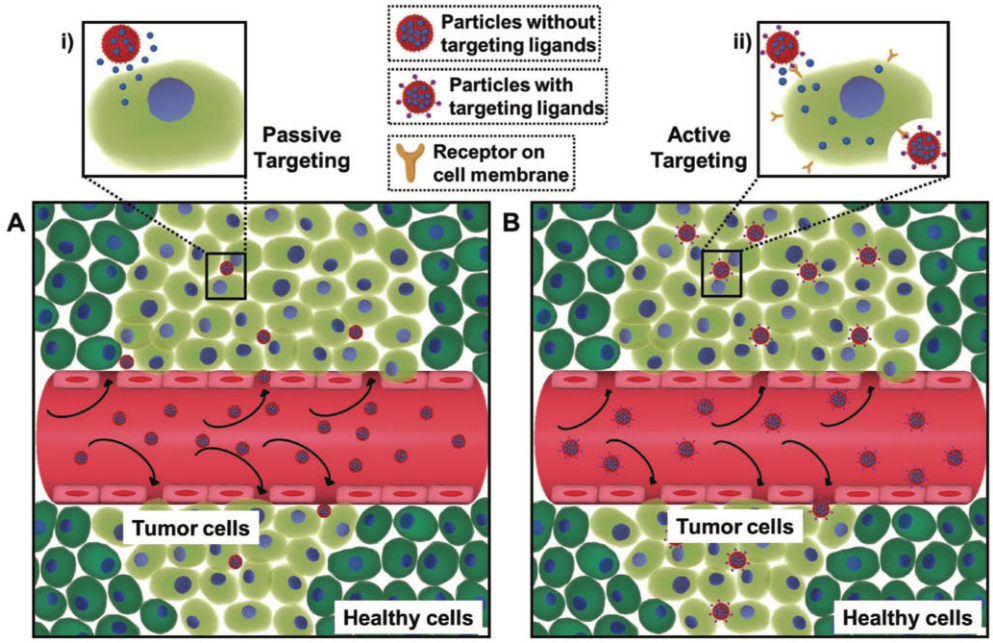

Figure 2. The passive targeting (A/i) *vs.* the active receptor targeting (B/ii) in solid tumors. Once in tumor parenchyma, targeting ligand-functionalized nanocarriers interact with surface receptors on tumor cells, which promotes receptor-mediated endocytosis of targeted particles and/or potentiates their retention in the tumor by means of receptor anchoring. Both the phenomena are thought to enhance specific accumulation of targeted nanocarriers in tumours expressing targeted receptors. Non-targeted nanocarriers do not leverage the above receptor-mediated mechanisms and thus are thought to enter tumor cells through "non-specific" internalization pathways. Characteristically, both targeted and non-targeted nanoparticles are thought to passively extravasate into tumors via hemodynamic forces and leaky tumor microvasculature (the EPR effect). Refer also to Fig. 1 and sections 2.1.2 – 2.1.3. (Reprinted from ref[14], page 3; © 2017, with permission from John Wiley and Sons).

Finally, what happens to our generic nanocarrier after it is engulfed by a tumor cell? Assuming the internalized nanoparticles are cargo-free and non-toxic to the cells, the main possible outcomes are either degradation, which typically happens within the acidic endosomal compartment, or re-cycling/exocytosis back to the extracellular compartment[55]. Selection between these routes is highly dependent on biology (*i.e.,* endocytosis apparatus and related machinery) of a given cell type, as well as on characteristics (most importantly, surface features) of a nanocarrier[56,57]. Still, in view of the compromised lymphatics in solid tumors, it appears that only a small fraction of the nanoparticles that undergo exocytosis or avoid cellular uptake could escape into systemic circulation[58]. Extended tumor retention due to entrapment in the extracellular matrix or engulfment by neighbouring tumor cells, fibroblasts or tissue macrophages, is thus the most likely outcome. With this, in the context of solid

malignancies, the life cycle of our generic nanocarrier could be considered over after the extravasation and initial cellular uptake events.

The processes outlined above reveal the astounding complexity of interactions and transition phases that a nanocarrier is likely to experience *en route* to the desired destination *in vivo*. Furthermore, the interaction complexity for a nanoformulation within the host organism appears to parallel those of the nanocarrier's design – for multicomponent carriers imply diverse interactions both between *autologous* structural components (such as ligand dissociation from a nanoparticle) and autologous component-specific interactions with environment (such as effects of blood adsorbates on targeting moieties and underlying nanosurface). Thus, nanoparticles of a more sophisticated structure (*e.g.,* functional shell- and ligand-decorated, multilayer), which comprise a good fraction of nanocarriers in current biomedical projects[5], should be generally expected to face an even higher number of interactions *in vivo*. Accordingly, the principal functional outcome (*i.e.,* tumor accumulation) quickly becomes a stunningly complex function of growing number of variables.

Clearly, both the EPR and ART models fall short of the described *in vivo* complexity (Table 1). Specifically, from the factors known to determine the fate of nanocarriers *in vivo*, neither of the models properly acknowledges active interactions of nanoparticles with the vascular wall (endothelial homing and active transport through endothelial cells) or a contribution of biocoronas to cellular interactions of nanocarriers. Furthermore, the staple EPR model globally disregards how nanoparticles interact with tumor cells after extravasation to tumor matrix. These very interactions, ultimately leading to internalization of nanocarriers and evidently important from the standpoint of their tissue accumulation, become partially addressed in the ART model, which, as said, otherwise represents a refined extension of the EPR model. Notwithstanding these principal shortcomings, the models of passive and active tumor targeting have been instrumental in the field and by and large continue to instruct nanocarrier-mediated delivery in oncology. Still, there is little doubt that in the future the current models would be superseded by more complex ones, paying homage to hitherto neglected aspects of tumor targeting (specifically, active interactions of nanocarriers with vascular endothelium and molecular mechanisms of endocytosis) and thus enabling more integrative outlook on the *in vivo* journey of nanocarriers to solid tumors.

As the current work is focused on a particular case of receptor targeting with a selected nanocarrier, which is convenient to think of in terms of the ART and EPR, I would elaborate more on these models in the following sections. Also, I will specifically discuss biocoronas and adsorption of biomolecules on nanocarriers *in vivo*, as well as provide an overview of main endocytosis mechanisms, known to mediate cellular uptake of nanoparticles. Both the latter aspects are important

determinants of tissue accumulation of nanocarriers, and as such should aid the reader in getting a good grasp of the actual experimental findings, presented herein, and putting them in a broader context.

Other important phases of the *in vivo* life cycle of nanocarriers (Table 1) are not detailed in the thesis, for these are best approached experimentally in relevant animal models (and the current work was solely done *in vitro*), but also in view of the manuscript length constraints. Further information on systemic pharmacokinetics of nanocarriers[12,13,16,21,59], including clearance/interaction with RES[34,60–63] and relevant immunity and toxicology aspects[22,64,65], microvascular hemodynamics and solute extravasation via filtration and diffusion in the context of nanocarrier-mediated delivery[31,32,45,46,66,67], as well as on lymphatic drainage of normal and malignant tissues[68–70], is available for the interested reader in the listed and many other works.

2.1.2 Enhanced permeability and retention (EPR): the model of passive uptake of nanocarriers in solid malignancies

As already mentioned, the EPR model conceptually instructed a great deal of efforts with nanocarrier-mediated delivery in oncology over the last three decades and as such represents a genuine milestone in the field[23,24,71–73]. As the name implies, the model principally builds up on the two specific pathophysiological traits of solid malignancies, a) increased permeability of tumor vasculature, allowing for enhanced extravasation of both small and high-molecular solutes, including agents of sub-micrometer size, into tumor parenchyma, and b) reduced tissue clearance of the extravasated compounds due to abnormal and malfunctioning lymphatics. As the compromised lymphatics predominantly affects clearance of the agents of bigger size, severely limited in their capacity to escape tumor tissue via diffusion[32], the combination of enhanced vascular leakiness and impaired tissue clearance (retention) collectively favours accumulation of high-molecular agents and nanoparticles in tumor parenchyma (Fig. 1).

The phenomenon of enhanced vascular permeability is typically explained in the context of grossly altered anatomical structure of the microcirculatory bed of solid malignancies and impaired local hemodynamics. Indeed, ultrastructural studies of tumor vessels revealed an array of irregularities. On a tissue level, the vasculature of solid tumors is characterized by appearance of the pathologically dilated vessels of increased tortuosity, featuring abnormal branching, which ultimately translates into pathological shunting and global loss of the strict hierarchical structure of the microvascular bed[74–77]. Such distorted vessel milieu is associated with drastically decreased velocity of blood flow, sludge of blood cells and frequent thrombotic events, which further compromise microvasculature and promote vascular stasis[31,32].

These effects are aggravated by solid stress and the associated tumor hypertension (also partially provoked by impaired lymphatic clearance; discussed below), which decrease the hydraulic pressure gradient, slowing down blood flow in tumor vessels even further[67,78].

On a level of a vascular wall, tumor microvessels feature axial thinning of the endothelium with depletion of tight junctions and the appearance of pathological gaps between endotheliocytes, which is accompanied by focal disintegration of basal membrane and failing pericyte support[76,79–82]. These ultrastructural alterations evidently undermine the integrity of the vascular wall, which compromises its function as of an active, tightly controlled and selectively permeable barrier and allows for enhanced and much less selective *passive* extravasation (by both filtration and diffusion) of small and high-molecular agents. The pathological gaps (also known as *fenestrae*) between tumor endothelial cells have received special attention in this regard – reported to be up to several micrometers wide and serving as "vascular exit gates*"* for near-micrometer or even bigger nanoparticles, these aberrant structures readily became a principal hallmark of the tumor vasculature, underpinning the leakiness facet of the EPR model[23,77,83,84].

Enhanced retention of the extravasated nanoparticles in tumor parenchyma is mainly attributed to distorted lymphatics. Solid tumors feature a depleted and structurally disarrayed lymphatic tree, with the majority of lymphatic vessels confined to the periphery of tumor lesions[38,48,67,85]. With this, lymphatic clearance is predominantly happening in the area of the outer tumor margins, while the bulk of the inner tumor mass has very little of functional drainage. As said, malfunctioning lymphatics predominantly affects clearance of high-molecular compounds, for the latter are severely diffusion-limited by virtue of their size and in effect can leave parenchyma only via conductive clearance with lymphatic fluid[32,37]. Contrary to this, extravasated low-molecular compounds do not face such a diffusion constraint and thus could still leave the tumor tissue even in the absence of proper lymphatic flow. Thus, vascular leakiness and tissue retention effects collectively enable the preferential accumulation of high-molecular agents and nanoparticles over small solutes in tumor tissue.

Another important prerequisite for efficient tissue accumulation of nanocarriers in the EPR model is their extended dwelling in systemic circulation[73,86,87]. As already mentioned, the latter effect is predominantly mediated by decreased renal clearance, for nanoparticles bigger than *ca* 5–6 nm face difficulties with passaging through the glomerular barrier. As the result, nanocarriers can stay in the circulation for up to several days, iteratively entering and leaving the tumor vasculature. Every tumor passage round leads to a seeping of a fraction of the administered dose into tumor parenchyma, where nanoparticles gradually accumulate.

The retention time in circulation also tends to increase if nanoparticles are *reluctant* to interact with normal endothelium and have decreased propensity to end up in the RES, which in the absence of efficient renal filtration becomes the predominant mode of nanoparticle clearance. These effects are typically achieved by preparation of nanocarriers of near-neutral or slightly negative surface charge, which mitigates their electrostatic adherence to the negatively charged healthy endothelium. Another common approach is to coat nanocarriers with special chemical moieties, such as poly(ethylene glycol) (PEG), known to inhibit opsonization of nanoparticles and their uptake by RES phagocytes[88–90].

Taken together, the EPR model stipulates that for efficient accumulation in tumor tissue, a nanocarrier has to be smaller than the endothelial fenestrae of tumor vessels (the EPR effect), but bigger than the size threshold of renal filtration (extended dwelling in circulation). Furthermore, a *stealth* surface, enabling RES evasion and potentiating retention of a nanocarrier in the systemic circulation, is also desirable.

By the mid-2010s, the bulk of nanocarriers for oncology applications were designed following the above dimensional and surface prerequisites, highlighting the governing role of the EPR model in the field. However, apart from a handful of liposomal and polymeric nanoformulations, most of the nanoparticles developed with the EPR concept in mind failed in the clinical setting despite demonstrating fair performance in animal models[91–93]. Almost uniformly, the major underlying reason for this failure appears to be a disappointedly low tumor accumulation rate, which was globally estimated to stay below 1 % of the administered dose[94]. Importantly, this was also the case even for the clinically approved nanoformulations – in fact, these gained approval mostly on the grounds of improved biocompatibility and toxicity profiles rather than their ability to enable enhanced delivery of a toxic cargo to tumor lesions[95,96]. Thereby, the whole nanooncology field arrived at a translational conundrum: literally dozens of nanoformulations reportedly demonstrate superior performance as vehicles for drug delivery in animal tumor models, yet in humans hardly any of these carriers significantly improve tumor accumulation of cargo drugs as compared to administration of the same drugs alone[50,97–99].

As it stands out, closer scrutiny would expose an array of inherent problems with the EPR model. To start with, the model is predominantly based on experimental evidence with nanocarriers in laboratory animals harbouring tumor xenografts (in most part, ectopical)[10,11,97]. Despite their undisputed role in cancer research, xenografts, however, only vaguely recapitulate the original solid human tumors in their complexity and heterogeneity, specifically on a tissue level[100,101]. In a typical case a xenograft represents an expanded progeny of the most aggressive and survival-fit clones out of the pool of the tumor cells, implanted into foreign environment of another species, lacking appropriate immune defence. Xenografts

feature tremendously accelerated growth rates – in a typical case, it takes several weeks for a xenograft in rodents *vs.* years in humans for a lesion to reach 1–2 cm in diameter. As the result, the earlier discussed alterations of the tumor vascular bed, frequently observed in xenografts and leveraged in the EPR model, in most part might as well represent xenograft-specific artefacts, reflecting host vascular response to the catastrophically expanding tumor mass[25,102]. As solid tumors in humans hardly ever proliferate that fast, surrounding tissues and the derived vasculature have much more time to adapt and respond to a growing malignant lesion, with the resulting tumor vasculature and the tumor itself evolving very differently as compared to experimental xenografts. The actual evidence with solid malignancies in humans appears to favour the last notion – endothelial fenestrae, considered for the main entry gates in the EPR model, appear to be a rare find in genuine microvessels of human tumors[103,104]. Vascular biology studies also steadily depict the renowned leakiness of tumor vasculature rather as an active phenomenon and not as a primary consequence of gross anatomical alterations of the microvasculature. This includes the active shuttling of molecules by endothelial cells of tumor vessels, mediated by specific endocytosis machinery and prompted by certain bioactive moieties, such as VEGF and histamine[77,104–107]. Taken together, these aspects clearly call for a careful re-evaluation of the enhanced permeability facet of the EPR model. Likewise, the notorious propensity of many solid tumors to disseminate primarily via lymphatic vessels might also call for a more accurate weighting of the enhanced retention component of the model[69,108].

All in all, tumor xenografts, established in laboratory animals with the current experimental techniques, in many ways are clearly not that same as the source human tumors, which by itself might suffice in explaining the discrepant performance of nanocarriers in preclinical and clinical settings[11,73,97]. A host of inter-species physiological differences that are likely to differentially impinge on pharmacokinetics and biodistribution of nanomedicines in humans and rodents (*e.g.,* immune surveillance & RES, hemodynamics) further supports this notion.

Besides the heavy bias towards tumor xenografts, the EPR model is evidently oversimplified and overlooks several vital components of the *in vivo* life cycle of a nanocarrier (Table 1). As said, the EPR model globally considers solid tumors as *permissive sponges*, allowing for enhanced influx and retention of high molecular agents, with both the processes being primarily mediated by *passive* physical factors (hemodynamics, diffusion, dimensional cut-offs). *Active* processes, *i.e.,* energy-dependent and tightly controlled events, mediated by specific molecular machinery on a level of a single cell or a tissue, such as endocytosis of nanoparticles by tumor cells or transendothelial transport, are neglected by the EPR model. Constant evolution of the functional surface of nanocarriers *in vivo* due to adsorption of biomacromolecules (biocorona) and the effects of the latter on interactions of

nanoparticles with vascular and tumor cells also go unrecognized. Yet, recent studies start putting endothelial biology in focus – and the active transvascular transport is beginning to emerge as a principal mediator of tissue accumulation of nanocarriers[43,104]. Instrumental role of the biocorona for *in vivo* fate of nanocarriers has also been compellingly demonstrated (discussed in 2.1.4).

To conclude, the EPR model provides quite a simplified perspective on *in vivo* journey of nanocarriers, which appears to be more pertinent for experimental tumor xenografts rather than the real-life human malignancies. With this, the persistent translational gap between animal experiments and trials with human subjects becomes easier to comprehend; the same applies to the limited *in vivo* performance of the majority of nanocarriers designed within the EPR framework. Improved understanding of tumor biology, endothelial physiology and active transvascular transport of nanoparticles, as well as of processes shaping functional interface of nanoparticles *in vivo* (biocoronas), is expected to yield more integrative and biologically relevant models of tumor targeting with nanocarriers, which are likely to instruct subsequent generations of more knowingly-designed nanoplatforms.

2.1.3 The active receptor targeting (ART) model for nanocarriers in solid tumors

2.1.3.1 The ART model: basic concepts and the current standpoint

The ART model emerged as a refinement of the EPR model that attempts to integrate all the principal components of its predecessor (*i.e.,* enhanced accumulation of nanocarriers in tumors due to leaky vasculature and impaired lymphatics) with specific receptor interactions of extravasated nanoparticles with tumor cells. To enable active targeting, *i.e.,* interaction with surface receptors of tumor cells, a nanocarrier has to be functionalized with respective high-affinity ligands, which makes a major prerequisite for the ART model. As said, the ART envisions that targeted nanocarriers firstly reach tumor sites by means of the EPR effect, being *passively* flown and sieved into tumor parenchyma by hemodynamic forces. After extravasation comes the *active* component of targeting, by which is typically implied either specific coupling between targeting ligands and targeted receptors (a nanocarrier *actively seeks contact* with a tumor cell) or energy-dependent (and hence, *active*) mechanisms of receptor-mediated endocytosis and nanocarrier uptake, provoked by ligand-receptor binding, or the combination of thereof (Fig. 2)[23,52,53]. In other words, the ART model supplements the passive EPR

model with an extra receptor targeting step that happens once a nanocarrier enters tumor parenchyma[a].

Binding of membranous receptors in tumor cells with targeting ligands on nanoparticles might be accompanied by receptor-mediated uptake (in cases when targeting ligand induces receptor internalization) or enhanced receptor-mediated retention of a nanocarrier in the immediate vicinity of targeted cells (in cases when ligand-receptor coupling does not lead to receptor endocytosis). As both these scenarios are commonly thought to potentiate the accumulation of nanocarriers in tumors, it comes as no surprise that the ART model quickly gained momentum, prompting development of the whole new class of targeted nanocarriers[109].

The ART model is easy to comprehend in the context of the broader tumor targeting concept in oncology[1,110,111]. Indeed, the idea of surface receptor targeting in tumors is not new – the last three decades have witnessed numerous examples of successful cancer targeting with high-affinity molecules, yielding a number of clinically-useful applications. The most colourful examples here are, perhaps, therapeutic antibodies for solid and haematological malignancies[51], antibody-drug conjugates[112,113], and radionuclide-bound peptide ligands of surface receptors, enabling both diagnostic imaging and treatment (a.k.a theranostics)[114,115]. Clearly, with such historic background, translation of the cancer targeting concept to nanocarriers was soon to follow.

Such a focusedness of the ART model on receptor-ligand coupling, however, brought along several important ramifications. Firstly, a nanocarrier must be decorated with a targeting moiety, for there could be no specific receptor targeting otherwise. Thereby, the ART readily puts all the nanoparticles without targeting ligands out of scope. With this, if taken explicitly, the ART model could not be considered for a global refinement of the EPR model, but rather should be viewed as a specific extension of the EPR for a particular subgroup of nanocarriers (*i.e.,* targeting ligand–functionalized). Secondly, "non-specific" endocytosis mechanisms, mediating cellular entry of nanoparticles in the absence of receptor engagement with targeting ligands (such as macropinocytosis and clathrin/caveolin-independent endocytosis; discussed in section 2.1.5), are overlooked in the ART, just as it was the case with the EPR model[52,116]. The same also applies to other important aspects of the *in vivo* life-cycle of a nanocarrier outside of immediate receptor interactions, such as biocorona and active transendothelial transport (Table 1) – here, the ART model tends to perpetuate the inherent breaches of the EPR model discussed

[a] There is one prominent exclusion from this scenario, which is receptor targeting of endothelial cells of tumor vasculature in an attempt to promote transcytosis of nanoparticles into tumor parenchyma. Vascular targeting represents a special case and is not detailed in the current work.

earlier (2.1.2). Lastly, targetability comes with *a certain price*. Decoration with targeting ligands not only endows nanoparticles with a new functional capacity, but also draws upon a number of challenges – not only on the linking chemistry and surface functionalization side, but, even more importantly, on the side of targetability evaluation. The latter appears to represent a characteristically weak point – as would be discussed in section 2.1.3.2, *in vitro* and *in vivo* approaches to targetability validation are all too often incomplete or inadequate, allowing no clarity with interpretation of obtained evidence with targeted nanoformulations. This in turn is likely to contribute to the disappointing results of targeted nanocarriers in the clinical setting (discussed below), questioning viability of the ART model as a whole.

Development efforts with targeted nanocarriers in the last decade have been enormous and research activity in this direction stays quite high. Following the success path of small-molecule targeted therapeutics, nanocarriers have been functionalized with multiple kinds of targeting ligands in an attempt to enhance selective tumor delivery and accumulation. Antibodies and their derivatives (*e.g.,* nanobodies and affibodies), natural and synthetic peptides, nucleic acids and aptamers, sugars, small-molecule drugs – all these moieties have been used in capacity of targeting ligands for a vast array of nanocarriers[111,117,118]. In fact, the current standpoint on the ART could be broadly described as follows: as long as 1) there is a surface receptor that is selectively or relatively selectively expressed in a tumor (*vs.* normal tissues), and 2) there is a ligand, which has reasonably high affinity to such receptor and could be anchored to a nanocarrier's surface, the resulting receptor-ligand pair appears worthy testing for a nanocarrier-mediated delivery. Admittedly, assuming the amount of works and diversity of approaches, a detailed review of the published targeted nanocarriers stands out as a nearly-impossible task. The interested reader is referred to surveys of particular subclasses of targeted nanocarriers instead (*e.g.,* antibody-functionalized nanoparticles[119,120]; nanoparticles targeting GPCRs[121,122], integrins[123], folate[124,125], or transferrin[126] receptors).

Altogether, the ART model brings numerous and very heterogeneous targeting strategies under one roof, with the common denominator being an *expectedly* positive link between tumor receptor targeting and accumulation of targeted nanocarriers in tumors. In practice, however, everything is far from being that simple – and the field of tumor receptor targeting with nanoparticles is swarming with contradictions[52,94,127–129]. On the one hand, there are literally hundreds of published carriers, reported to show supreme accumulation in tumor cells *in vitro* and tumor xenografts by virtue of specific receptor targeting[109]. On the other hand, we have a number of opposite cases, reporting no clear advantage of receptor-targeted nanocarriers over non-targeted counterparts[11,25,52]. The clinical evaluation pipeline is also rather telltale: targeted nanocarriers typically fail the scrutiny of trials with human subjects. In fact, as of the late 2010s, none of the receptor-targeted

nanocarriers is endorsed by FDA or EMA[b] for clinical oncology applications[25,92,95,130]. Thus, the current status with targeted nanocarriers not only closely resembles the one of the nanoparticles designed to employ the EPR effect, but appears even more disappointing and confusing.

In an attempt to expose the roots of the problem and to highlight inherent complexity of the receptor targeting approach, in the following section I would focus on a particular subgroup of nanocarriers, designed to target somatostatin receptors (SSTRs). SSTRs are relatively well studied and represent very successful targets for molecular therapies in solid cancers (reviewed in section 2.1.6), which naturally makes them attractive for targeting with nanocarriers. Equally important, SSTR-targeted nanoformulations have an impressive research track, encompassing varying nanoparticle types and chemical solutions for SSTR targeting (nearly 4 dozen of original SSTR-targeted nanocarriers have been developed and published over the last 13 years; Table 2). With this, the selected SSTR case could serve as a valid proxy for the majority of nanocarriers designed to target other receptor classes and thus could be used to draw more general conclusions about the current state of the ART model in oncology.

2.1.3.2 Targetability validation and lessons from SSTR targeting with nanocarriers

As receptor targeting comprises the principal component of the ART model, ligand-receptor interaction studies should naturally be central in a targeted nanocarrier's evaluation pipeline. Furthermore, in contrast to the EPR effect, which is solely a tissue/organ-scale phenomenon and thus could be only reliably studied *in vivo* or in advanced *ex vivo* tissue-scale set-ups (*e.g.,* isolated perfused organs), receptor targeting by nanoparticles could be comprehensively evaluated in cell cultures *in vitro*[c]. *In vivo* studies of receptor engagement with targeted ligands, on the contrary, pose a much more challenging task, frequently calling for tailored and technically demanding solutions[131–133].

What aspects are vital for a robust targetability evaluation *in vitro*? On the side of a targeted nanocarrier, the following has to be ensured:

[b] Food and Drug Administration (FDA) and European Medicines Agency (EMA) – principal pharmacological regulators in the USA and the EU, respectively.

[c] Conventional *in vitro* uptake studies of non-targeted nanocarriers by cells growing in 2D primarily reflect internalization on a cellular level (endocytosis) and have nothing to do with vascular permeability and retention of nanocarriers in tumor parenchyma, which are the hallmarks of the EPR model.

Firstly, a nanoformulation has to carry a sensible amount of targeting ligands – enough to trigger measurable binding/receptor response in a testing system, which is expected to be used for targetability evaluation. Secondly, targeting ligands ought to be properly positioned on a nanocarrier's surface, which implies adequate orientation of a ligand's pharmacophore (the motif, responsible for receptor binding) and its accessibility for targeted receptors. Thirdly, targeting ligands have to be anchored to nanoparticles in a solid fashion, staying surface-bound even under complex biologic conditions in the presence of surface adsorbates (*e.g.,* in blood serum/plasma, destined to be the final medium for the majority of nanocarriers *in vivo*). In the absence of proper anchorage, the ligands could easily liberate from the nanosurface into liquid phase (phenomenon of ligand shedding; II). The consequences of such ligand liberation are clearly detrimental for receptor targeting, for nanocarriers not only lose their potential to engage targeted receptors, but might also experience competition for receptor binding with the liberated ligands. Last, but not least, ligands on the nanosurface are required to maintain the ability to engage targeted receptors despite adsorption of biological macromolecules to a nanoformulation (biocorona formation, section 2.1.4), since no efficient targeting could be expected *in vivo* otherwise.

On the side of an *in vitro* system for targetability evaluation, the main requirement is that a system should incorporate targeted receptors in a physiological or nearly-physiological state, capable of binding targeting ligands within the expected affinity range (for a free ligand). Receptor type-specific events, emerging upon ligand binding, such as downstream receptor signaling, internalization or associated events, and the ability to trace such in a system, are likely to make an extra advantage. Furthermore, it is highly desirable that a system provides a quantitative or semi-quantitative response to targeting ligands, which is convenient to capture and analyse. Finally, and perhaps most importantly, the system needs to be compatible with complex media, such as cell culture medium with proteins or blood serum/plasma, allowing *in vitro* targetability evaluation under biologically-relevant conditions, mimicking those encountered *in vivo*.

With the above prerequisites combined, most of the commonly used biophysical techniques for studies of ligand-receptor binding, such as surface plasmon resonance, isothermal titration calorimetry and analytical ultracentrifugation, have only limited applicability for the purpose, mostly on the grounds of their poor compatibility with complex biotic media[134–136]. Besides, methods of this sort typically require purified receptors (solubilized or immobilized on a surface), and receptor isolation in certain cases might be quite challenging. Furthermore, even when purified receptors retain the ability to bind ligands, they typically lack cognate environment and partners required for adequate downstream responses (*e.g.,* scaffold proteins and effector molecules, partaking in receptor signaling/internalization),

which naturally precludes or severely limits probing of the latter. However, in many cases, biophysical methods could be still efficiently used for *in vitro* targetability evaluation of nanocarriers under simplistic conditions, such as aqueous buffers.

In effect, this leaves us with living cells–based *in vitro* assays – these not only retain targeted receptors in a physiological environment (*i.e.,* dwelling in plasma membranes of living cells), but are generally compatible with complex biotic media, as the latter are required for cellular growth and maintenance. Technical solutions for ligand-receptor studies in living cells are currently manifold and tailored approaches are thus could be established for a majority of targeting pairs. This ranges from competition/displacement studies with free labelled ligands/antagonists to reporter assays, leveraging receptor signaling, internalization or associated events for proxies of receptor-ligand binding[137,138]. The cAMP *in vitro* targetability bioassay, presented in works I and II herein, belongs to the latter group of indirect techniques (see also ref[139]).

After this short survey of prerequisites for *in vitro* targetability evaluation, we could proceed with analysis of the SSTR-targeted nanocarriers published so far (as of mid-January 2021; Table 2). A literature survey identified 44 original research papers on the topic, published over 13 years. Here, we find a broad array of nanocarrier types, from conventional liposomes, solid metal nanoparticles, quantum dots and varying polymeric nanoparticles, to "exotic" formulations, such as nanogels, nanofibrills and nanoworms. Different peptide-based SSTR ligands were used as targeting moieties (most often, octreotide). Nearly all the studies in question evaluated nanocarriers for targetability *in vitro* (43/44); a significant fraction also undertook *in vivo* studies (34/44; typically, in rodents harbouring ectopic tumor xenografts)[d].

If we consider *in vitro* targetability evaluation, a highly frustrating pattern emerges. In the first place, just 4 studies out of the overall lot (4/44 or <10 %) utilized some dedicated technique to gauge the ability of targeting ligands to bind targeted receptors (highlighted in bold within the «Methods» column of Table 2). In two cases, the authors relied on ligand-evoked receptor signaling (calcium flux assay) in living cells with targeted receptor expression; in two others, free ligand displacement (competition) experiments with targeted receptors in isolated cellular membranes took place. All the remaining 40 studies did not involve any technique to confirm ligand-receptor engagement at all.

Next comes the aspect of integrity of a targeted nanocarrier under the utilized experimental conditions. As said, the phenomenon of targeting ligand shedding

[d] To the best of our knowledge, no results of clinical trials (*i.e.,* in human subjects) with SSTR-targeted nanoparticles have been reported as of January 2021.

poses a serious risk of false-positives and could easily invalidate experimental conclusions with targeted nanocarriers if left unattended. This issue appears to be especially pertinent for nanocarriers with non-covalent ligand functionalization, which renders ligand shedding more plausible (specifically, under the complex conditions *in vivo*). None (0 %) of the 44 studies took appropriate measures to exclude the possible presence of free targeting ligands in liquid phase during *in vitro* experiments with targeted nanocarriers. Some measures, though clearly insufficient, to exclude ligand shedding were taken in 2 studies (Table 2); yet, all the remaining studies do not even appear to acknowledge possible existence of such a phenomenon.

Then, the aspect of nanocarrier opsonization with biological macromolecules in complex solutions and effects of biocoronas on targetability. Tremendous importance of adsorbates for ultimate cellular interactions of nanocarriers was recognized more than a decade ago and the accumulated evidence thus far depicts biocorona as one of the principal determinants of the *in vivo* fate of nanocarriers in general (discussed in 2.1.4). Yet, none (0 %) of the studies with SSTR-targeted nanoparticles evaluated possible effects of biocorona on targetability *in vitro*. Neither taken were measures to evaluate targeting peptide shedding from nanocarriers in complex media, under adsorption of biosolutes to a surface of nanoparticles.

Concerning *in vitro* targetability testing systems, another "technical issue" stands out prominently. Thought it goes without saying that a receptor targeting event requires both receptors and ligands to occur, the presence of the former in cell lines and derived models (*e.g.,* membranous preparations) used for *in vitro* experiments with targeted nanocarriers was confirmed in less than one quarter of the studies (10/44). In the majority of cases, authors seemingly rest contented on the grounds that the cell lines they were using[e] had been earlier SSTR-profiled by others. Quite often, SSTR-positivity (or negativity, in case of no-SSTR control cells) of the utilized cells was just taken for granted without providing any supporting evidence or explanation. However, the well-documented phenomenon of a continuous genetic and phenotypic drift in immortalized cells, as well as numerous reports of confused identity or misidentification of cell lines upon extended passaging and lab-to-lab transfer[140,141], clearly depict such approaches as overtly risky and error-prone. Indeed, evaluation of a targeted nanocarrier in receptor-negative cells when taking such cultures for receptor-positive or *vice versa*, could readily lead to erroneous conclusions on targetability and its attributive events, such as cellular uptake of

[e] (studies in Table 2): though the implied cell types are the same, the actual origins (*e.g.,* source repository) of the cells in question typically differ between the earlier work (original SSTR profiling) and the later work with nanoparticles; special steps to validate identity of cell cultures are usually not reported.

nanocarriers. The issue of all too often inadequate receptor profiling in case of SSTR targeting is further aggravated by the presence of multiple SSTR subtypes and their frequent co-existence in different combinations in many cell types (discussed in 2.1.6). As the majority of SSTR ligands can bind several SSTR subtypes with varying affinities, meticulous receptor profiling of an *in vitro* model for targetability testing emerges as a virtually indispensable step. Yet, inadequate or incomplete SSTR profiling appears to be the rule rather than exception (Table 2, «Testing model/TR profiling» column).

Table 2. SSTR-targeted nanoparticles: literature survey (published research articles as of mid-January 2021).

NP / SIZE[#1] REF	TARGETING LIGAND (TL) / ANCHORING TO NPs	*IN VITRO* TARGETABILITY EVALUATION						*IN VIVO*[‡1-2] STUDIES
		Methods	Testing model[&1-2] / Targeted Receptor (TR) profiling[&3]	Targeting ligand shedding[§]	Comparator for targeting validation	Corona effects on targeting	Enough evidence to confirm targeting ?	
Liposomes; *ca* 150-170 nm *[2008; Food Chem. Toxicol.]* [142]	Octreotide/ covalent[¶1]	Comparative cellular uptake/toxicity	TR+ cell line/ TR profiling n/r	n/s	No-TL counterpart	n/s	NO	n/s
Iron oxide NPs; *ca* 10 nm (TEM) *[2009; Acta radiol.]* [143]	Octreotide/ covalent	Comparative cellular uptake (+ free TL (fTL) competition)/toxicity	TR+ cell line/ TR profiling+	n/s	No-TL counterpart	n/s	NO	Xenografting: [tumor uptake]
Liposomes; *ca* 110 nm *[2010; Nanotech.]* [144]	Octreotide/ covalent[¶1]	Comparative cellular uptake /toxicity/apoptosis (+fTL competition)	TR-high *vs.* TR-low cells (allogeneic)/ TR profiling n/r	n/s	No-TL counterpart	n/s	NO	Xenografting: [biodistribution (BD)/tumor uptake]
Liposomes; *ca* 100 nm *[2010; Mol. Pharm.]* [145]	Octreotide/ covalent[¶1]	Comparative cellular uptake (+fTL competition)/toxicity	TR-high *vs.* TR-low cells (allogeneic)/ TR profiling+	n/s	No-TL counterpart	n/s	NO	Xenografting: [pharmacokinetics (PKA)/BD/tumor uptake & proliferation]
Liposomes; *ca* 130-150 nm *[2011; Mol. Pharm.]* [146]	Octreotide/ covalent[¶1]	Comparative cellular uptake (+fTL competition)/toxicity	TR+ cell line/ TR profiling n/r	n/s	No-TL counterpart	n/s	NO	Xenografting: [tumor proliferation]
Polymeric micelles; *ca* 60-75 nm *[2011; Pharm. Res.]* [147]	Octreotide/ covalent[¶2]	Comparative cellular uptake	TR+ cell line/ TR profiling n/r	n/s	No-TL counterpart	n/s	NO	Xenografting: [tumor proliferation]

Liposomes; *ca* 90 nm *[2012; Pharm. Res.]* [148]	Octreotide/ covalent¶1	Comparative cellular uptake	TR+ cell line/ TR profiling n/r	n/s	No-TL counterpart	n/s	NO	Xenografting: [tumor proliferation/PKA]
Liposomes; *ca* 120 nm *[2012; J. Control. Release]* [149]	Octreotate ([Tyr3]-TATE)/ covalent¶1	Comparative cellular uptake	TR+ cell line/ TR profiling+	n/s	No-TL counterpart	n/s	NO	Xenografting: [PKA/BD/tumor uptake]
Polymeric micelles; *ca* 210-240 nm *[2012; Biomaterials]* [150]	Octreotide/ covalent¶2	Comparative cellular uptake (+ fTL competition)/toxicity/ apoptosis	TR-high *vs.* TR-low cells (allogeneic)/ TR profiling n/r	n/s	No-TL counterpart	n/s	NO	Xenografting: [BD/tumor uptake & proliferation]
Polymeric micelles; *ca* 100-140 nm *[2012; J. Pharm. Sci.]* [151]	Octreotide/ covalent¶2	Comparative cellular uptake & apoptosis (*vs.* fTL competition)/toxicity	TR-high *vs.* TR-low cells (allogeneic)/ TR profiling n/r	n/s	No-TL counterpart	n/s	NO	n/s
1) Micelles, *ca* 20 nm; 2) Liposomes, *ca* 100 nm *[2012; Nanomedicine Nanotechnology, Biol. Med.]* [152]	Tyr-3-octreotide/ covalent¶1	**Competition (*vs.* free radiolabeled Sst14) for TR on isolated plasma membranes**; cellular binding (*vs.* fTL: internalized fraction *vs.* plasma membrane-bound fraction)	TR+ cell line/ TR profiling n/r	n/s	fTL	n/s	**+/-** (non-corona)	BD (TL-NP *vs.* no-TL-NP) in healthy animals; xenografting [TL-NP *vs.* fTL: BD/tumor uptake]
Gold nanorods; *ca* 50x10 nm (TEM) *[2012; Nanoscale]* [153]	Octreotide/ covalent	Comparative cellular uptake /toxicity	TR+ cell line/ TR profiling n/r	n/s	No-TL counterpart	n/s	NO	n/s
Liposomes; *ca* 115 nm *[2013; Pharm. Res.]* [154]	Octreotide/ covalent¶1	Comparative cellular binding (internalized fraction + plasma membrane-bound NP fraction; *vs.* fTL competition)	TR+ cell line/ TR profiling n/r	n/s	No-TL counterpart	n/s	NO	Xenografting: [grafts of TR-high *vs.* TR-low cells, syngeneic (TR profiling n/r): BD/tumor uptake]

Polymeric micelles; *ca* 70 nm *[2013; Nanoscale]* [155]	Octreotide/ covalent¶2	Comparative cellular uptake /toxicity	TR+ cell line/ TR profiling n/r	n/s	No-TL counterpart	n/s	NO	n/s
Nanostructured lipid carriers; *ca* 100-125 nm *[2013; Int. J. Pharm.]* [156]	Octreotide/ covalent¶1	Comparative cellular uptake (also *vs.* fTL and varying endocytosis inhibitors)/ toxicity	TR-high *vs.* TR-low cells (allogeneic)/ TR profiling n/r	n/s	Comparisons between NP subtypes, carrying varying loads of TL	n/s	NO	Xenografting: [TL-NP *vs.* no-TL-NP in TR+ grafts: BD/PKA/tumor uptake & proliferation; TR profiling of the grafted cells n/r]
1) PAMAM#2 dendrimers, *ca* 1,5 nm; 2) Gold NPs, *ca* 20 nm (TEM) *[2015; J. Nanosci. Nanotechnol.]* [157]	Tyr-3-octreotide/ covalent	Comparative cellular binding (internalized NPs + plasma membrane-associated NPs)	TR+ cell line; TR profiling n/r	n/s	No-TL counterpart	n/s	NO	Xenografting: [BD/tumor uptake (*vs.* fTL)]
Polymeric micelles; *ca* 70 nm *[2016; Int. J. Nanomedicine]* [158]	Octreotide/ covalent¶2	Comparative cellular uptake/toxicity	TR-high *vs.* TR-low cells (allogeneic)/ TR profiling n/r	n/s	No-TL counterpart	n/s	NO	Xenografting: [BD/tumor uptake & proliferation]
Gold NPs; *ca* 20-25 nm *[2016; Drug Dev. Ind. Pharm.]* [159]	Sst14/ non-covalent (electrostatic adsorption)	Comparative cellular uptake (+SSTR antagonist competition)	TR-high *vs.* TR-low cells (allogeneic)/ TR profiling+	n/s	No-TL counterpart	n/s	NO	n/s
Polymeric micelles; *ca* 66 nm *[2016; Biomaterials]* [160]	Octreotide/ covalent¶2	Comparative cellular uptake/toxicity	TR-high *vs.* TR-low cells (allogeneic)/ TR profiling n/r	n/s	No-TL counterpart	n/s	NO	Xenografting: [tumor proliferation]

Solid lipid NPs[#3]; *ca* 180 nm *[2016; Acta Biomater.]* [161]	Tyr-3-octreotide/ covalent[¶1]	Comparative apoptosis (+fTL competition)/ toxicity/ uptake/ HUVEC tube formation assay	TR-high *vs.* TR-low cells (allogeneic)/ TR profiling incomplete (only done for TR-high cells *in vivo*)	n/s	No-TL counterpart	n/s	NO	Xenografting: [TR-high cells: tumor uptake (*vs.* fTL competition)/ proliferation/ BD]
Nanographene oxide NPs; *ca* 30-35 nm *[2016; Small]* [162]	Octreotide/ covalent	Comparative cellular uptake & toxicity (+fTL competition)	TR-high *vs.* TR-low cells (allogeneic)/ TR profiling n/r	n/s	No-TL counterpart	n/s	NO	Xenografting: [BD & tumor uptake (*vs.* fTL competition)/ proliferation]
Polymeric micelles; *ca* 60 nm *[2016; Biomaterials]* [163]	KE108/ covalent[¶2]	Comparative cellular uptake & toxicity	TR-high *vs.* TR-low cells (allogeneic)/ TR profiling incomplete (only TR+ cells)	n/s	No-TL counterpart	n/s	NO	Xenografting: [tumor uptake & proliferation]
PMAA[#4] single-chain polymeric NPs; *ca* 45 nm *[2016; Biomacromolecules]* [164]	PTR86/ covalent	n/s	n/a	n/s	No-TL counterpart	n/s	NO	Xenografting: [tumor uptake& BD]/ TR profiling of the grafted cells n/r
Nanofibrils of peptide amphiphiles; *ca* 4 nm (d; TEM) *[2016; Biomacromolecules]*[165]	Octreotide/ covalent	Comparative cellular uptake & toxicity	TR-high *vs.* TR-low cells (allogeneic)/ TR profiling n/r	n/s	No-TL counterpart	n/s	NO	n/s
Liposomes; *ca* 100 nm *[2016; Drug Deliv.]* [166]	Octreotide/ covalent[¶1]	Comparative cellular uptake & toxicity	TR-high *vs.* TR-low cells (allogeneic)/ TR profiling+	n/s	No-TL counterpart	n/s	NO	Xenografting: [tumor proliferation & PKA]

Branched block copolymer NPs; *ca* 55 nm *[2016; Biomacromolecules]* [167]	Octreotide/ covalent	**Competition (*vs.* free radiolabeled Sst14) for TR binding on isolated plasma membranes**	TR+ cell line; TR profiling n/r	n/s	No-TL counterpart	n/s	**+/-** (non-corona)	Xenografting: [tumor uptake & BD]/ TR profiling of the grafted cells (TR-high *vs.* TR-low; allogeneic) n/r
Nanospheres of supramolecular peptide co-polymers; *ca* 170 nm *[2017; ChemNanoMat]* [168]	PTR3207-86/covalent	Comparative cellular uptake	TR-high *vs.* TR-low cells (allogeneic)/ TR profiling n/r	n/s	fTL	n/s	NO	Xenografting: [tumor uptake/BD]
Liposomes; *ca* 120 nm *[2017; Cancer Lett.]* [169]	Tyr-3-octreotide/ covalent[¶1]	Comparative cellular uptake/toxicity (+fTL competition)/apoptosis/ invasion (Boyden chamber)/ HUVEC tube formation assay	TR+ cell lines (allogeneic)/ TR profiling+	n/s	No-TL counterpart	n/s	NO	Xenografting: [tumor proliferation (incl apoptosis and vasculature profiling)/BD]; CAM[‡3]: [angiogenesis]
Nanogel (comacromer-based nanospheres); *ca* 40 nm (TEM) *[2017; Mater. Sci. Eng.]* [170]	Octreotide/ covalent	Comparative cellular uptake/toxicity/apoptosis	TR+ cell line/ TR profiling n/r	n/s	No-TL counterpart	n/s	NO	Bioimaging &toxicity in healthy animals
PLGA[#5] NPs; *ca* 80 nm *[2017; Oncotarget]* [171]	Synthetic peptide derivative of Sst14/ covalent	Comparative cellular uptake/toxicity/apoptosis /migration/colony formation (agar)	TR+ cell lines (allogeneic)/ TR profiling n/r	n/s	No-TL counterpart	n/s	NO	Xenografting: [tumor uptake&proliferation/ PKA/BD]

Iron oxide nanoworms; *ca* 90 nm *[2017; Colloids Surfaces B Biointerfaces]* [172]	PTR86/ covalent	Comparative cellular uptake/toxicity	TR+ cell line/ TR profiling n/r	+/- [§§]	Cadaverine[+]-tagged counterpart	n/s	NO	Xenografting: [tumor uptake/BD]
Quantum dots; size n/r *[2018; Iran. J. Pharm. Res.]* [173]	Sst14/ covalent	Comparative cellular uptake (+competition with fTL)	TR+ cell line/ TR profiling n/r	n/s	No-TL counterpart	n/s	NO	n/s
Hybrid polymer NPs; *ca* 190 nm *[2018; Acta Biomater.]*[174]	Lanreotide/ covalent	Comparative cellular uptake (+competition with fTL)/toxicity/apoptosis	TR+ cell lines (allogeneic)/ TR profiling n/r	n/s	No-TL counterpart	n/s	NO	Xenografting: [tumor uptake & proliferation/ BD]
Ordered multidomain protein complexes; *ca* 20 nm (AFM) *[2018; Adv. Sci.]* [175]	Sst14/ Non-covalent	**SSTR2–calcium flux assay (TL-NP in TR-high *vs.* TR-low cells, syngeneic);** comparative cellular uptake/toxicity (TR-high *vs.* TR-low cells, allogeneic)	TR-high *vs.* TR-low cells/ TR profiling n/r	n/s	No-TL counterpart/ empty medium	n/s	**+/-** [◆] (non-corona)	CAM[‡3]: [tumor proliferation/ apoptosis/ angiogenesis]
Magnetic liposomes; *ca* 160 nm *[2018; Nanomedicine (Lond).]* [176]	Octreotide/ non-covalent (electrostatic adsorption)	Comparative cellular uptake/toxicity	TR-high *vs.* TR-low cells (allogeneic)/ TR profiling n/r	n/s	No-TL counterpart	n/s	NO	Xenografting: [tumor uptake & proliferation/ BD]
Hybrid protein nanoconstructs; *ca* 6 nm *[2018 Chem. - An Asian J.;]* [177]	Sst14/ covalent	**SSTR2–calcium flux assay (TR-high *vs.* TR-low cells, syngeneic);** comparative cellular uptake/toxicity (TR-high *vs.* TR-low cells, allogeneic)	TR-high *vs.* TR-low cells/ TR profiling n/r	**+/-**[§§§]	No-TL counterpart	n/s	**+/-** (non-corona)	n/s

Quantum dots; *ca* 600 nm *[2018; Saudi Pharm. J.]* [178]	Vapreotide/ covalent	Comparative cellular uptake (+competition with fTL)	TR+ cell line/ TR profiling n/r	n/s	No-TL counterpart	n/s	NO	BD in healthy animals
Chitosan-molecular beacon NPs; *ca* 80 nm (TEM) *[2018; Drug Deliv.]* [179]	Octreotide/ covalent	Comparative cellular uptake	TR+ cells (allogeneic)/ TR profiling+	n/s	No-TL counterpart	n/s	NO	Xenografting and a syngeneic orthotopic transgenic tumor model: [tumor uptake]
PVA/PLA[#6] NPs; *ca* 190 nm *[2019; Pharm. Res.]* [180]	Octreotide/ non-covalent	Toxicity	TR+ cell line/ TR profiling n/r	n/s	no-treatment control	n/s	NO	Xenografting: [*vs.* no-TL-NPs: tumor uptake/ BD]
Organic melatonin NPs; *ca* 10-15 nm *[2019; Nanoscale]* [181]	Octreotide/ covalent	Toxicity	TR+ *vs.* TR- cells (allogeneic)/ TR profiling+	n/s	no-treatment control	n/s	NO	Xenografting: [TR-high *vs.* TR-low lesions: tumor uptake/ BD]
Copper sulfide NPs; *ca* 180 nm *[2019; Nanomedicine Nanotechnology, Biol. Med.]* [182]	Lanreotide/ non-covalent	Comparative cellular uptake (+competition with fTL)/ toxicity/apoptosis/ migration	TR+ cells (allogeneic)/ TR profiling n/r	n/s	No-TL counterpart	n/s	NO	Xenografting: [tumor uptake & proliferation/ BD]
Trimethylchitosan emulsomes; *ca* 130 nm *[2019; J. Liposome Res.]* [183]	Octreotide/ covalent[¶1]	Comparative cellular uptake/ toxicity	TR+ cell line/ TR profiling n/r	n/s	No-TL counterpart	n/s	NO	n/s
Quantum dots; *ca* 280 nm *[2020; Pharm. Res.]* [184]	Octreotide/ covalent	Comparative cellular uptake (+competition with fTL)	TR-high *vs.* TR-low cells (allogeneic)/ TR profiling n/r	n/s	No-TL counterpart	n/s	NO	BD in healthy animals

Gold NPs; *ca* 20 nm (TEM) *[2020 Mater. Sci. Eng.;]* [185]	Lanreotide/ non-covalent (electrostatic adsorption)	Comparative cellular uptake (+competition with fTL)/toxicity	TR-high *vs.* TR-low cells (allogeneic)/ TR profiling n/r	n/s	No-TL counterpart	n/s	NO	n/s

#1 dimensions in solution for TL-decorated NPs (DLS-derived hydrodynamic d) are shown, if not stated otherwise.
#2 polyamidoamine.
#3 the same nanocarrier was also used in [186].
#4 poly(methacrylic acid).
#5 poly(lactic-co-glycolic acid).
#6 poly(vinyl alcohol)/polylactic acid.
¶1 (for liposomes, lipid micelles and some lipid-based formulations): TL is covalently bound to a linker, the latter is "inserted" into NPs by virtue of hydrophobic association.
¶2 (for polymeric micelles): TL is covalently linked to elementary "building blocks" of NPs, yet the resulting NPs are comprised of a multitude of "blocks" that are non-covalently bound.
&1 (*TR+ cell line)* – a single SSTR-positive cell line was used; (*TR-high vs. TR-low cells)* – at least two distinct cell lines of varying SSTR abundance were utilized for NP characterization.
&2 when two or more distinct cell lines are utilized for NP characterization: *syngeneic* – implies cell lines under comparison belong to the same strain and differ only in terms of TR expression (*e.g.,* CHO cells with endogenous SSTR2 expression *vs.* CHO with SSTR2 overexpression or knockout/down-regulation); *allogeneic* – implies cell lines originate from different tissues of the same species, or were established in different species (*e.g.,* human lung cancer and human liver hepatoma cells, or human breast cancer and mouse mammary/skin cancer cell lines).
&3 (*TR profiling+*) – authors characterized SSTR abundance (mRNA transcripts and/or protein levels) in the utilized cell lines (also includes cases when profiling was not comprehensive, *e.g.,* Sst14 that binds all SSTR subtypes was used for TL , but levels of just SSTR2 was measured); (*TR profiling n/r (not reported))* – SSTR abundance in the utilized cell lines was not evaluated or details of SSTR profiling/origins of the cell lines are not explicitly reported (also including cases when authors refer to earlier SSTR profiling of allegedly the same cell strains by other research teams).
§ did the authors take steps to ensure TL stays bound to NPs under the utilized conditions (an interference from fTL in the experimental readout)?
§§ measures taken lack sufficient sensitivity/resolution (conventional fluorescent microscopy).
§§§ possible false-positives from liberated TL (shedding) were not excluded reliably (the method used lacks sensitivity).
‡1 experiments performed in rodents (mice/rats) upon systemic i.v. injection of NPs, if not specified otherwise.
‡2 for xenografting experiments, the same cells as in *in vitro* studies were used, if not specified otherwise.
‡3 topical administration.
⊹ has dissimilar structure and size as compared to the active TL.
◆comparison with a non-targeted NP and TL shedding studies are lacking for a conclusive statement.

AFM – atomic force microscopy; BD – biodistribution; CAM – chick chorioallantoic membrane; d – diameter; n/s – not studied; NP – nanoparticle; PKA – pharmacokinetics;TEM – transmission electron microscopy; (f)TL – (free, not bound to NP) targeting ligand; TR – targeted receptor (*i.e.,* SSTR).

Admittedly, omittance or incomplete evaluation of any of the discussed aspects could suffice in raising concerns about the validity of experimental conclusions on *in vitro* targetability of a given nanocarrier. Several breaches in experimental design, strictly speaking, would preclude any targetability claims, calling for re-evaluation of a nanocarrier under the refined experimental setup. It emerges from Table 2 that issues with the experimental approach to *in vitro* targetability validation of nanoparticles tend to cluster. Even in the very few works, where the authors did resort to special *in vitro* methods for ligand-receptor studies, other issues, such as inadequate evaluation of nanocarrier stability (ligand shedding) and incomplete SSTR profiling, still crawl in, hindering conclusive statement on *in vitro* targetability of the studied nanoparticles even under simplistic conditions (a buffer or rectified media). What is more, sound evidence on targetability of the listed SSTR-targeted nanocarriers in the presence of biocorona, which is a proxy scenario for *in vivo* administration of nanoformulations, is simply non-existent (Table 2, column «Corona effects on targeting»).

Notwithstanding the above issues, all the reviewed papers report the nanocarriers in question as capable of efficient SSTR targeting *in vitro*. Characteristically, conclusions on targetability are almost exclusively drawn from *comparative cellular uptake and toxicity studies* (occasionally supplemented with evaluation of how nanoparticles affect cell death/apoptosis, capacity to grow in 3D and other *phenotypical* events), where a targeted nanocarrier is compared to a respective non-targeted counterpart, carrying no ligands on its surface (Table 2). Quite often, both types of nanoparticles are loaded with a toxic cargo (typically, a hydrophobic small-molecule drug, such as doxorubicin), and the observed difference in cargo-associated events (toxicity, apoptosis, cell cycle alterations) are further leveraged as a proof of selective receptor-mediated intracellular cargo delivery with targeted nanocarriers. In selected cases, the experiments also involve competition with free targeting ligands or SSTR antagonists, which is devised to further endorse the specificity of the observed response to targeted nanoparticles. The comparisons between targeted and non-targeted carriers tend to be performed in either a single SSTR-positive cell line or in a combination of distinct cell strains of varying SSTR abundance (typically, SSTR-high *vs.* SSTR-low cells).

Even if we put aside the nearly-ubiquitous issues with ligand shedding and SSTR profiling and focus only on the studies without biocorona formation on nanocarriers, such an approach to targetability validation still misses to address the point, for ligand-receptor interactions are not confirmed by evidence from appropriate techniques devised to measure ligand-receptor coupling, but are *indirectly deduced from late events well downstream of and not necessarily coupled to receptor-ligand binding*, such as cellular internalization, toxicity, apoptosis, etc. In fact, all the listed and similar outcomes of interaction of nanoparticles with cells might well happen

irrespectively of any specific engagement between targeting ligands and targeted receptors and could have other explanations besides the actual targeting. A few simulations would come handy to further elucidate this point.

Consider one typical scenario: a targeted nanocarrier is evaluated for uptake in two unrelated cellular strains, featuring different levels of SSTR expression. A higher uptake in SSTR-high cells *vs.* SSTR-low cells tends to be attributed to receptor targeting and this evidence is used to proclaim *in vitro* targetability. However, distinct cell lines (a.k.a *allogeneic*, refer to «Testing model/TR profiling» column and footnote[&2] of Table 2) are quite likely to feature distinct endocytosis machinery – in fact, this is something that should be expected[187–190] – and thus the observed discrepant internalization rates could be mainly explained by inherent biological differences between the cell types under comparison and have not much to do with varying SSTR abundance and/or SSTR targeting.

Now, let's consider the reverse scenario, which is also very frequently encountered: a targeted nanocarrier is compared to a non-targeted counterpart (almost exclusively bare nanoparticles lacking any targeting moieties; Table 2) for an uptake in a single cell line positive for SSTR. Uptake differences between the nanoparticles here are again used to confirm targeting. Yet, the compared nanocarriers have distinct functional surfaces, for one nanoparticle type carries ligands on its surface and the other does not. Even under the simplest conditions, such as aqueous buffer, this very difference almost inevitably translates into discrepant hydrodynamic size/surface charge/surface geometry/hydrophobicity of targeted and non-targeted carriers, which in turn could differentially affect colloidal stability of nanoformulations and their interactions with cells, impinging on the resulting uptake rates[23,191–193]. Similar surface effects tend to become much more pronounced in complex media, when targeting ligand's coating could alter corona composition, leading to profound effects on cellular interactions of nanocarriers[194,195] (refer also to section 5.4.2). Evidently, assuming these factors, the differential uptake of targeted and not-targeted nanoparticles could hardly serve by itself as a conclusive proof of receptor targeting.

Then, consider a more complex setup, which is a fusion of the former two: a targeted nanocarrier is evaluated for uptake against a non-targeted counterpart in two unrelated cell type (SSTR-high *vs.* SSTR-low). Here, the same confounders, *i.e.,* unbalanced surface effects as a consequence of ligand functionalization *vs.* absence of thereof and the likely discrepant internalization machinery of cell strains under comparison, are still in force, thus not allowing to unambiguously attribute any cellular uptake differences between nanocarriers to SSTR targeting. Even if we take a step further and perform uptake studies in closely-related cellular strains that only differ in terms of SSTR expression (a.k.a *syngeneic*, refer to footnote[&2] of Table 2), which is very seldomly done, the unbalanced surface effects still remain unattended.

Finally, if we increase the rigor of uptake studies further by introducing competition with SSTR agonists (or antagonists) in a free form in the comparison of targeted *vs.* non-targeted particles in syngeneic SSTR-high *vs.* SSTR-low cells, validation of targeting based solely on differential uptake rates is still problematic. For the discrepant functional surfaces of the compared nanocarriers are still there, and competition/blocking with a free ligand tends to bring more questions than answers (specifically, when free ligands evoke downstream receptor responses that might affect the ground cellular state – how such phenomena could possible impinge on the resulting uptake of nanoparticles by cells, especially featuring distinct levels of targeted receptors, is very difficult to evaluate; the same might also apply to receptor antagonists, when *silent* binding event might still affect basal receptor signaling and/or receptor's cooperation with other receptors/effectors).

All in all, *comparative studies of targetability-attributive events, such as cellular uptake of nanoparticles, are inherently problematic when are used to establish specific receptor targeting*, for such a *backwards* approach allows no certainty with evidence interpretation in terms of receptor targeting and its consequences. The problem gets even worse, once nanocarriers under comparison are loaded with non-neutral cargo (*e.g.,* cytotoxic drugs) – extra effects of the latter on the measured cellular outcomes introduce additional variables, and deconvolution of the of trigger-effect chains (*i.e., this* happens due to receptor targeting and *that* does not) becomes ever more challenging. Importantly, the above issues could hardly be fully circumvented even by introducing complex experimental designs (*i.e.,* syngeneic SSTR-high *vs.* SSTR-low cells, free ligand competition)[f], as explained earlier. Besides, the latter approaches to characterization of nanocarriers are quite seldomly encountered in real life and tend to be substituted with less rigorous experimental frameworks (Table 2). These in turn are frequently haunted by other issues, such as incomplete receptor profiling and failures to evaluate possible targeting ligand shedding and biocorona effects on targeting. Admittedly, such a conjuncture tends to preclude robust targetability evaluation, leaving many question marks behind.

[f] There is one exclusion though: comparative studies of cellular events (uptake, toxicity, etc.) could be used to infer targetability if undertaken under rigorously matched experimental conditions when all the variables but ligand-receptor coupling are fully balanced. Pertinent examples could include comparative evaluation of a targeted carrier *vs.* a sham (inactive) ligand-functionalized counterpart (to mitigate the surface differences between the nanoparticles in question) in a single SSTR-positive cell strain or, even better, in syngeneic SSTR-high vs. SSTR-low cells. Besides, such designs also ought to incorporate evaluation of targeting ligand shedding. Sadly, such prerequisites combined are exceedingly rarely met in practice (Table 2).

Yet, the solution to the described and nearly universal problem with *in vitro* targetability evaluation of nanocarriers appears to be rather straightforward. As said, ligand-receptor cooperation is in the very center of the targetability concept. Thus, in order to reliably evaluate attributive events of receptor targeting, *i.e.,* whether and how binding of targeting ligands to surface receptors affects uptake of nanoparticles by cells and their well-being (toxicity, apoptosis, etc.), including the effects ascribed to cargo delivered by targeted nanocarriers, *the actual targeting has to be confirmed and evaluated in the first place.* It was already pointed out that *in vitro* solutions for ligand-receptor studies are currently manifold and thus a tailored approach could be readily envisioned for the majority of the nanoformulations. With having *in vitro* targetability confirmed beyond doubt, evaluation and proper interpretation of targetability-attributive events become a rather straightforward task. Yet, just the reverse scenario appears to dominate the field (Table 2), which I believe is strongly contributing to the general confusion about the ART model, hampering translational efforts with targeted nanocarriers.

The very similar (and perhaps even more pronounced) problem with targetability evaluation also exists *in vivo*. As emerges from Table 2 («*In vivo* studies» column), none of the studies with SSTR-targeted nanocarriers involved appropriate methods to confirm that targeted particles could verily bind targeted receptors in tumor tissues *in situ*. Instead, conclusions on targeting (which were almost exclusively affirmative) were solely based on the attributive events, such as tissue accumulation and tumor-inhibiting activity of nanocarriers, with pharmacokinetics and biodistribution studies used as additional support in selected cases.

We already discussed some inherent problems with targetability evaluation *in vitro* based on events downstream of and not necessarily related to ligand-receptor binding – the very same issues not only stay valid for studies *in vivo*, but gain further weight by virtue of the increased environmental complexity for nanoparticles. The *in vivo* passage of nanocarriers is long and arduous (Table 1), conditions keep changing and barriers to traverse are many on the way to a targeted tissue. The bionanointerface (corona) evolves along the journey and processes of natural decay (for biodegradable carriers and targeting ligands prone to degradation *in vivo*) generally proceed at a higher pace as compared to *in vitro* conditions. Besides, a fraction of i.v. administered dose of nanoparticles tends to end up in tumors anyhow (in part, by virtue of mechanisms, explained in the previous section on the EPR)[23,97]. So, if a given targeted nanocarrier accumulates to a higher extent in tumor xenografts as compared to its non-targeted counterpart, does this evidence prove specific tumor receptor targeting and represent its very consequence? Admittedly, the answer is "NO", for in the absence of conclusive data on receptor-ligand binding *in situ*, such an outcome might be explained by a number of alternative mechanisms that might

or might not involve targeted receptor-targeting ligand interaction. Further examples would help to illustrate this point.

Consider the earlier discussed surface non-equality of ligand-decorated and bare non-targeted nanoparticles. Ligand functionalization is likely to affect adsorption of biomacromolecules onto nanoparticles *in vivo*, culminating in dissimilar (structurally and/or compositionally) biocoronas of targeted and non-targeted carriers (see also 5.4.2). Dissimilarities in coronas, in turn, might translate into different retention times of nanocarriers in circulation or unevenly affect their interactions with the RES. Similar effects might also concern endothelial uptake and transcytosis of nanoparticles, as well as their recognition and internalization by tumor cells[194,195]. Most importantly, even slight differences in any of these processes might suffice in leading to different tumor accumulation rates of targeted *vs.* non-targeted nanoparticles.

Then, let's take another aspect – targeting ligand shedding by nanoparticles *in vivo*. Admittedly, liberation of ligands by nanocarriers in systemic circulation might trigger profound responses in various *in vivo* compartments by virtue of stimulation of targeted receptors in off-target sites. In fact, targeted receptors are quite rarely expressed exclusively in tumor lesions – in the majority of cases, we rather should be talking about relative overexpression as compared to normal tissues[196]. Thus, in principle, off-target effects are to be expected upon ligand liberation. For instance, in case of SSTR targeting, ligand shedding might affect both the systemic and local tumor hemodynamics, for SSTR are known to be expressed and functional in the heart, as well as in endothelium of normal and tumor vessels[197–201]. Similar effects might also accompany ligand shedding in tumor parenchyma – here, free ligand-evoked receptor signaling might affect ground state and endocytosis in tumor cells, shaping the resulting cellular uptake of nanocarriers. In the absence of meticulous stability studies, confirming integrity of targeted nanocarriers both in blood and tissue compartments, differential uptake rates of targeted *vs.* non-targeted nanoparticles are hardly possible to explain in terms of the active receptor targeting.

In fact, in view of the enormous complexity of *in vivo* conditions and the reviewed shortcomings of the standard approaches to *in vivo* evaluation of nanocarriers (on top of things, most of *in vivo* evidence comes from tumor xenograft studies – the limitations of this methodology were highlighted in section 2.1.2), it would not be an exaggeration to state that SSTR targeting with nanoparticles *in vivo* remains poorly understood (Table 2). In other words, we still do know, what the actual attributive effects of SSTR targeting with nanocarriers *in vivo* are – most importantly, whether SSTR targeting translates into improved uptake of nanocarriers in tumor parenchyma or not.

What could be the ways to proceed further in this regard? It appears prudent to start experimental evaluation of targeted nanocarriers from comprehensive *in vitro* characterization. Only with having targetability and its attributive effects evaluated *in vitro* (preferentially, also in the presence of biocorona), could a targeted nanoformulation be further subjected to *in vivo* scrutiny. In terms of *in vivo* characterization, nanoparticle evaluation pipeline, among other things (stability, biodistribution, clearance, toxicity, etc.) has to include a pertinent technique to confirm receptor engagement with targeting ligands in a tumor tissue (*in situ*), in a similar manner to preceding *in vitro* studies. In many cases, this is likely to require a tailored approach with development and validation of a custom methodology[131–133]: possible examples could include *in vivo* imaging (*e.g.,* multiphoton) of labelled nanocarriers and surface receptors in tumor cells or characterization of tumor receptor signaling by means of appropriate reporters *in vivo* or in tissue samples *ex vivo* after prior treatment with nanocarriers (the latter approach is especially sensitive to ligand shedding, which has to be excluded). A failure to gauge ligand-receptor binding in tumors *in vivo* is very likely to perpetuate the principal problem with *in vitro* characterization of nanoparticles, *i.e.,* inability to confirm receptor targeting with nanoparticles and the ensuing inability to establish casual links between targeting and its attributive events.

To conclude, after reviewing the SSTR-targeted nanocarriers reported so far, the conflicting views on the utility of the ART model and the problems with clinical translations of targeted nanoformulations should become easier to comprehend. So, a seemingly simple and intuitively *catchy* concept of tumor receptor targeting proves to be a hard nut to crack once extrapolated to nanoparticles. As it stands out, functionalization of nanoparticles with targeting ligands brings over a host of technical challenges both on chemistry and biology sides, drastically increasing the complexity of evaluation (*in vitro* and especially *in vivo*) of targeted carriers as compared to their non-targeted counterparts. As it has been discussed herein, the details to address are many and lack of proper attention to seemingly "minor" aspects of targeting might lead to profound problems with experimental evidence and its interpretation. When such issues accumulate and persist with time, the general perspective inevitably gets blurred.

Besides, as already pointed out, the ART model inherits pre-existing limitations of the EPR model, *i.e., in vivo* journey of nanocarriers to targeted lesions is still primarily thought of in terms of hemodynamic forces and leaky tumor vasculature, while processes of active transport of nanocarriers through vascular wall, similarly to surface adsorption (biocorona) effects *in vivo* remain overlooked. Future advances with nanocarrier-mediated delivery appear unlikely without introduction of newer integrative models for tumor targeting, better acknowledging *in vivo* complexity

(specifically, tumor and vascular biology) and wittingly leveraging relevant processes at nanobiointerface.

2.1.3.3 Other issues of receptor targeting and the steps forward

In this section, I would briefly discuss a few other pertinent aspects of active receptor targeting. The first concerns selection of a negative control for targetability evaluation. The established practice in this regard is to resort to a non-targeted ligand–functionalized nanocarrier, which quite often is also the immediate synthetic predecessor of the ultimate targeted formulation («Comparator for targeting validation» column of Table 2). This practice is, however, suboptimal and in certain cases might hinder interpretation of evidence from comparative studies of targeted *vs.* non-targeted nanoparticles. The explanation resides in surface effects or, more precisely put, a non-equality of functional surfaces of nanoparticles under comparison. Indeed, a surface covered with ligands and the respective bare surface comprise two distinct entities, which are clearly different in terms of free energy, geometry and surface charge[23]. This by itself under certain conditions might be sufficient to invalidate direct comparisons between non-targeted and targeted nanoparticles. For instance, consider a frequent situation, when functionalization with targeting ligands alters the surface charge of a nanocarrier (Table 2, refs[156,176,185]): evidently, comparison of cellular uptakes of near-neutral control particles and targeting ligand-decorated particles that obtained a clearly positive (or negative) surface charge after functionalization is a futile task when the targetability-associated uptake is in focus, for charge effects and targetability effects could hardly be deconvoluted.

The problem of non-equality of functional surfaces becomes even more pronounced once nanocarriers enter complex media and biocorona build-up intervenes. As already pointed out, a pre-existing layer of ligands is likely to affect adsorption processes, thereby targeted and non-targeted carriers acquire significantly different biocoronas. In view of the importance of coronas for cellular interactions of nanoparticles (reviewed in section 2.1.4), the targeted and non-targeted particles might literally emerge as two absolutely different species after corona formation *in vivo*, which in effect would hinder (or preclude) meaningful comparisons between them.

One practically feasible solution to this problem is to abandon conventional bare negative controls for inactive (scrambled) ligand controls, *i.e.,* nanoparticles decorated with structurally close yet functionally-inactive ligands. In other words, a scrambled ligand is designed and validated in such a way that it retains strong structural resemblance to the active targeting moiety (in terms of structure, size, and charge), but loses the specific affinity to targeted receptors. In case of antibody-

functionalized nanocarriers, this approach could entail utilization of isotype controls (unspecific antibody of the same class)[202,203]. The resulting nanocarriers, functionalized with either an active ligand or a scrambled ligand via the same approach under identical conditions, are expected to end up with very close functional surfaces (naturally, provided conjugation efficacies and the resulting ligand loads are even). This, in turn, would allow to keep biocorona effects in check, revealing the actual input of receptor targeting in cellular uptake of nanocarriers and other phenotypic outcomes of interaction of nanoparticles with cells. Despite the fundamental nature of the described problem with negative controls, it stays poorly recognized – none of the studies with SSTR-targeted nanocarriers took deliberate steps to design and validate inactive ligand-functionalized counterparts for the targeted nanocarriers (Table 2). Significance of this for interpretation of the experimental evidence (specifically, *in vivo*) with the published nanocarriers is left to the reader to judge.

The second aspect I would like to highlight is how targeting ligands are presented from a nanosurface. Evidently, ligand orientation is of utmost importance: targeting moieties should be linked to nanocarriers in such a way that their receptor-binding domains (a.k.a pharmacophores) stay exposed and available for receptor binding, *i.e.,* facing outwards from the surface of a nanoparticle. Despite the seeming self-evidence of such a requirement and numerous means of chemical conjugation, it is not that seldom that directional anchoring of ligands is not properly ensured (for instance, refs[159,176,182,185] of Table 2). Possible detrimental consequences of the latter for efficiency of targeting are easy to comprehend.

Apart from ligand orientation, efficiency of ligand-receptor coupling might be also profoundly affected by density and/or distribution of ligands on a nanosurface (steric hindrance and ligand multivalence phenomena), so the latter aspects should be recognized and, preferably, also addressed experimentally[204–206]. "Cumulative" affinity of a nanocarrier to a targeted cell is intuitively proportional to the number of ligand-receptor pairs. However, in practice this does not always translate into enhanced cellular uptake of nanoparticles – there are reports of superior performance (tumor uptake-wise) of less densely decorated nanocarriers *vs.* ligand-heavy counterparts[202,207–209]. Very little is currently known about how specific types of surface receptors bind and respond (also, ligand-induced receptor clustering phenomenon) to multiple ligands, patterned on a surface[210–213]; in case of SSTR, the evidence in this regard is next to non-existent. Future studies are likely to shed more light on ligand multivalence and the related phenomena, which might emerge as important determinants of cellular responses to artificial nanomaterials. Instrumental role of sensitive techniques for probing of ligand-receptor binding is difficult to overestimate in this regard.

Finally, a few words on biology of targeted receptors. As mentioned earlier, the ART model takes a rather simplistic position here – the targeted receptors are considered as *hooks* or *sticky patches* that bind targeting ligands and either *pull* them inside the cells (via receptor-mediated endocytosis) or simply keep them bound (*anchorage*), with both outcomes believed to promote accumulation of nanocarriers in tumors. Yet, each receptor subtype is unique – not only in terms of ligand selectivity, but also in terms of the nature of ligand-evoked responses. The latter are very diverse and receptor type–specific, and might include downstream receptor signaling (numerous effectors could be involved, such as cAMP, calcium/IP_3, nitric oxide, kinase/phosphatase-mediated relay), receptor internalization and intracellular trafficking, receptor clustering (hetero/homo- or oligomerization) and cooperation with scaffold proteins, enzymatic receptor processing, etc.[214,215]. Most important though is that in most cases *receptor activation events are not neutral for a receptor-presenting cell* – in fact, the very opposite is true, for receptors and associated signaling relay mechanisms evolutionally emerged as specific sensors for external clues, designed to adjust signal-receiving cells to the ever-changing environment[215]. This notion also *apriori* applies to cases of targeting with neutral ligands, which are meant to bind cognate receptors without evoking their activation, such as antibodies to certain receptor epitopes or "silent" receptor antagonist. Indeed, a seemingly "silent" binding might impinge on basal receptor signaling or cooperative events the receptor in question partakes in[216–219], or simply interfere with binding of incoming active ligands, thereby "prospectively" modifying cellular state. In fact, actual neutrality of binding in terms of cellular responses could be only established in dedicated studies; before that, candidate "silent" ligands should not be considered for neutral moieties.

However, the ART model tends to overlook the above aspects and possible effects of targeting ligand-evoked signaling in receptor-presenting cells frequently stay unrecognized (with a possible exclusion of ligands, know to induce toxicity/apoptosis – the later outcomes are typically measured; this is also pertinent for SSTR targeting (Table 2)). As said, ligand binding almost always induces some changes in signal-receiving cells – thereby, a sound evaluation of targeting-attributive events (*e.g.,* cellular uptake of nanocarriers) is only possible once ligand-receptor engagement-specific effects on cellular physiology are recognized and measured. Clearly, this calls for a receptor-specific approach. For instance, consider cases where ligand-evoked receptor signaling might lead to down-regulation of cellular endocytosis machinery[220–223] – conceivably, the latter effect might override a positive input of receptor targeting (*i.e.,* increased affinity of particles to cells), culminating in a net decrease of cellular uptake of targeted nanocarriers. A similar scenario might also apply to SSTR2/5 targeting (discussed in sections 5.4.3 – 5.4.4).

To sum up, the very receptor biology and diversity indicate that the *one-size-fits-all* approach to receptor targeting, currently endorsed by the ART model, is overly-simplified, which is likely to contribute to the confusion about practical usefulness of tumor receptor targeting with nanocarriers. I believe that years to come would witness the advance of more-tailored conceptual perspectives on receptor targeting with nanocarriers, better recognizing biology of particular receptor types and operating in terms of specific receptor-ligand pairs featuring distinct response patterns in targeted cells. Once carefully evaluated against an array of nanocarriers of varying size and functional surface, this refined paradigm is likely to untangle the targeting problem, eventually exposing particular targeting pairs (ligands *vs.* receptors) that would enable enhanced tumor delivery when knowingly integrated with defined types of nanoparticles.

2.1.4 Adsorption of biomolecules on nanoparticles: the concepts of biocorona and bionanointerface

The importance of biocorona for the ultimate *in vivo* performance of nanocarriers has been already stressed a number of times in the preceding chapters. Now, we would consider the phenomenon of surface adsorption of biomacromolecules and the related aspects in more detail.

To start with, nanoparticles in solution share an inherent propensity to adsorb solutes – from simple molecules, such as water, to low and high-molecular weight compounds – on their surface[224,225]. As it is typically the case with *basic* phenomena, the underlying physics of this seemingly simple process is intricately complex and could only be properly understood in the context of thermodynamics, surface free energy, weak interaction forces, adsorption theories and adsorption isotherm models. These concepts and related aspects are not covered herein – the interested reader is referred to surface chemistry textbooks and selected works on the topic instead (for instance, refs[226–228]). However, in very simple terms, adsorption of solutes on nanoparticles could be thought of in terms of excess of free energy on their surface, "urging" nanomaterials to adsorb solutes, which steers the nanoparticle/solutes/solvent system towards thermodynamic equilibrium. Based on the above, surface adsorption of biomolecules can be considered as an indispensable component of the system under real life conditions and thus virtually all nanoformulations in complex solutions will be acquiring coronas.

Adsorption of biomoieties on surface of materials grafted into living systems (*e.g.,* artificial heart valves, joints, vascular prostheses, bone mimetics, etc.) has been recognized and intensively studied for more than half a century. Most importantly, it has been firmly established that adsorbates (especially, proteins) serve as *master regulators* of how exogenous materials are recognized by acceptor organisms. In

other words, surface-adsorbed molecules globally shape the nature of biological responses to grafted materials in host cells and tissues[227,229]. Somewhat surprisingly, significance of bioadsorbates for nanoparticles in the same regard was widely acknowledged only recently, in 2007[230]. Subsequent years witnessed mounting research in the field, which is currently drawing more and more attention[14,15]. As of now, the main standpoints on the biocorona of nanocarriers appear as follows.

Firstly, biomacromolecules inevitably adhere to nanoparticles once these enter complex environment of living organisms. In case of humans and standard *in vivo* models (rodents), distinct bodily compartments feature quite distinct liquid phases, be it blood, lymph, gastric juice, cerebrospinal fluid or extracellular fluid of parenchymal organs. However, despite pronounced quantitative and qualitative differences, all the bodily fluids contain the same general classes of biological macromolecules – proteins, sugars, lipids, nucleic acids and derivatives of thereof[231,232]. Thus, whichever biocompartment a nanocarrier enters, it ends up decorated with quite a complex sheath of adsorbates that might include a host of biomolecules of the listed classes in varying combinations (up to *ca* three hundred distinct proteins were reported to adsorb on selected nanocarrier types[233]). The process is quite rapid – happens on a second's scale in case of proteins[233], and predominantly mediated by weak interactions (*i.e.,* van-der-Waals, Coulomb and hydrophobic forces, as well as hydrogen bonding)[224,234]. Adsorption pattern and kinetics are heavily dependent on features of a nanocarrier – material, size, shape, surface curvature, roughness and charge, presence of surface moieties (*e.g.,* PEG, linkers, targeting ligands) and the way these are arranged on a surface – all these factors have been reported to affect adsorption and resulting biocorona structure (Fig. 3)[194,235–243]. On the other side, adsorption is also a complex function of temperature, time, and a number of parameters of the liquid phase (*e.g.,* concentrations of solutes, structure and charge of solutes under particular conditions, nature of solvent, ionic strength, viscosity, flow *vs.* absence of flow, shear forces)[225,244–249]. Taken together, assuming the enormous number of variables on both ends (a nanocarrier *vs.* a biologic compartment it is administered into) and the complexity of their interplay *in vivo*, functional relations between the physico-chemical features of a given nanocarrier and the resulting adsorption pattern in a given compartment *in vivo* remain poorly understood. In other words, currently it is quite difficult to reliably predict what kind of corona (quality- and quantity-wise) would arise on a given nanocarrier under particular conditions *in vivo*.

Instability of biocorona under changing microenvironment makes the things even more complex. Passage of a nanocarrier from one medium to another, *e.g.,* from blood to tissue upon extravasation or from extracellular matrix to endocytic compartment upon cellular uptake, is likely to bring along significant rearrangements of corona structure – for instance, a fraction of adsorbed moieties from the earlier

compartment being displaced by another solute/s of the present one[250–253]. In essence, such processes of corona evolution accompany all the major steps of the *in vivo* passage of nanoparticles (Table 1), underlying highly dynamic nature of *in vivo* bio-nanointerfaces.

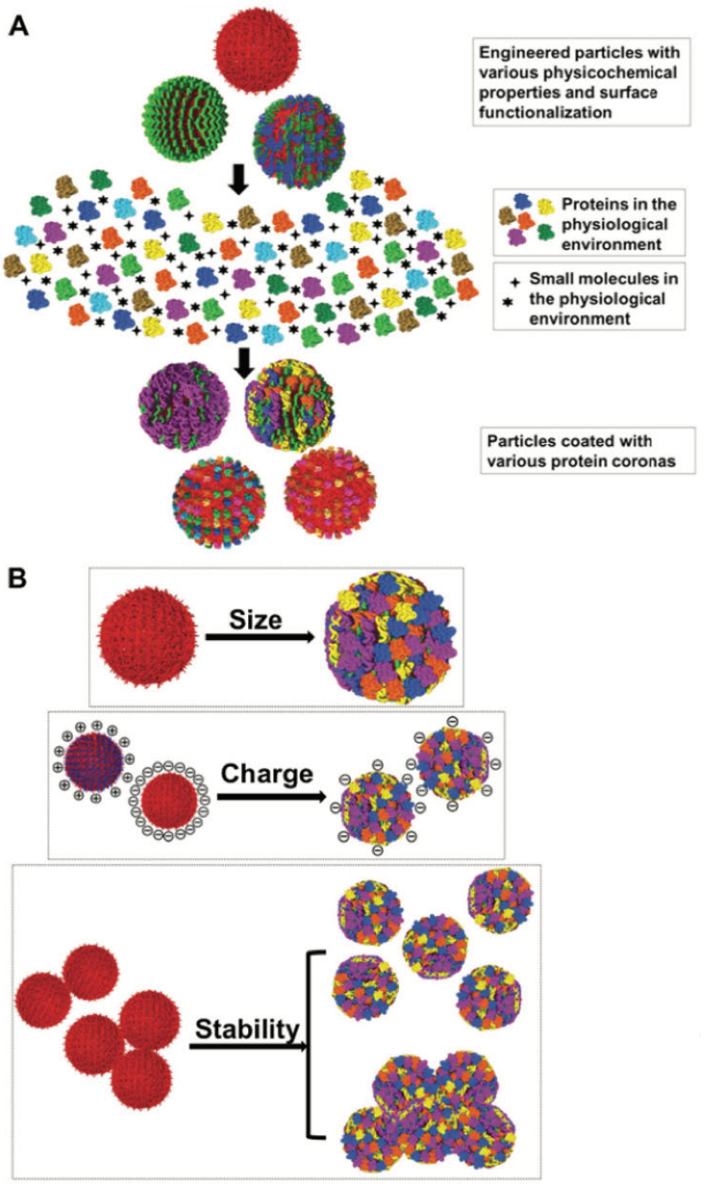

Figure 3. (A) Biocorona composition to a high degree is determined by features of nanoparticles. (B) In turn, biocoronas affect physicochemical properties of nanoparticles such as size, surface charge and colloidal stability. Further details are in the main text (Reprinted from ref[14], page 8; © 2017, with permission from John Wiley and Sons).

Secondly, corona build-up significantly affects the basic properties of nanocarriers (Fig. 3). Evidently, adsorbates increase physical dimensions of nanoformulations (typically, manifested by an increment in hydrodynamic diameter) and tend to alter their net surface charge[224,225]. These alterations are not only likely to impinge on solubility and colloidal stability of nanocarriers[225,254,255], but also to affect *in vivo* processes know to be sensitive to size and charge of nanoparticles (such as retention in blood, interaction with RES and endocytosis[16,192]). Further, biocorona might affect biotransformation and degradation of nanocarriers *in vivo* (*e.g.,* by modifying enzymatic reactions)[256,257], as well as have significant implications for kinetics of cargo release[258]. As pertains receptor-targeted delivery (the ART model, 2.1.3), biocorona could interfere with efficient targeting, *e.g.,* by virtue of "burying" targeting ligands and preventing coupling with targeted receptors (shielding phenomenon)[203,259–261] or by promoting targeting ligand displacement from nanocarrier surface (ligand shedding phenomenon, sections 5.3.4 – 5.3.6).

Thirdly, and perhaps the most important of all, biomacromolecules that adsorb on the surface of nanocarriers, *are not inert moieties* when considered from the standpoint of cellular interactions. Nanoparticles enshrouded with proteins, sugars, lipids and other solutes of *in vivo* liquids could evoke adsorbate-specific responses in cells bearing receptors to adsorbed moieties. And though we still do not have a good grasp of such corona-mediated interactions, the relevant evidence continues to mount: complex and specific effects of corona components on pharmacokinetics, biodistribution and toxicity of nanoparticles, as well as immunity, have been reported[262–266]. Thereby, biocoronas could as well be broadly considered as heterogeneous ensembles of endogenous ligands with complex *targeting potential*, autonomously arising on surface of nanocarriers *in vivo*. However, in contrast to a purposeful ligand functionalization by chemical means in the lab, the former process is governed by yet poorly understood laws, is problematic to predict and control, and tends to yield combinatorial *decors* of dozens of possible targeting moieties. Evidently, an impact of such a "natural functionalization" on possible cellular interactions of nanoparticles is likely to be highly intricate and case-specific (a given type of nanocarrier *vs.* particular conditions). Besides, adsorption on a nanosurface could also affect the structure of biomolecules, *e.g.,* by triggering protein unfolding. Possible consequences of the latter could be manifold, including alterations in colloidal stability of nanoformulations and unpredicted immune responses[267,268]. This adds yet another dimension to the complexity of the biocorona phenomenon.

What do we have in the end? As chemical solutions to entirely prevent surface adsorption of biomolecules are currently unavailable[14], nanomaterials would inevitably acquire coronas in complex solutions, be it bodily fluids *in vivo* or cell culture media in *in vitro* works. Adsorption processes are fast, enshrouding nanomaterials with complex biocoronas in a matter of seconds. With this, pristine

surface features of a nanocarrier, *i.e.,* the way it emerged after synthesis (a.k.a *synthetic identity*), are very short-lived in biotic environments – for corona almost instantaneously endows a nanocarrier with a novel *biologic identity*[269]. Biocorona profoundly alters ground features of a nanoformulation (size, surface charge, decay pattern and kinetics of drug release). What is more, the novel bioidentity also shapes the resulting cellular interaction of nanocarriers, impinging on the major phases of their *in vivo* life cycle, including extravasation, cellular uptake, RES surveillance and clearance. Collectively, the impact of the biocorona on *in vivo* performance of nanoparticles is so profound, that it would not be an exaggeration to state that the same nanocarrier *before* and *after* administration into a living organism represents two distinct entities that could be hardly compared.

Adsorption of biomacromolecules on a nanosurface is a very complex function of multitude of variables, both on the side of a nanocarrier and a microenvironment it enters. We are just beginning to understand the "rules" governing corona formation and robust *in silico* means to predict corona structure for a given carrier under particular condition are currently unavailable. Thus, biocorona structure and its contribution to *in vivo* interactions of a given nanoformulation could only be evaluated in dedicated studies. The same also fully applies to *in vitro* works with living cells, where nanocarriers rapidly adsorb biomolecules after spiking in culture media (especially, when the latter contain serum). Noteworthy, in view of profound differences between *in vitro* and *in vivo* conditions, the respective coronas of a given nanocarrier also tend to bear significant dissimilarities[270,271]. This fact should not however discourage from comprehensive *in vitro* characterization of nanoparticles – *in vitro* evidence should rather guide and instruct subsequent progression to *in vivo* evaluation phase. As discussed earlier (section 2.1.3), the biocorona aspect is absolutely critical and calls for experimental rigor when it comes to characterization of receptor-targeted nanocarriers.

To conclude, at the present technological state, biocorona is an inevitable and ubiquitous component of interaction of nanocarriers with living matter. The functional significance of biocoronas is hardly possible to overestimate. Mindfulness of this phenomenon is a must; disregard, oversimplification or inadequate experimental evaluation are all very likely to lead astray, undermining developmental efforts with nanocarrier-aided delivery.

2.1.5 Endocytosis of nanomedicines: a brief overview

The endocytosis concept encompasses a wide array of heterogeneous mechanisms utilized by living cells to internalize diverse entities, from liquids, ions, metabolic precursors and proteins to complex microorganisms, such as bacteria and viruses. A cell is very selective to what to let inside and what not – and endocytosis machinery

evolved respectively to allow for cargo-specific, tightly-controlled cellular entry and addressed delivery (intracellular and/or transcellular)[215,272–274]. Evidently, the processes in question are extremely complex, dynamic and intertwined – and despite years of focused research, we still do not have a holistic in-depth understanding of the molecular machinery in operation at uptake of particular types of internalized cargo. Thus, in this short section, I would not be reviewing particular endocytosis pathways in detail – rather, I would try to succinctly summarize the selected general aspects, which are important to keep in mind when considering cellular uptake of nanomedicines.

Evolution equipped cells with specialized molecular mechanisms to engulf and process numerous types of cargo – and there is a number of distinct entry routes for smaller entities, such as ions, carbohydrates, vitamins, fatty and amino acids, and entities of bigger size, such as proteins, protein complexes, exosomes and viruses. The first group entails a host of highly-specialized transporters (typically, composed of plasma membrane-spanning protein complexes), specifically suited for recognition and uptake of respective moieties. Pertinent examples are ion[275], glucose[276] and amino acid transporters[277]. Nanocarriers, however, do not have much to do with this group of entry mechanisms, mainly on the ground of their size. Their dimensions rather make nanocarriers a subject of the second group of internalization mechanisms, tailored for processing of bulkier cargo[57,278,279]. The apparatus in question here could be broadly categorized into five categories: 1) clathrin-dependent endocytosis (ClaDE), 2) caveolin-dependent endocytosis (CavDE), 3) clathrin/caveolin-independent endocytosis (non-CCE); 4) macropinocytosis and 5) phagocytosis (Fig. 4)[g]. Hereafter, I would very briefly introduce the reader to the listed internalization machineries, while leaving the fine details to textbooks and selected review articles (*e.g.,* endocytosis in general[215,272,280], ClaDE[281], CavDE[282], non-CCE[283,284], macropinocytosis[285], and phagocytosis[286]).

[g] Apart from the listed *conventional* endocytosis pathways, nanoparticles have also been reported to enter cells via alternative mechanisms, *e.g.,* by membrane fusion when nanocarriers (typically, liposomes) of certain surface functionalization could be integrated by cellular plasma membranes, whilst a payload is released into cytoplasm[372–375]. Such mechanisms are not discussed in the thesis.

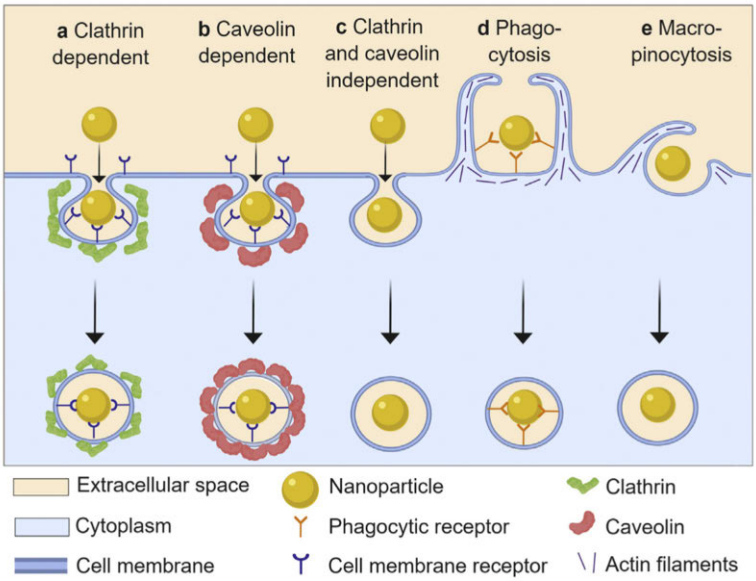

Figure 4. Major endocytosis pathways of nanocarriers. (Reprinted from ref[279], page 70; © 2019, with permission from Elsevier).

ClaDE is typically thought to encompass processes of receptor-mediated uptake of proteins and protein complexes and thus this very pathway is most frequently implied when the term *receptor-mediated endocytosis* is used. At a glance, ClaDE starts from a cargo recognition by respective surface receptors, which triggers cooperative events of receptor clustering and plasma membrane invagination in the vicinity of the cargo being prepared for internalization. Aided by intracellular clathrin and adaptor proteins, stabilizing the in-growing membranous invagination (thus the name of ClaDE), the cargo-engulfing pit (an endosome-to-be) is eventually closed and severed from the plasma membrane (aided by another protein, dynamin), setting off for intracellular trafficking and sorting.

CavDE represents another type of receptor-dependent endocytosis, employing distinct molecular machinery. However, its operational principle is broadly similar to the one of ClaDE: a cargo prompts specific membranous receptors on acceptor cells, which initiates internalization cascade, culminating in cargo wrapping in plasma membrane (flask-shaped vesicles, stabilized with caveolin proteins – hence the term), vesicle scission and shuttling into cytoplasm. As opposed to ClaDE, which frequently delivers cargo to late endosomal/lysosomal compartment, CavDE is known to favour endoplasmic reticulum and Golgi apparatus for final destinations of internalized moieties. CavDE is also implicated in transcytosis (*i.e.,* active shuttling of cargo through specialized polar cells, such as endothelial cells, enterocytes, and kidney tubular cells), specifically in the vasculature.

Macropinocytosis is generally considered for a cargo-nonspecific internalization mechanism that mediates uptake of liquids and solutes. Here, cytoskeleton actively partakes in forming plasma membrane protrusions (a.k.a membrane ruffles), with the latter engulfing *drops* of surrounding liquid together with solutes, bringing *the catch* to intracellular compartment.

Phagocytosis is a particular type of endocytosis, which is in operation in highly specialized cells (a.k.a professional phagocytes), comprising the vital part of RES (*e.g.,* certain types of lymphocytes, dendritic cells and tissue macrophages). Phagocytosis normally requires recognition of a cargo by specialized surface receptors of phagocytes, such as scavenger receptors, complement receptors and receptors of Fc fragment of antibodies – and if a cargo bears respective ligands (collectively called *opsonins*) on its surface, it is likely to be engulfed by a phagocytic cell. The ultimate cargo destiny in this case is typically an enzymatic digestion in phagolysosomes.

Non-CCE is a collective term, describing a group of internalization mechanisms employing neither clathrin nor caveolin for cargo processing. The molecular mechanism of non-CCE are not that well-understood as compared to ClaDE and CavDE and thus remain an area of active research – yet, non-CCE is thought to initiate upon cargo contact with particular regions of plasma membranes enriched in cholesterol and sphingolipids (a.k.a lipid rafts), which mediates recognition and sparks up downstream internalization machinery (a number of possible mediators have been implied in this regards, including flotillins and small GTPases RhoA, CDC42 and ARF6), actively shuttling the cargo across the plasma membrane[278,284].

Nanocarriers have been reported to utilize all the listed types of endocytosis pathways[278,279,287,288]. Yet, despite evident dissimilarities, these pathways also share a number of cardinal features, which are important to bear in mind. In particular, all of them are *active* (*i.e.,* energy-dependent) and are tightly regulated on multiple levels. Endocytosis is also highly sensitive to the nature and characteristics of the engulfed cargo – ClaDE, CavDE, and phagocytosis are all initiated by cargo recognition by specific surface receptors, non-CCE is leveraging particular cargo-plasma membrane interactions in the region of lipid rafts, and macropinocytosis, thought seemingly non-cargo-specific, is steered by dedicated signaling machinery of upstream receptors, sensing metabolic requirements of a cell and thus switching on macropinocytosis via cytoskeleton to meet specific cellular demands. Another thing to keep in mind is that distinct endocytosis pathways might as well utilize common effectors and converge at various points. Also, several endocytosis pathways might co-exist and be active in a given cell[278,279,289]. Besides, the nature of available/active internalization machinery is highly dependent on cellular commitment and specialization. As already mentioned, phagocytosis is a prominent capacity of professional phagocytes. Macropinocytosis is important for antigen

processing in selected types of immune cells[285]. Likewise, CavDE is known to be active in endothelial cells, enabling transendothelial passage (transcytosis) of bulky solutes such as albumin and lipoproteins[274,290]. The described dependence of internalization machinery on cellular specialization is important to account for when considering targeting particular cellular populations or examining possible interactions of nanoparticles in complex cellular environments (such as solid tumors, comprised, apart from tumor cells, of a number of other cell types, such as fibroblasts, tissue macrophages, lymphocytes, vascular cells, etc.).

Then, a relation between structural and surface parameters of a nanocarrier and resulting internalization pathway(s) in cells. Enormous amount of studies has been undertaken in this regard[191,192,297,298,193,194,291–296] – however, our understanding of how particular features of a nanoparticle could affect the way it would be internalized by a given cell type is quite far from complete and robust *in silico* tools to predict endocytosis patterns of nanocarriers are still elusive. In fact, the global conclusion from endocytosis studies with nanoparticles thus far could be summarized as follows: nearly every parameter of a nanocarrier – including material it's made of and its elasticity, physical dimensions, shape, surface curvature, surface charge and functionalization – could affect endocytosis of a nanocarrier in a given cell type, yet the ultimate effect is very difficult to predict reliably. Indeed, all of the listed variables on a nanocarrier's side have been reported to affect endocytosis, however the directionality of effects stays ill-defined, since the experimental evidence is highly conflicting (as nicely reviewed in ref[289], listing a number of examples when a defined modification of single parameter of a nanocarrier translated into opposite effects on endocytosis in similar or related models).

The case is further complicated by the fact that many studies did not properly account for or overlooked biocorona effects on endocytosis (specifically, in the "early days", *i.e.,* before mid-2010s, when biocoronas got wide recognition in the field)[279,289]. As discussed in the preceding section (2.1.4), biocoronas provide the final biological identity for nanocarriers both *in vivo* and under complex conditions *in vitro* (assays with living cells in culture media), instructing the cells how to recognize and engulf nanoparticles. With this, much of evidence from endocytosis studies of nanoparticles has to be approached and interpreted with certain care.

Objective difficulties with experimental evaluation of endocytosis, such as inherent problems with specificity and toxicity of inhibitors, frequently used for dissection of internalization routes, as well as paucity of highly pathway-specific tracers[56,188,299], add up to the above. Endocytosis modulation by virtue of silencing/KO or overexpression of involved effectors could provide viable solutions, but is neither entirely problem-free – specifically assuming some degree of redundancy in endocytosis pathways and not infrequent involvement of particular effectors in several pathways (such as dynamin in case of ClaDE and CavDE).

All in all, the complexity and frequent co-existence of internalization pathways, vicissitudes of endocytosis studies and a host of variables (physicochemical features, *multiplied* by effects of biocorona) on the side of nanoparticles together boldly underline the magnitude of a challenge *to make nanocarriers work as desired* in living systems. Deep understanding of endocytosis, enabling ability to predict how a particularly-designed nanocarrier would be engulfed, sorted and processed in a given cell *in vivo* in the presence of biocorona, would be empowering, bridging rational design of nanoparticles with their ultimate *in vivo* performance, which is the utmost goal of smart nanomedicine. Undoubtedly, we are not there yet. The importance of future research in this direction (specifically, of carefully controlled studies of nanocarriers bearing biocoronas) is hardly possible to overestimate.

Finally, particular endocytosis pathways appear to dictate the ultimate intracellular destination for the engulfed cargo[278,279,287]. As said, ClaDE most often leads to entrapment of the cargo in acidic endosomes, whilst CavDE is more likely to route internalized moieties to Golgi apparatus and endoplasmic reticulum. However, here we also miss detailed understanding of the relevant processes and cannot reliably predict in which intracellular compartment/s of a given cell would a particular nanocarrier end up in after internalization. Neither can we reliable predict whether (and in what manner) a particular nanocarrier would be subjected to intracellular sorting or exocytosis. Admittedly, the question of *the final destination* of nanomedicines is also of tremendous practical importance. Not much could be expected from a nanoformulation in terms of cargo delivery and treatment efficacy, if it is predominantly cleared by RES phagocytes or ends up in lysosomes of tumor cells (where, similarly to phagolysosomes of RES cells, the payload is digested and expunged). Characteristically, both these scenarios are rather typical for nanocarriers *in vivo*[62,278,288], which evidently poses yet another barrier for nanomedicine in oncology. In an attempt to bypass the all-to-frequent entrapment of nanocarriers in lysosomes, a number of *escape* solutions have been devised, including fusogenic carriers and nanoparticles employing *proton sponge effect* (the latter is believed to lead to endosomal rupture and release of nanoparticles into cytoplasm). Further information on these approaches is available for the interested reader elsewhere (for instance, ref[300]). Future structure-function studies would hopefully provide alternative and more efficient solutions to this long-standing issue, enabling precise intracellular routing (including efficient targeting of nucleus or intracellular organelles, such as mitochondria) of nanocarriers by virtue of rational design, based on holistic understanding of endocytosis and relevant nanobiointeractions.

2.1.6 MSN as nanocarriers and SSTR as targets: a synopsis and selected targeting-relevant aspects

In this last section of the Introduction, I provide a brief overview of the targeting pair (MSN as carriers and SSTR as targeted receptors), highlighting selected targeting-relevant aspects, which are important to keep in mind when interpreting the experimental approach and the data presented in the following chapters. In-depth surveys of MSN, covering chemical synthesis and functionalization, as well as comprehensive perspectives on SSTR biology in health and disease, are available for the reader in selected works on the topic (refs provided below).

Firstly, mesoporous silica nanoparticles (MSN) as targeted nanocarriers. MSN comprise a well-established class of nanoformulations with an impressive track in biomedical applications. Built of amorphous silicon oxide (SiO_2, a.k.a silica), MSN are naturally degradable in aqueous solutions, biocompatible and feature generally favourable toxicity profile, which is instrumental for utilization in living systems. Chemical solutions for MSN synthesis and functionalization are currently manifold, which makes MSN a rather flexible nanoplatform, allowing for preparation of a multitude of derivates, featuring distinct size, shape and surface features. The latter aspect is specifically important – MSN could be functionalized with diverse tags of biomedical utility – from affinity moieties, such as antibodies and peptides, serving in capacity of targeting ligands, to molecules enabling varying modes of visualization and tracking, such as fluorophores, metals and PET/MRI tracers. Furthermore, complex combinatorial decors of several distinct tags are also possible to achieve with the current chemical means. Likewise, a number of advanced hybrid designs (*e.g.,* MSN in lipid shells) and solutions for "active" interactions of MSN with environment (*e.g.,* enzyme-responsive or magnetic MSN) have been reported. Most importantly though, MSN have an excellent cargo-loading capacity, enabled by mesopores (*i.e.,* a structured meshwork of "pits" on MSN surface with a typical diameter of 2–4 nm; mesopores could be also enlarged up to 30–50 nm to allow for stacking of bulkier cargo) – the latter endow MSN with a grand surface-to-volume ratio (600–1000 m^2/g) and could accommodate high loads (up to *ca* 35 % of MSN weight) of varying cargo types, such as cytotoxic drugs or small interfering RNAs for oncology applications.

However, most of the listed MSN advantages were not of particular relevance in the context of the present study – for its major aim was to expose how SSTR targeting affects cellular uptake of nanocarriers *in vitro*. With this, we primarily focused on *in vitro* ligand-receptor interactions and endocytosis of nanocarriers, while other aspects, such as cargo loading & release, intracellular trafficking and degradation of nanocarriers, were not addressed in the thesis. In principle, other nanocarrier types (*e.g.,* liposomes, metal or polymeric nanoparticles) featuring close dimensional and surface features to the MSN evaluated herein, could have been also utilized for the

purpose (though interpolation of the evidence from one carrier type to another still ought to be done with reasonable caution, despite their close similarities). Thus, the selection of a nanocarrier in our case was primarily instructed by the availability of the technological platform and the solutions for targeting ligand functionalization, as well as the prior *in vitro* and *in vivo* expertise with MSN (within longstanding collaborations between the author's host lab, specialized in molecular biology and headed by Prof. Sahlgren, and chemistry-focused labs of Prof. Rosenholm and Prof. Lindén, developing MSN)[301–304].

Broad overview of MSN in biomedical applications[305–308], including pharmacokinetics, clearance and toxicity[309–316], as well as further details on MSN synthesis and functionalization[317–321], could be obtained from the selected references.

Then, SSTR as targets for nanoparticles. SSTR belong to the GPCR superfamily and have a typical structure of 7 transmembrane domain-spanning proteins. Five distinct SSTR subtypes (namely, SSTR1, 2, 3, 4 and 5) have been described in humans – the receptors are rather close in size (the shortest and the longest subtypes, SSTR5 and 3, are comprised of 364 and 418 amino acids, respectively), share high sequence homology of core regions (50–70 %) and are encoded by intronless genes. Besides, several truncated variants of SSTR5 have been reported, yet these appear to arise mostly in malignancies and their functional relevance remains poorly understood. The general mode of SSTR operation is also typical of GPCR, *i.e.,* ligand recognition and binding by the extracellular regions of SSTR evoke conformational changes in receptor structure, which leads to recruitment of effector proteins and allosteric regulators, such as G proteins, G protein-coupled receptor kinases (GRK) and arrestins to the intracellular regions (intracellular loops and C-tail) of the receptor. Downstream SSTR signaling is mainly mediated by G proteins, while GRKs and arrestins promote SSTR endocytosis (ClaDE; section 2.1.5) and terminate signal transduction[h]. Depending on SSTR subtype and nature of agonist, the internalized ligand-receptor complex is either subjected to lysosomal degradation or dissociates in endosomes, with SSTR being re-shuttled back to the plasma membrane.

SSTR are expressed in different cell types and tissues in human body, including central neural system (CNS), endocrine glands, gonads, pancreas, gastrointestinal tract, kidney, immune cells, and vasculature. Receptor profile (*i.e.,* abundance of particular SSTR subtypes) tends to significantly vary from tissue to tissue; multiple SSTR subtypes are not infrequently co-expressed in different levels and combinations in a single cell. Endogenous SSTR ligands, somatostatin-14 and

[h] Some GPCR have been reported to continue signaling even when in endosomes[376,377]. However, whether this also applies to SSTR, is presently unknown.

somatostatin-28 (Sst14 and Sst28; named after the respective number of structural amino acids), as well as closely homologous cortistatins, are short cyclic peptides that share high affinity (low-nanomolar range) to all SSTR subtypes. Characteristically, the endogenous SSTR ligands are rather short-lived (rapidly degraded in blood, with a half-life not exceeding several minutes), which might explain their local production in varying tissues, enabling paracrine signaling (*i.e.,* ligand-secreting and SSTR-bearing cells are in the vicinity of each other in the same tissue compartment).

Physiological effects attributed to SSTR are quite diverse and appear to be receptor type- and tissue-specific. However, apart from the CNS, where the SSTR axis serves as a complex modulator of neuronal signaling, consequences of SSTR activation in other cells and tissues could be generally characterized as inhibitory. The prototypic effect is the inhibition of hormonal release from the anterior pituitary – the negative effect of SSTR on blood growth hormone levels gave rise the nomenclature of the receptor/ligand class. Besides the pituitary, SSTR inhibit synthesis and secretion of a number of hormones and bioamines (such as serotonin) by other endocrine glands and cells of diffuse endocrine system. The inhibitory effects are not confined to the hormonal release though – SSTR also down-regulate excretory activity of exocrine pancreas and intestinal tract, inhibit intestinal motility and contractility of the gallbladder. SSTR activation could also trigger specific responses in certain subpopulations of immune cells, as well as affect vascular tone. The inhibitory activity of SSTR tends to be retained in certain types of cancer with SSTR expression – specifically, SSTR activation in tumors has been associated with inhibition of proliferation, induction of apoptosis and downregulation of angiogenesis.

To a significant extent, the described inhibitory SSTR effects in normal and malignant cells appear to be mediated by common signaling mechanisms shared by all the subtypes of SSTR (Fig. 5). More specifically, all SSTR subtypes inhibit adenylyl cyclases via Gαi subunits of G proteins, which leads to depletion of intracellular 3′-5′-cyclic adenosine monophosphate (cAMP). The drop in cAMP, combined with plasma membrane hyperpolarization and decrease in cytoplasmic calcium levels due to activation of inwardly-rectifying potassium channels (which are positively coupled to SSTR), are collectively thought to mediate inhibitory effects of SSTR on exocytosis. Antiproliferative effects of SSTR are more complex and less understood, but appear to be mediated (at least, partially) by certain types of phosphotyrosine phosphatases, such as SHP-1 and SHP-2. Once activated by SSTR, SHP-1 and SHP-2 modulate MAPK/ERK and PI3K/Akt/mTOR pathways downstream of receptor tyrosine kinases, thus *counteracting* positive effects of the latter on cellular metabolism, proliferation and survival. Late transcriptional effects

of cAMP (*i.e.,* altered expression of cAMP-dependent genes due to cAMP depletion) might also supplement the above mechanisms.

However, apart from these commonalities, SSTR subtypes are quite distinct in many ways, including expression pattern, signaling, receptor internalization and trafficking, as well as the nature of evoked responses in host cells, and thus should be regarded as individual entities and not taken collectively for an "indiscrete ensemble". SSTR subtype individuality is further endorsed by the ability of all SSTR subtypes to form homodimers and/or heterodimers (not only with other SSTR subtypes, but also with another GPCR and non-GPCR, such as dopamine/opioid receptors and EGFR) featuring altered signaling and internalization responses to ligands, as well as high degree of dependence of SSTR effects on specialization and availability of specific signaling effectors in a given cell.

As already mentioned, SSTR (specifically, subtypes 2 and 5) are quite commonly expressed by certain types of solid malignancies, such as pituitary adenomas, neuroendocrine tumors of gut and pancreas, as well as colorectal and cervical cancer. Selective targeting of SSTR of tumors became possible due to many years of focused medicinal chemistry research, yielding an array of synthetic analogues of endogenous SSTR ligands (most notably, octreotide) featuring extended *in vivo* stability. Somatostatin analogues not only established themselves as rather efficient stand-alone targeted pharmaceutics for tumor control, but also made the basis for another class of targeted compounds, *i.e.,* radionuclide–SSTR ligand conjugates. The latter combine antiproliferative activity of SSTR ligands with their ability for addressed delivery of radio-emitters to SSTR-positive tumors. Conjugate binding to SSTR culminates in internalization of the ligand-radionuclide complex by tumor cells, thereby anti-tumor SSTR signaling is augmented by a topical radiotherapy. The resulting treatment modality, collectively called as PRRT (peptide receptor radionuclide therapy), together with monoclonal anti-tumor antibodies represents one of the most successful types of targeted therapy developed so far and is currently rapidly entering clinical oncology armaments in Europe and the United States.

With this, extrapolation of the SSTR targeting paradigm to synthetic nanocarriers was to be expected and appears rather logical. However, as I hope I have managed to demonstrate in the preceding chapters, nanocarriers *are not* small- molecule drugs, even when conjugated with such in the capacity of targeting moieties – rather, they comprise a distinct class of agents that feature a higher level of complexity and obey to other, still rather poorly understood rules when it comes to interactions on cellular, tissue and organismal levels. There is no question currently whether SSTR analogues and their radionuclide conjugates can bind and get endocytosed together with SSTR by tumor cells *in vivo* – we known they successfully *do* so[322]. Thereby, we have an established positive correlation between SSTR abundance and SSTR ligand uptake in targeted tumors – yet, whether a similar scenario is also broadly valid for SSTR

ligand-functionalized nanocarriers, I believe remains an open question as of now. The current work was meant to contribute to this very topic.

Detailed information on SSTR biology is available from the selected comprehensive reviews[4,323,324]; further info on SSTR signaling[325–327], internalization and trafficking[328], SSTR dimerization[329,330], SSTR ligands[3,331–333] and PRRT[115,334,335] could be found in the specified references.

After this rather lengthy (but necessary) introduction to the nanocarrier-mediated delivery, I would proceed with the review of the actual experimental approach and the derived evidence with the SSTR-targeted MSN.

► **Figure 5.** Somatostatin receptors: common signaling mechanisms as exemplified by SSTR2.

Ligand-activated somatostatin receptor subtype 2 (SST2) inhibits adenylyl cyclases (AC) via Gαi, leading to a decrease in intracellular cAMP levels. Depletion of cAMP, in turn, downregulates exocytosis and inhibits cAMP-dependent protein kinase A (PKA); the latter effect impinges on transcription of cAMP-dependent genes (*i.e.,* genes bearing cAMP-responsive elements (CREB) within promoters). Antisecretory activity SSTR2 is further enhanced by membrane hyperpolarisation and drop in cytoplasmic calcium, mediated by activation of G protein-coupled inwardly-rectifying potassium channels (GIRK) and downregulation of voltage-operated calcium channels (VOCC). SSTR2 also activates nonreceptor protein tyrosine phosphatases SHP-1 and SHP-2 – these are thought to mediate antiproliferative and antiangiogenic SSTR2 effects via inhibition of PI3K/Akt/mTOR and RAF1/MEK1/ERK pathways, propagating signals from receptor tyrosine kinases (RTK), as well as via modulation of NOS (nitric oxide synthase) pathway.

The described signaling machinery, mediating antisecretory and antiproliferative effects of SSTR2, is broadly shared by all SSTR subtypes. However, different SSTR subtypes have been also reported to utilize distinct signaling mechanisms, which underlines specific nature and function of every given SSTR subtype. For instance, SSTR2, 3 and 5 have been reported to activate phospholipase C (PLC; seemingly, via dissimilar effectors), modulating MAPK pathway and leading to elevation of intracellular calcium; SST1, 3 and 4 were shown to negatively regulate sodium/hydrogen exchanger 1 (NHE1), decreasing extracellular acidification rate. Further info on SSTR signaling – in refs[325,327]. (Reprinted from ref[4], page 781; CC BY 4.0 (https://creativecommons.org/licenses/by/4.0/)).

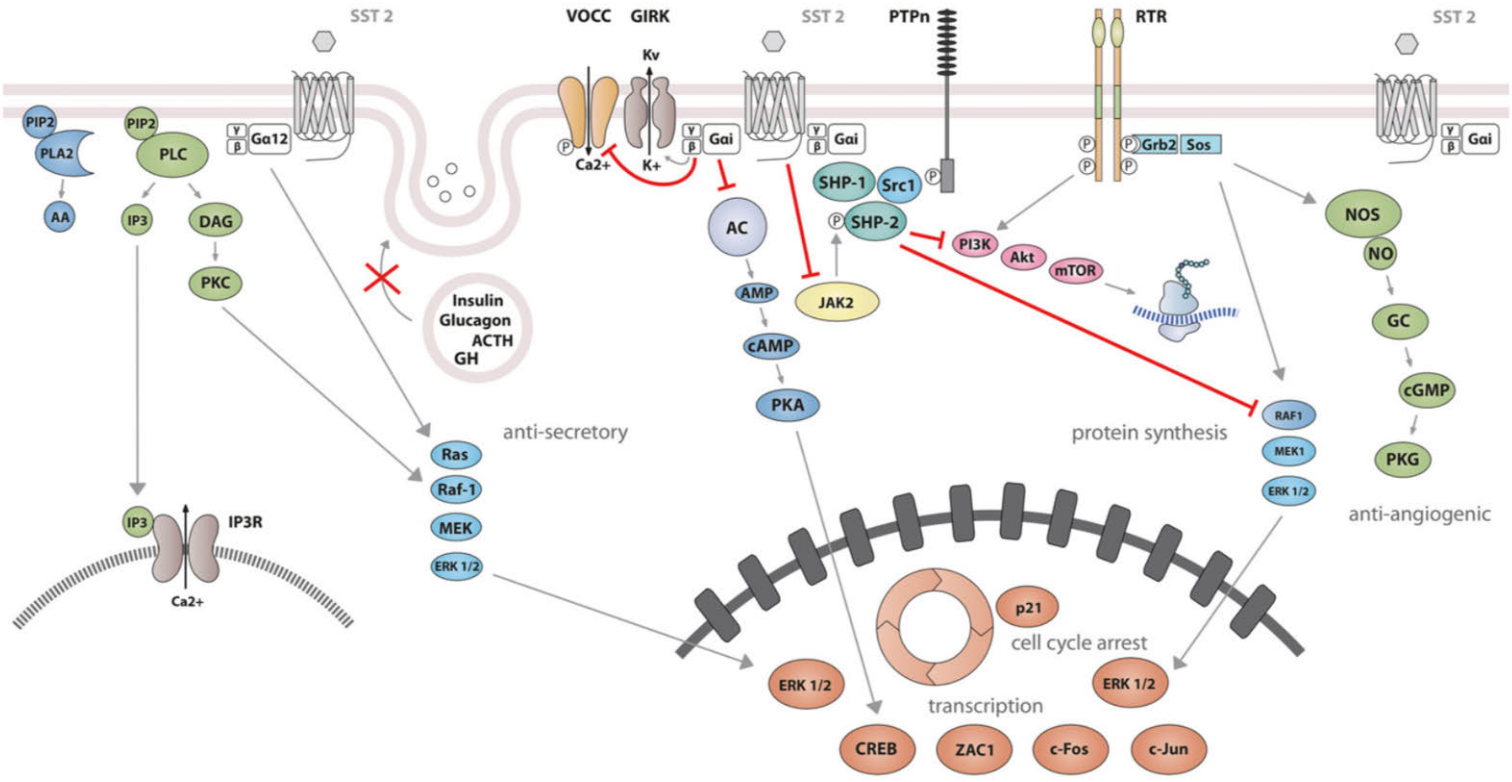

Figure 5. (the legend is on the previous page)

3 Aims

The major objective of the thesis was to evaluate the applicability of the active receptor targeting model to particular cellular receptors (SSTR5 and SSTR2) and a synthetic nanocarrier (MSN with diameter of *ca* 100–200 nm in dry state) under biologically-relevant conditions *in vitro*. In other words, we wanted to know if specific binding of SSTR on plasma membranes of living cells with high affinity SSTR ligands attached to the surface of MSN would lead to enhanced cellular accumulation of nanoparticles. The answer to this question was expected to instruct the decision on subsequent *in vivo* evaluation for the selected nanocarrier (*i.e.,* whether the developed targeted MSN merit evaluation in animal models), and to improve our understanding of SSTR5/2 role in the context of nanoparticle-aided tumor delivery.

To this, the following specific aims have been set:

- To design, synthetize and characterize by physicochemical means nanoparticles of mesoporous silica, functionalized with either high affinity SSTR peptides or inactive scrambled peptide (actively-targeted and control MSN, respectively) (I, II)
- To establish *in vitro* targetability bioassay capable of gauging SSTR activation in living cells by targeting peptides on MSN under biologically-relevant conditions (I)
- To evaluate *in vitro* targetability of the resulting MSN both under protein-depleted and serum-enriched conditions, in an attempt to find specific MSN type/s that could bind SSTR despite adsorption of serum proteins (I, II)
- To develop cell models with differential expression of SSTR5/2 and to utilize these for *in vitro* uptake experiments with the targetability-validated MSN, aiming to expose the input of SSTR5/2 engagement with targeting peptides into the net MSN internalization (I, III)

4 Materials and Methods

The chapter provides an overview of experimental techniques, utilized by the author within the projects encompassing the thesis. As the immediate chemical aspects, such as MSN synthesis and physicochemical characterization by appropriate methods, were principally covered by the collaborators (trained chemists), these techniques are not fully detailed in the thesis. Further information on experimental methodology can be found in the experimental sections and contribution statements of the publications I–III.

Table 3. Experimental techniques utilized in the thesis.

TECHNIQUE	PUBLICATION
CONVENTIONAL (2D) CELL CULTURE	I, II, III
FLOW CYTOMETRY (FC)	
- immunolabelling of viable non-fixed or PFA-fixed and permeabilized cells	I, III
- FC-aided cell sorting (FACS)	I, III
- cellular uptake of nanoparticles	III
cAMP ANALYSES	
- kinetic tracing of cAMP in living cells with GloSensor-22F probe	I, II
- AlphaScreen cAMP assay (antibody-based luminescent assay with cell lysates)	I
WORKS WITH NUCLEIC ACIDS	
- genomic DNA (gDNA) extraction from cells	I, III
- PCR	I, III
- agarose gel electrophoresis of PCR products/plasmids	I, III
- gel/column purification of PCR products	I, III
- restriction digest of DNA	I, III
- assembly of plasmid vectors (cloning)	I, III
○ conventional cohesive-end cloning with restriction enzymes and *T4/T7* ligases	I, III
○ TOPO-TA cloning	I
○ Gibson assembly	I
- CRISPR/Cas9 gene editing	III

BACTERIAL WORKS	
- in-house preparation of electro-competent *E.coli*	I
- transformation of electro- and/or chemically-competent *E.coli*	I, III
- bacterial colony PCR	I, III
- plasmid extraction (mini/midi/maxi–preps)	I, III
CELL PROLIFERATION/VIABILITY *IN VITRO* ASSAYS	
- mitochondrial respiration-based colorimetric cell viability assay (CCK-8)	II, III
- confluence-based cell proliferation analysis with Incucyte HD	III
FLUORESCENT CONFOCAL MICROSCOPY	
- cellular uptake of nanoparticles	III
PHYSICOCHEMICAL CHARACTERIZATION OF NANOPARTICLES	
- dynamic light scattering (DLS)	I, II
- targeting peptide load measurements (absorbance of supernatant fractions for MSN pre- and post-peptide conjugation)	I

Table 4. Wild type cell lines utilized in the thesis.

CELL LINE	DESCRIPTION	PUBLICATION
HEK293	Human embryonic kidney cell line	I, II, III
PC3	Human prostate cancer cell line	I
MCF7	Human breast cancer cell line	I, II
MD-MB-231	Human breast cancer cell line	I
BON1 (a.k.a BON/SSTR$_{WT}$)	Human pancreatic endocrine cancer cell line	I, III
QGP1	Human pancreatic endocrine cancer cell line	I
U87-MG	Human glioblastoma cell line	I

Table 5. Genetically engineered cell lines, specifically generated for the studies within the thesis.

CELL LINE	DESCRIPTION	PUBLICATION
HEK-GS (a.k.a HEK/SSTR$_{WT}$)	HEK293 cell line with stable expression of GloSensor-22F cAMP probe (GS22/cAMP)	I, III
HEK-GS/SSTR2 (a.k.a HEK/SSTR2$_{OE}$)	HEK293 cell line with stable co-expression of GS22/cAMP and human SSTR2	I, II, III
HEK-GS/SSTR3	HEK293 cell line with stable co-expression of GS22/cAMP and human SSTR3	I, II
HEK-GS/SSTR5 (a.k.a HEK/SSTR5$_{OE}$)	HEK293 cell line with stable co-expression of GS22/cAMP and human SSTR5	I, II, III
HEK/SSTR5$_{KO}$	SSTR5 knockout (clone B8); established in HEK-GS via Cas9/CRISPR	III
BON-GS	BON1 cell line with stable expression of GS22/cAMP	I
BON/SSTR5$_{OE}$	BON1 cell line with stable co-expression of GS22/cAMP and human SSTR5	III
BON/SSTR5$_{KO}$	SSTR5 knockout (clone A11); established in BON1 via Cas9/CRISPR	III

4.1 Cell culture (I, II, III)

HEK293 wild type (WT) cells and the derived strains were cultured in Dulbecco's Modified Eagle's Medium/Nutrient Mixture F-12 (DMEM/F-12; Gibco). BON1 WT cells and the derived strains were propagated in 50/50 (v/v) mixture of DMEM (Sigma) and F12K (Kaighn's; Gibco). MCF7, MD-MB-231 and U87-MG cell lines were maintained in DMEM (Sigma). QGP-1 and PC3 cell lines were cultured in RPMI-1640 (Sigma). If not specified otherwise, all the media were supplemented with 10 % (w/v) heat-inactivated foetal bovine serum (iFBS; Biowest), 50 U/ml of penicillin and 50 µg/ml streptomycin (Gibco). The cells were maintained at +37 °C in humidified atmosphere with 5 % CO_2 (a.k.a standard conditions). Cell counts were done with TC20 automated cell counter (Bio-Rad Labs).

The sources of WT cell lines (Table 4) are specified in the respective papers. All the genetically modified cell lines (Table 5) were derived from the respective WT strains in-house.

4.2 Generation of genetically-engineered cell lines (I, III)

4.2.1 General procedures with nucleic acids (I, III)

The concentration of nucleic acids was measured with NanoDrop 1000 spectrophotometer (Thermo Fisher Scientific). For gel-purification of PCR products and plasmids intended for cloning or sequencing, visualization of DNA in agarose gel was carried out with either ethidium bromide (EtBr) or Midori Advance stain under LED light of 470 nm (Fastgene Blue LED Illuminator; Nippon Genetics) in order to avoid DNA damage by UV light. Sanger sequencing (SangerSeq) of PCR products and plasmids was performed at either Finnish Microarray and Sequencing Centre, Turku Centre for Biotechnology, Finland or at Macrogen Europe, the Netherlands.

4.2.1.1 Synthetic DNA fragments (oligos and gBlocks) and plasmids (I, III)

The oligos were obtained from either TAG Copenhagen A/S (Denmark) or Integrated DNA Technologies (IDT, USA) and came with standard desalting. Explicit information on primers is provided in Table 6. Each primer was assigned a unique identification number (PID#), and these are used throughout the text for unambiguous identification of particular primers employed in certain experiments.

CRISPR/Cas9 construct for human *SSTR5* targeting is described in Table S1 (III). Annotated sequences of plasmid vectors are available from the respective original publications.

Table 6. Primers utilized in the thesis.

PRIMER ID#	PRIMER SEQUENCE (5'- 3')	DESCRIPTION	PUBLICATION
#1	gcgtacgatggattacaaa gatgatgatgataaggagc ccctgttcccagcctccac	Amplification and cloning of *SSTR5* WT coding sequence (CDS) from human gDNA; product of 1129 bp (#1+2 as a pair)	I
#2	gcgcgccagcttgctggtct gcataagcc	Amplification and cloning of *SSTR5* WT CDS from human gDNA; product of 1129 bp (#1+2 as a pair)	I
#3	taatacgactcactataggg	Screen and sequencing of inserts ligated into pcDNA 3.1/V5-His TOPO-TA vector; product of 267 bp + the length of insert (#3+4 as a pair)	I
#4	ctagaaggcacagtcgag gc	Screen and sequencing of inserts ligated into pcDNA 3.1/V5-His TOPO-TA vector; product of 267 bp + the length of insert (#3+4 as a pair)	I
#5	cggtttgactcacggggat	Screen and sequencing of inserts ligated into AmCyan-P2A-mCherry vector; product of 341 bp + the length of insert (#5+6 as a pair)	I
#6	gcgcatgaactccttgatga	Screen and sequencing of inserts ligated into AmCyan-P2A-mCherry vector; product of 341 bp + the length of insert (#5+6 as a pair)	I
#7	acctgccaaccaaagcga gaac	Screen and sequencing of inserts ligated into pMiniT vector; product of 246 bp + the length of insert (#7+8 as a pair)	I
#8	tcagggttattgtctcatgag cg	Screen and sequencing of inserts ligated into pMiniT vector; product of 246 bp + the length of insert (#7+8 as a pair)	I
#9	aaccgtcagatcccgtctcc cgtacgatgtacccatacg atg	Preparation of *SSTR2HA* CDS for ligation into AmCyan-P2A-mCherry plasmid via Gibson assembly; product of 1180 bp (#9+10 as a pair)	I
#10	aagttagtagctccgcttcc gatactggtttggaggtctc	Preparation of *SSTR2HA* CDS for ligation into AmCyan-P2A-mCherry plasmid via Gibson assembly; product of 1180 bp (#9+10 as a pair)	I
#11	gcgtacgatgtacccatac gatgttccagattacgctga catggcggatgagccactc aa	Amplification and cloning of *SSTR2* WT CDS from human gDNA; product of 1147 bp (#11+12 as a pair)	I

#12	gcgcgcgatactggtttggaggtctccat	Amplification and cloning of *SSTR2* WT CDS from human gDNA; product of 1147 bp (#11+12 as a pair)	I
#13	gcgtacgatggaacaaaaactcatctcagaagaggatctggacatgcttcatccatcatcggt	Amplification and cloning of *SSTR3* WT CDS from human gDNA; product of 1297 bp (#13+14 as a pair)	I
#14	gcgcgccaggtagctgatgcgcatcgtgc	Amplification and cloning of *SSTR3* WT CDS from human gDNA; product of 1297 bp (#13+14 as a pair)	I
#15	tttttgtgatgctcgtcagg	Assembly of CRISPR/Cas9 plasmid for human *SSTR5* targeting (colony PCR (#15+16 as a pair) and SangerSeq)	III
#16	gggcgtacttggcatatgat	Assembly of CRISPR/Cas9 plasmid for human *SSTR5* targeting (colony PCR (#15+16 as a pair) and SangerSeq)	III
#17	gtgattcccggccaagctaa	Screen for alterations in *SSTR5* CDS after Cas9-mediated mutagenesis (PCR (#17+18 as a pair) and SangerSeq)	III
#18	ttagaggggatggtcggtca	Screen for alterations in *SSTR5* CDS after Cas9-mediated mutagenesis (PCR (#17+18 as a pair) and SangerSeq)	III

4.2.1.2 PCR screen of bacterial colonies (I, III)

Transformed bacteria were seeded on LB-agar (1.5 % w/v) plates supplemented with appropriate selection agents and incubated ON at desired temperature. The next day, once the bacterial colonies had reached sufficient size (at least 1–2 mm), a few dozens of colonies were randomly picked with sterile wooden toothpicks, using a fresh toothpick for every single colony. A toothpick with bacteria was dipped for 1–2 s into one well of a 96-well PCR plate prefilled with 5 µl of ultrapure water supplemented with 20 µg/ml of RNase A (Sigma), then removed and dipped for another few seconds into a corresponding single well of a 96-well polystyrene round-bottom plate for suspension cultures (Greiner), prefilled with 150 µl/well of LB medium with appropriate selection antibiotic. Suchwise, two replicate 96-well plates were prepared simultaneously: the first one to be used for actual screening by PCR (*screen plate*), and the second one serving as a *living stock* of all the clones that underwent PCR (*stock plate*), allowing for maintenance and expansion of the selected clones once screen PCR results became available.

The *stock plate* was covered with a lid and incubated on a thermoshaker (Thermomixer Comfort, Eppendorf AG) at +37 °C and 400 RPM for 8–12 h; then the plate was transferred to +4 °C for storage. The *screen plate* was further spiked with 10 µl/well of master mix, yielding a final reaction volume of 15 µl/well, containing 0.01 U/µl of DNA polymerase (Biotools, B&M Labs, S.A.), 333 µM of

dNTPs, 0.167 μM of forward and reverse primers in 1x standard buffer for the polymerase. The reactions were run on a thermocycler using the following conditions: #1) +98 °C for 2 min; #2) +94 °C for 45 s; #3) +55–59 °C for 30 s (annealing temperature was primer-specific); #4) +72 °C for 60 s/1000 bp of the amplicon's length, then back to step#2, for 35 cycles overall; #5) +72 °C for 5 min. The primers were purposely designed to either produce no product in the absence of the correct insert (*e.g.,* with one primer landing in the backbone and the other having a complementary region within the insert) or to produce products of sensibly different size for cases of no insert/insert present. The resulting PCR products were resolved on agarose gels and visualized with EtBr. A small set (typically 4–8) of the correct clones was retrieved from the *stock plate,* expanded in larger volumes of liquid LB with appropriate selection agents, and processed for plasmid preparations. The latter were validated with SangerSeq.

4.2.2 Generation of cells with stable expression of luminescent cAMP sensor and SSTR (I, III)

4.2.2.1 Isolation of human genomic DNA (I)

Human gDNA was isolated from the buccal epithelial cells of the author (VMP) via the express method[336]. In brief, after having buccal smears obtained, the cotton-covered tips of the presterilized wooden swabs were severed with scissors and transferred to sterile 1.5 ml microcentrifuge tubes (1 cotton tip per tube), containing 600 μl of 50 mM NaOH. The samples were vortexed once and placed on a thermoblock for 5 min at +95 °C. The lysis procedure was terminated by adding of 60 μl of 1 M Tris-HCl, pH 8.0 per tube with subsequent vigorous vortexing for 10 s. The samples were further centrifuged at 13,000*xg* for 1 min at RT and the supernatant was transferred to fresh 1.5 ml tubes for either immediate use or storage at -80 °C.

4.2.2.2 Amplification and tagging of coding sequences of human *SSTR2, 3* and *5* (I)

The full coding sequences (CDS) of *SSTR2*, *3* and *5* (HUGO Gene Nomenclature Committee symbol/ID (HGNC): *SSTR2/11331, SSTR3/11332* and *SSTR5/11334*) were amplified from the freshly isolated human gDNA with the high-fidelity DNA polymerase (KOD Xtreme Hot Start; Merck Millipore) as follows: 1x Xtreme buffer, 0.4 mM dNTPs, 0.3 μM of forward and reverse primers each (PID#11+12 for *SSTR2*_HA, #13+14 for *SSTR3*_Myc, #1+2 for *SSTR5*_Flag; Table 6), 0.02 U/μl of DNA polymerase, 2–10 μl of gDNA, ultrapure water to a final volume of 50 μl. The

reactions were run on a thermocycler at the following conditions: #1) +94 °C for 2 min; #2) +98 °C for 7 s; #3) +57 °C for 30 s; #4) +68 °C for 90 s, then back to step#2, for 35 cycles overall. After validation of the accuracy of PCR by agarose gel electrophoresis (AGE), the amplified CDS were either directly isolated from the reaction mixtures or subjected to gel-purification with NucleoSpin columns (Macherey-Nagel) according to the manufacturer's instructions.

4.2.2.3 Generation of expression vector for human *SSTR5* (I)

For cloning into pcDNA3.1/V5-His TOPO-TA mammalian expression vector (Invitrogen), the purified *SSTR5*_Flag CDS were 3'-adenylated with 2.5 U of *Taq* polymerase (Qiagen) in 50 µl of 1x*Taq* polymerase reaction buffer with 0.4 mM of dATPs for 10 min at +72 °C on a thermocycler. The resulting 3'-adenylated products were ligated into pcDNA3.1/V5-His TOPO-TA vector according the manufacturer's instructions and the 1–2 µl of ligation reaction was transformed into 10-β chemically competent *E. coli* (New England Biolabs (NEB)). The transformants were seeded on LB plates with 1.5 % (w/v) agar (LB-agar) and 50 µg/ml ampicillin; the plates were left ON in the incubator at +37°C. Next day, the evolved bacterial colonies were screened by PCR (PID#3+4, Table 6), as described. The clones harbouring the correct insert were processed for minipreps with NucleoSpin Plasmid EasyPure (Macherey-Nagel) and verified with SangerSeq.

To obtain the mammalian expression vector for human *SSTR5* coupled to mCherry fluorescent protein via P2A linker (SSTR5_Flag-P2A-mCherry; accession #LT962381 at European Nucleotide Archive), *SSTR5*_Flag sequence was further subcloned into AmCyan-P2A-mCherry plasmid[337] (#45350; AddGene repository), as described below. *SSTR5* CDS was cut out from the earlier generated pcDNA 3.1/V5-His TOPO-TA plasmid via double-digest with *BsiWI* (NEB) and *BssHII* (Promega) and gel-purified. The derived isolate was directionally cloned with *T4* DNA ligase (NEB) into *BsmBI* (NEB)-linearized and gel-purified AmCyan-P2A-mCherry plasmid. The ligation products were transformed into in-house generated electrocompetent HS996 *E. coli*[338] and the transformants were seeded on LB-agar (1.5% w/v) plates supplemented with 50 µg/ml of kanamycin. The evolved colonies were PCR-screened (PID#5+6, Table 6) and SangerSeq-verified. The seq-validated clones were used for large-scale plasmid preparations (NucleoBond Xtra Maxi Plus; Macherey-Nagel).

4.2.2.4 Generation of expression vectors for human *SSTR2* and *3* (I)

SSTR2_HA-P2A-mCherry and SSTR3_Myc-P2A-mCherry expression plasmids (accession #LT962382 and #LT962383, respectively; European Nucleotide Archive)

have been assembled via 2-step procedure, involving a common first step and a disparate second step.

For the initial step, PCR-amplified and purified *SSTR2*_HA and *SSTR3*_Myc CDS were cloned into linearized pMiniT plasmid (NEB PCR cloning kit), as suggested by the provider. The ligation products were used for transformation of 10-β chemically competent *E. coli* (NEB), and the transformants were plated on LB-agar (1.5 % w/v) with 100 μg/ml of ampicillin. The clones bearing the right insert were identified by colony PCR and validated by SangerSeq (PID#7+8, Table 6). The verified clones were further processed for mid-scale plasmid preparation with GeneJET Plasmid Midiprep Kit (Thermo Scientific).

The second step in SSTR2_HA-P2A-mCherry vector generation involved subcloning of *SSTR2*_HA CDS into AmCyan-P2A-mCherry plasmid. For this, *SSTR2*_HA CDS was PCR-amplified from pMiniT vector utilizing high-fidelity KOD Xtreme Hot Start DNA polymerase and primers carrying 5-prime overhangs (PID#9+10, Table 6) to the ultimate expression plasmid. The PCR products were gel-purified and ligated into *BsmBI* (NEB)-linearized and gel-purified AmCyan-P2A-mCherry plasmid via Gibson assembly (NEB)[339]. The resulting ligation reaction was purified with YM-100 kDa centrifugal filter unit (Merck Millipore) and transformed into DH10-β electrocompetent *E.coli* (NEB) employing Electroporator 2510 (Eppendorf AG), at 1350 V, 600 Ω and 10 μF . The transformants were seeded on LB-agar (1.5 % w/v) plates supplemented with 15–25 μg/ml kanamycin and kept ON at +37 °C. The evolved bacterial colonies were PCR-screened (PID#5+6, Table 6) and validated by SangerSeq.

For the assembly of SSTR3_Myc-P2A-mCherry plasmid, pMiniT-SSTR3_Myc vector was double digested with *BsiWI* (NEB) and *BssHII* (Promega), and the released *SSTR3*_Myc CDS was gel-purified. Finally, *SSTR3*_Myc sequence was cloned into *BsmBI* (NEB)-linearized and gel-purified AmCyan-P2A-mCherry plasmid with *T4* ligase (NEB). The ligation reaction was used for transformation of DH10-β electrocompetent *E.coli*, with the ensuing selection and PCR screen of the evolved bacterial colonies carried out as described for SSTR2_HA-P2A-mCherry vector.

4.2.2.5 Transfection and isolation of cells, stably co-expressing SSTR and GS22/cAMP (I, III)

HEK293 cells, stably expressing GS22/cAMP probe (HEK-GS), had been generated in-house and characterized earlier[340]. To obtain double-stable cell lines, co-expressing GS22/cAMP and a desired SSTR subtype, HEK-GS cells were transfected with SSTR2_HA-P2A-mCherry, SSTR3_Myc-P2A-mCherry or SSTR5_Flag-P2A-mCherry plasmids. Transfections were carried out with Xfect

polymer (Clontech Laboratories), according to the manufacturer's instructions. After 4–6 weeks of continuous selection with 500 μg/ml geneticin (G418; Roche), the evolved stable populations were sorted at least twice with FACSAria IIu cell sorter (Becton-Dickinson) to collect the brightest fraction of mCherry-positive cells. As *mCherry* and *SSTR* are transcriptionally coupled via P2A linker[341], the respective proteins are expected to accumulate in proportional amounts in plasmid-expressing cells, which makes a rationale for the above FC-aided enrichment approach. BON1, stably expressing GS22/cAMP (BON-GS), and BON1 with stable co-expression of GS22/cAMP and human *SSTR5* (BON/SSTR5$_{OE}$), were derived and characterized in a similar fashion.

4.2.3 Generation of *SSTR5* knockout cells (III)

To generate SSTR5-null cells, we resorted to a simultaneous expression of two gRNAs and *S.pyogenes* Cas9 from a single plasmid vector, following the procedures of ref[342,343], with some modifications. As human *SSTR5* is intronless and has a reasonably short coding sequence (1095 bp; consensus CDS#10429.1 in CCDS database), by selecting a pair of gRNAs, flanking the most of the CDS (III, Table S1), we were expecting to obtain a fraction of mutant clones with the flanked *SSTR5* fragment deleted, thus increasing the likelihood of efficient gene disruption (KO) and facilitating the screen of the procured clones by means of regular agarose gel electrophoresis of PCR products. After selection of the gRNAs with CasFinder software[344] (available at http://arep.med.harvard.edu/CasFinder/), the targeting pair was assembled *in silico* and obtained as a synthetic gene, with subsequent ligation into pSpCas9(BB)-2A-Puro plasmid[345] (PX459, #48139 of Addgene repository) with *T7* ligase and *BbsI*, as described in ref[343]. The ligation products were used for transformation of chemically-competent 10β E. coli (NEB). The bacterial colonies, evolved on LB-agar plates supplemented with 100 μg/ml of ampicillin after ON incubation at +37 °C, were screened by PCR (PID#15+16, Table 6). Selected colonies, exhibiting PCR products of the expected size on agarose gels, were further validated with SangerSeq and used for the targeting plasmid isolation (NucleoBond Xtra Maxi Plus; Macherey-Nagel).

For *SSTR5* targeting, the cells were seeded into 6-well plates (as 2.5 or 4.0×10^5 cells/well in case of BON1 and HEK293 cells, respectively) in 2 ml of the respective complete medium and left ON in the incubator. Next day, the cells were transfected with the *SSTR5* targeting plasmid with Xfect reagent, as suggested by the manufacturer. 48–72 h after transfection, the cells were subjected to puromycin selection (InvivoGen; at 1.0 and 1.25 μg/ml in the appropriate complete medium for BON1 and HEK293, respectively) that lasted for 5–7 days. Next, the evolved oligoclonal populations that overcame the selection were allowed to expand for 1–2

extra weeks and then further passaged into 96-well plates by means of limiting dilution, with the intention of having less than 1 cell/well (target cell density – 0.6 cells/well). After another 10–14 days, once the procured monoclonal populations had reached sufficient size (occupying at least 1/4 of a well's surface upon visual inspection), the clones were harvested by trypsinization, with *ca* 1/3 of the cells used for culture continuation and frozen stocks preparation, and the remaining 2/3 of the cellular mass utilized to screen for Cas9-induced genetic rearrangements, as follows. Firstly, we isolated gDNA from the cells in question with the Mouse Direct PCR kit (Bimake; conditions per single sample: the harvested cells were washed once with 1xPBS, pelleted by centrifugation, cleared of the wash, resuspended in 40 µl of buffer L, supplemented with 0.8 µl of protease, and incubated on a thermocycler at +55 °C for 45 min, then at +95 °C for 5 min). Next, the resulting gDNA preps were PCR-amplified with primers, flanking CDS of *SSTR5* (PID#17+18, Table 6; PCR conditions: 1.5 µl of DNA extract, 200 nM of both the primers, 25 µl of 2x MasterMix from the specified Mouse Direct PCR kit and H_20 *quantum satis*, till the final reaction volume of 50 µl; cycling conditions: #1) 5 min at +94 °C; #2) 20 s at +94 °C; #3) 30 s at +61 °C; #4) 50 s at +72 °C, then back to step #2, for 35x cycles overall; #5) 5 min at +72 °C) and resolved on agarose gels. Selected mutants, harbouring gross rearrangements of *SSTR5* CDS, as evident by a clear size shift of a screened sample's PCR product as compared to the WT product upon gel electrophoresis, were further validated by SangerSeq, performed on the gel-purified PCR products (NucleoSpin Gel & PCR clean-up; Macherey-Nagel) with primers #17 and #18 for FW and RW reads, respectively (Table 6). As a final step, the *SSTR5*-null clones were also validated on a protein level by immunolabelling & FC analysis, as described.

4.3 Immunolabelling and flow cytometry analysis (I, III)

The cells to be immunolabelled were propagated in either 25- or 75-cm^2 flasks in the appropriate complete medium under the standard conditions. On the day of analysis, the cells were harvested by trypsinization and counted. The aliquots with required number of cells were then pelleted by centrifugation, cleared of supernatants (SNs), and resuspended in 1xPBS (ice-cold). From this point onwards, the procedure followed either the protocol for live cell immunolabelling or the protocol with fixation and permeabilization, as described below. When required, such as in paper I, both the protocols were carried out in parallel. If not specified otherwise, all the subsequent steps, including centrifugation, were performed at +4 °C, all the reagents were pre-cooled to ≤+4 °C, and the cells constantly kept on ice, protected from light.

4.3.1 Immunolabelling of viable non-permeabilized cells (I)

The cells were dispensed into a 96-well plate (round bottom, for suspension cultures; Greiner) as 0.5–1×10^6 cells per well. The plate was spun down once (600x*g*, 4 min), SNs removed and the cells resuspended in 100 µl/well of either stain buffer (SB; 1xPBS with 10 % (w/v) FBS and 1 % (v/v) normal donkey serum (Jackson ImmunoResearch); no-stain controls and secondary antibody–only controls) or SB with appropriate concentration of primary antibody (Ab; samples). After incubation for 30 min, the cells were washed twice with SB and resuspended in 150 µl/well of either SB (no-stain controls) or SB with appropriate concentration of secondary Ab (samples and secondary Ab–only controls). After another round of incubation (30 min), the cells were washed three times with SB. Next, the cells were fixed (15 min at RT) in 150 µl/well of 2 % (w/v) paraformaldehyde (PFA) in 1xPBS. Finally, the plate was spun down, the cells were cleared of PFA and resuspended in 150 µl/well of 1xPBS. The samples were kept at +4 °C protected from light (wrapped in aluminium foil) till FC analysis.

4.3.2 Immunolabelling of paraformaldehyde-fixed and saponin-permeabilized cells (I, III)

The cells were pelleted by centrifugation, cleared of SNs and fixed in 2 % (w/v) PFA in 1xPBS for 15 min at RT. After fixation, the samples were centrifuged and cleared of PFA, resuspended in 1xPBS and dispensed into the round-bottom 96-well plates for suspension cultures, aiming to have 0.5–1×10^6 cells per well. Then, the cells were pelleted by centrifugation, cleared of 1xPBS, resuspended in 200 µl/well of permeabilization buffer (PB; SB supplemented with 0.1 % (w/v) saponin) and left on ice for 10–15 min to allow for permeabilization and blocking. Next, the plate was spun down, PB was removed and the cells were resuspended in 100 µl/well of either PB or PB with a primary Ab (no-stain controls or samples, respectively). After 30 min of incubation, the cells were pelleted by centrifugation, cleared of the SN and washed 3x times with PB. Then, the cells were resuspended in 200 µl/well of either PB (no-stain controls) or PB with a secondary Ab (samples and secondary Ab-only controls), and left to incubate further for 30 min. After three more washes with PB, as described above, the cells were suspended in 150 µl/well of 0.5 % (w/v) of PFA in 1xPBS, and kept at +4 °C protected from light till FC analysis.

4.3.3 Antibodies (I, III)

Primary Abs recognizing intracellular epitopes that were used on permeabilized cells: anti-SSTR2 (MAB4224, R&D systems; mouse monoclonal Ab (mAb); 1:250), anti-SSTR3 (UMB-5, Abcam; rabbit mAb; 1:800), anti-SSTR5 (UMB-4, Abcam;

rabbit mAb; 1:1000). Primary Abs recognizing exposed plasma membrane-bound epitopes that were used on non-permeabilized cells: anti-HA tag (A190-107, Bethyl; goat polyclonal Ab (pAb); 1:1000), anti-Myc tag (9E10, Developmental Studies Hybridoma Bank; mouse mAb; 3 μg/ml), anti-Flag tag (F7425, Sigma; rabbit pAb; 1:600). Anti-β-tubulin primary Ab (9F3, Cell Signaling; rabbit mAb; 1:400) was used on both permeabilized and non-permeabilized cells for control of adequacy of plasma membrane permeabilization or absence of thereof, respectively. Secondary Abs (all – Invitrogen, Alexa488-conjugated, raised in donkey, 1:2000): anti-goat (A11055), anti-mouse (A21202), anti-rabbit (A21206).

4.3.4 FC analysis of immunolabelled cells (I, III)

FC analysis was performed on LSRII cytometer (Becton-Dickinson; provided by Turku Bioscience). After gating for the target cell population (FSC area *vs.* SSC area) and exclusion of the cellular *doublets* (FSC height *vs.* FSC width; SSC height *vs.* SSC width), we strived to collect ≥ 10,000 events. The samples were exited with 488 nm laser and the emission was captured on *log* scale with [505 nm longpass / (530/30) nm bandpass] filter set. Data analysis and histogram plotting were carried out with Flowing Software 2.5.1 (available at http://flowingsoftware.btk.fi/index.php?page=1).

4.4 Handling of nanoparticles for biological tests (I, II, III)

MSN suspensions were prepared fresh immediately before experiments from the lyophilized stock, kept at -20 °C as small single-use pre-weighted aliquots. After removal from the freezer and brief centrifugation to collect all the particulate material, an aliquot of MSN was resuspended in HEPES buffer (25 mM, pH 7.4) of RT to the desired concentration by vigorous vortexing and further processed on a waterbath sonicator (FinnSonic m03; FinnSonic Oy) for 3 rounds of 10 min each, with additional vortexing in between. The sonication was done in deionized H_20 of <10 °C, with water temperature controlled by timely addition of ice. Before usage, the resulting MSN preps were further diluted in a desired solvent to 10x of the final working concentration.

For the preformed corona studies, the freshly-sonicated suspensions of MSN were further diluted to 1500 μg/ml in either DMEM/F-12 mix with 10 % (w/v) of iFBS (corona samples; final serum concentration during incubation – 7 % (w/v)) or HEPES buffer (25 mM, pH 7.4; control samples), with subsequent incubation for 1 h on a thermoshaker (Thermomixer Comfort, Eppendorf AG) at 850 RPM and +37°C. After the incubation, MSN were further diluted to 10x of the final working

concentration in the corresponding solvent (*i.e.,* HEPES or the medium+10 % iFBS) and used immediately. For collection of supernatants, MSN and controls were spun at 15,650x*g* for 5 min at RT, after which the SN fractions were carefully removed by pipetting and transferred to fresh tubes.

4.5 cAMP assays (I, II)

4.5.1 Measuring intracellular cAMP in living cells with the luminescent cAMP probe (a.k.a targetability bioassay; I and II)

The experimental protocol and approaches to data processing for the targetability bioassay are explicitly covered in paper I of the thesis. In brief, the cells with stable expression of GloSensor-22F cAMP probe (sensor cells) were seeded one day before the experiment into tissue culture-treated polystyrene 96-well plates with light-tight walls and translucent bottom (ViewPlate-96, PerkinElmer) as 60,000 cells per well in the 150 µl of cell type–specific medium, and incubated ON (+37 °C in humidified atmosphere with 5 % CO_2). Next day, before the assay, the old culture medium was removed and the wells were refilled with 45 µl of the freshly prepared inducing medium (IndMed), comprised of 2 % (v/v) of GloSensor reagent (Promega; corresponds to the final working concentration of 0.612 mg/ml, with the original stock of 30.6 mg/ml in 10 mM HEPES, pH 7.5) and 200 µM of the non-specific phosphodiesterase inhibitor 3-isobutyl-1-methylxanthine (IMBX; Sigma) in the assay-specific medium. In case of MSN corona studies, DMEM/F-12 medium (50/50, v/v) with 10 % (w/v) of iFBS was used for that purpose (a.k.a $Med_{10\%FBS}$, yielding $IndMed_{10\%FBS}$); for other setups, a mix of the above medium and CO_2-independent medium (Gibco; 4v of DMEM/F12 per 5v of CO_2-independent medium), supplemented with 0.1 % (w/v) of bovine serum albumin (BSA), was used (a.k.a $Med_{0.1\%BSA}$, yielding $IndMed_{0.1\%BSA}$). After equilibration for 45 min at RT in the dark, the plate was inserted into a multiwell plate reader (EnSight; PerkinElmer) and the light output – denoted as a *baseline signal* – was captured in a kinetic fashion, *i.e.,* the selected wells on a plate were repeatedly captured in a desired sequence, for 15–20 min at RT. Next, the plate was removed from the reader and the wells were spiked with either 5 µl of freshly prepared solutions, having all the desired components at 10x of the final concentration, or respective controls. Final concentration of forskolin (FSK) in the assay equalled 10 µM, if not specified otherwise. FSK was not subjected to heat exposure or centrifugation (in the context of peptide/MSN thermal stability or peptide shedding assays, respectively), but its working solutions were prepared simultaneously with the actual study preps and kept for the same time at RT before being mixed with the actual preps to yield the final

10x co-mixes. After spiking, the plate was immediately re-inserted into the reader and the luminescence (now denoted as *induced signal*) was further captured in the same kinetic mode for the time required (typically, for 45–60 min). The described assay conditions (*i.e.,* at RT, IndMed with 2 % of GloSensor reagent and 200 μM of IBMX, stimulation with 10 μM of FSK) are referred to as "standard" throughout the text.

The registered luminescent reads were used for plotting of intracellular cAMP kinetic curves (luminescence *vs.* time), with the latter processed to baseline signal – subtracted Area Under the Curve (AUC) values with the help of either the respective operator of GraphPad Prism software or a custom-written script, both employing trapezoidal rule and producing similar results[346]. The derived AUC values were further normalized to AUC of FSK, taken for 100 % (if not specified otherwise), and the resulting %FSK-AUC indices used for inferential statistics.

4.5.2 Measuring cAMP with AlphaScreen technology (I)

AlphaScreen cAMP Detection Kit (PerkinElmer) was used as suggested by the manufacturer, with minor modifications. In brief, the cells were plated in a suitable vessel (25- or 75-cm^2 flask) and propagated in appropriate complete medium for 1–2 days before the assay. On the day of analysis, the cells were detached by trypsinization and counted. The required number of the cells was suspended in Stimulation Buffer (a cell type-specific Induction Medium as described for GS22/cAMP assay with 200 μM of IBMX) of RT, yielding a suspension of 4,000 cells/μl. After incubation for 15–20 min at RT, the suspension was mixed with equal volume (1:1) of 10x Acceptor Beads solution in Stimulation Buffer and the resulting suspension was transferred to a 384-well polystyrene plate (AlphaPlate-384; PerkinElmer) as 5 μl/well, producing a load of 10,000 cells/well. Next, the wells were spiked with 5 μl/well of the Induction Mix, consisting of 20 μM of FSK with or without octreotide (2x final concentration) dissolved in Stimulation Buffer, and the plate was left for 10 min at RT in the dark to allow for cAMP accumulation. At the end of the incubation period, all the wells were spiked with 15 μl of 1.67x mix of biotin-cAMP (41.7 nM) and streptavidin donor beads (33.3 μg/ml) in 1x Immunoassay Buffer, with the Mix being freshly prepared and preincubated for 30 min at RT in the dark before addition to the cells. Then, the plate was sealed with an adhesive film and left for 1 h at RT to allow for cell lysis and cAMP liberation. The assay plate also incorporated a set of wells with cAMP standards covering a range of cAMP concentrations from 0 to 1 μM prepared in the same Stimulation Buffer. The standards were processed in parallel with the sample wells, all done in three technical replicates. As a final step, the plate was read on AlphaScreen technology-compatible platereader (EnSight; PerkinElmer). The signal from cAMP standards

served for reconstruction of the standard curve, with the latter being used for deduction of the absolute cAMP values in the cells treated with FSK and varying concentrations of octreotide.

4.6 *In vitro* assays for cell proliferation/viability (II, III)

4.6.1 CCK-8 assay (II, III)

Cell Counting Kit-8 assay (CCK-8; Dojindo Europe), which is mitochondrial respiration–based *in vitro* colorimetric cell viability test, was performed after the vendor's suggestions, as follows. The cells were seeded into flat-bottom 96-well plates (Greiner) in 95 µl/well of cell type–specific complete medium without antibiotics and left to incubate ON under the standard conditions. Cell seeding density for BON1 and HEK293 (including the derived SSTR-engineered clones) was 10^3 and 1.5×10^4 cells/well, respectively. Next day, without prior medium exchange, the cells were spiked with 10 µl/well of 10x analyte solutions (either peptides or freshly-prepared MSN, paper I or III) or respective controls, yielding desired 1x working concentrations (1:10 dilution; 5 µl of the original medium volume was taken for expected evaporation losses with ON incubation, thus the starting medium volume by the moment of treatment initiation was assumed to equal 90 µl/well), and the plates were returned to the incubator. 2 hours before the assay's termination points, *i.e.,* 24 h and 48 h of treatment, 10 µl of CCK-8 reagent was added to the cells without prior medium exchange, and the plates were placed back to the incubator and kept there till the specified time points had been reached. The assay was terminated with absorbance read at 450 nm (Abs@450nm; with EnSight plate reader; PerkinElmer). After subtraction of the average blank values (corresponding to Abs@450nm of cell-specific medium without cells), the resulting values were normalized to average Abs@450nm of non-treated cells (taken for 100 %), giving the final normalized viability rate.

4.6.2 Confluence-based cell proliferation analysis with Incucyte HD (III)

Conditions for cell seeding, incubation and treatment – as specified in Section 4.6.1. After treatment administration on Day 2 (MSN or matching no-treatment controls), the plates were inserted into Incucyte HD live cell imager (Essen BioScience), integrated with the cell culture incubator (+37 °C, humidified atmosphere with 5 % CO_2), and immediately subjected to continuous phase-contrast imaging (1 snapshot every 30–60 min, up to 46 h (if combined with CCK-8, otherwise – till 48 h) from

the moment of treatment initiation). As the plates were placed into the imager within 5–10 min of treatment, the first imaging time point was taken for the time point "0" in terms of the subsequent image analysis. No medium exchange or other perturbations were performed during the imaging. Confluence analysis, reflective of the surface occupancy by cells in a given field of view (FoV; with 100 % corresponding to full confluence), was performed with Incucyte software (build 2010A Rev3; Confluence v.1.5 operator) on time-lapse series of the captured phase-contrast images.

4.7 Uptake of nanoparticles by living cells *in vitro* (III)

4.7.1 MSN uptake studies with FC (III)

BON1 and HEK239 cells were seeded into 96-well plates (flat-bottom; Greiner) as 1.0 or 4.0×10^4 cells per well in 95 µl of the respective complete medium and left ON in the incubator under the standard conditions. Next day, the plates were retrieved from the incubator and spiked with 10 µl/well of either freshly-prepared 10x MSN suspensions or appropriate controls, without prior medium exchange (yielding 1:10 dilution to the final 1x working concentration, with 5 µl of the original medium volume counted for expected evaporation loss with ON incubation). The plates were then returned to the incubator and kept at the standard conditions for the time required (2 h or 24 h) to allow for MSN internalization. Once the incubation time had elapsed, the plates were retrieved from the incubator and the cells were prepared for FC analysis, as follows.

The incubation medium was removed and the cells were washed with 1xPBS and harvested by trypsinization. After trypsin quenching by addition of the equal volume of complete medium, the resulting cellular suspensions were transferred to a round-bottom 96-well plate for non-adherent cultures (Greiner) and the cells were pelleted by centrifugation (at 600x*g* and +4 °C for 4 min). SNs were removed, and the pellets were washed once with 1xPBS. Then, the cells were fixed with 100 µl/well of 4 % (w/v) PFA in 1xPBS, for 10 min at RT in the dark. Finally, the cells were cleared of the fixative by centrifugation, as described, and resuspended in 125 µl/well of 0.5 % (w/v) PFA in 1xPBS. The resulting suspensions were stored at +4 °C in the dark till FC analysis.

FC was performed on LSRFortessa cytometer (Becton-Dickinson; at Turku Bioscience), following the general protocol described in section 4.3.4. After gating and exclusion of cellular aggregates, ≥ 20,000 the gated events were collected. As the MSN were decorated with ATTO647N red fluorophore, the samples were excited with 640 nm laser and the emission was registered on *log* scale with (670/14) nm

bandpass filter. We kept the cytometer settings constant for all MSN uptake experiments, with the exception of a single run, where the red laser intensity was slightly decreased. The reads from the latter experiment are explicitly highlighted in the charts.

A freeware package Flowing Software 2.5.1 was utilized for raw FC data processing and histogram plotting. Absolute fluorescence intensities (FI) of the samples were estimated as median values of the respective population distributions ("emission intensity *vs.* number of events" histograms), after subtraction of the median FI of the non-MSN-treated population (a.k.a autofluorescence control, AFC). Importantly, to correct for the varying brightness of the nanoparticles (relative FI of MSN, MSN_{SP3} and MSN_{OC3} at 680 nm – 1.0, 0.6 and 1.2, respectively (II, Table S1)), AFC-corrected median FI values were normalized accordingly. The resulting $_{corr}$MedFI values were used to calculate *MSN dose-normalized relative uptake rate* (%; estimated for a given nanoparticle dose as $_{corr}$MedFI (MSN_{SP3}) / $_{corr}$MedFI (MSN), with the latter value taken for 100%) and *MSN_{SP3} / MSN_{OC3} relative flux* (AU; estimated as $_{corr}$MedFI (MSN_{SP3}) / $_{corr}$MedFI (MSN_{OC3})). Ratiometric nature of both the above indices mitigated possible cytometry hardware-related effects, such as varying laser power, on the experimental readout, thus enabling robust inter-run quantitate comparisons and inferential statistics.

4.7.2 MSN uptake studies with fluorescence microscopy (III)

BON1 and HEK239 were seeded as 5×10^4 or $1–2\times10^5$ cells in 800 µl of appropriate complete medium with antibiotics per well, onto glass coverslips (round, d = 12mm, #1; Mentzel-Glaser), inserted into 24-well plates (flat-bottom, Greiner) as 1 coverslip/well, and left to incubate ON under the standard conditions. Before cell seeding, the coverslips were sterilized with 70 % (v/v) ethanol in water and copiously washed with 1xPBS. In case of HEK293 cells and the derived strains, coverslip sterilization was followed by pre-coating with poly-D-lysine (0.01 % w/v, 50,000–150,000 Da, Gibco; each coverslip was fully submerged in poly-D-lysine and left to incubate for 20 min at RT, after which the coating solution was removed and the coverslip was washed twice with ample volume of 1xPBS), to facilitate cell attachment. No coverslip precoating was done in case of BON1, for these cells featured strong adhesion to glass.

Next day, the plates were removed from the incubator, cleared of the old medium, refilled with 360 µl/well of fresh pre-warmed (+37 °C) cell type-specific complete medium and spiked with 40 µl/well of either freshly-prepared 10x MSN suspensions or appropriate controls (1:10 dilution to a final 1x working concentration). The plates were placed back to the incubator and further kept there at the standard conditions for 2 h or 24 h. Once the incubation period was over, the

cells on the coverslips were cleared of the treatment medium, washed two times with 1xPBS and fixed with 4 % (w/v) PFA in 1xPBS for 10 min. To allow for cytoskeletal stain with phalloidin, the cells were further permeabilized with 0.1 % (v/v) Triton X-100 in 1xPBS for 15 min. Next, the coverslips were cleared of the permeabilization buffer, washed once with 1xPBS and left to incubate for 15 min in 5 % (w/v) FBS in 1xPBS (a.k.a blocking buffer). For actin labelling, the coverslips were further immersed for 30 min in 100 nM ATTO488-phalloidin (ATTO-TEC GmbH; stock of 10 μM in 100 % methanol) in the blocking buffer. After successive washings (at least 4x times) with 1xPBS, the cells were counterstained with DAPI dihydrochloride (Sigma; working concentration of 285.5 nM in 1xPBS of RT) for 5 min, washed two more times with 1xPBS and once with deionized water, after which the coverslips were mounted onto glass slides (Mentzel-Glaser) with ProLong Gold antifade reagent (Molecular Probes), as recommended by the manufacturer. All the steps of microscopy samples preparation, from PFA fixation till coverslip mounting, were performed at RT and with RT-equilibrated reagents, under minimized exposure to light. The resulting slides were stored at +4 °C in light-tight chambers before being subjected to microscopic examination.

Fluorescence microscopy was performed with 3i CSU-W1 spinning disk confocal microscope, equipped with Hamamatsu sCMOS Orca Flash4.0 camera (provided by Turku Bioscience). ATTO647N (nanoparticles), ATTO488 (cytoskeleton), and DAPI (cell nuclei) were excited with 640 nm, 488 nm, and 405 nm solid state lasers, with emission sequentially (no channel-to-channel bleed-through) captured with the help of [692/40nm], [525/30nm], and [445/45nm] filters, respectively. Image acquisition settings for each of the fluorophores, *i.e.,* laser power and camera exposure time, were kept constant, thus enabling inter-run and cross-sample comparisons. Image processing, including reconstruction of z-stacks and the derived maximal intensity and 3D projections, were performed with freeware Fiji package (available at https://imagej.net/Fiji[347]). The resulting figures were assembled with Biorender software (at https://biorender.com).

4.8 Curve fitting and inferential statistics (I, II, III)

All statistical tests were carried out with Prism package (GraphPad Software). Dose-response curve fitting and IC_{50} calculations were performed using "*log (inhibitor) vs. response – Variable slope*" [$Y=Bottom+(Top-Bottom)/(1+10^{(LogIC50-X)\times HillSlope})$] operator of Prism software. Further information on the utilized statistical tests is specified in figure legends and the Experimental sections of publications I–III.

5 Results and Discussion

5.1 Development and validation of the *in vitro* targetability bioassay (I, II)

The selection of *in vitro* targetability assay was instructed by the targeting pair (SSTR and cognate high-affinity peptides as the targeted receptors and targeting ligands, respectively) and compatibility of the method with living cells. The latter aspect was deemed specifically important, for the live cell assay format would have allowed for facile control of the environment nanocarriers were administered into and had to traverse to get in physical contact with the acceptor cells, whilst simultaneously maintaining responsiveness of the acceptor cells and the targeted receptors to external clues. Furthermore, the assay had to provide SSTR-specific and quantitative readout and to encompass the physiological range of SSTR affinities (low-to-mid nanomolar in terms of ligand concentration).

Such the prerequisites, combined with the universal ability of all the five SSTR subtypes to negatively regulate intracellular cAMP and availability of sensitive living cells–compatible cAMP probes, prompted us to select the intracellular cAMP pathway for measuring SSTR activity. To this end, we opted to use a luminescent GloSensor-22F (GS22/cAMP) probe, originally introduced by[348]. GS22/cAMP is based on a circularly permutated firefly (*Photinus pyralis*) luciferase fused with a regulatory subunit IIβ of protein kinase A. The latter acts as cAMP responsive element, which restores a functional conformation of luciferase upon cAMP binding, leading to cAMP-dependent light emission in the presence of luciferin (I, Fig. 1A). GS22/cAMP has a wide dynamic range (0.003–100 μM of cAMP) and excellent linearity of response, ultimately providing for an up to 800-fold signal-to-noise ratio. The sensor is also compatible with both transiently and stably transfected cell lines, as well as primary cell cultures[340,349].

5.1.1 Cells with low SSTR expression constitute a poor model for quantitative targetability evaluation (I)

As a first step, we evaluated if GS22/cAMP could measure ligand-provoked SSTR signaling in cells with endogenous SSTR expression. For this, we selected two

unrelated cell lines, human embryonic kidney cell line 293 (HEK293) and human pancreatic endocrine carcinoma cell line (BON1), reported to express SSTR2/3/4/5 and SSTR2/5, respectively[350–354]. From these maternal cell lines, we derived oligoclonal populations with stable overexpression of GS22/cAMP (a.k.a HEK-GS and BON-GS). HEK-GS and BON-GS acted as robust cAMP sensors, reliably capturing positive increments in intracellular cAMP upon exposure to FSK and non-selective agonist of β-adrenoreceptors isoproterenol (I, Fig. S1).

Next, we studied the effects of SSTR activation with cognate ligands on intracellular cAMP in HEK-GS and BON-GS. SSTR ligand provocation studies were performed with simultaneous addition of 10 μM FSK (I, Fig. S1A-B). A potent natural activator of ACs[355–357], FSK boosted intracellular cAMP stores, which facilitated detection of even minor negative effects on cAMP downstream of SSTRs.

HEK-GS and BON-GS demonstrated poor overall cAMP response to octreotide (OC), with cAMP inhibition only becoming evident with the high peptide doses (≥ 500 nM). Low OC concentrations (1–10 nM) induced a moderate increment in cAMP levels in both of the sensor lines, leaving the signal kinetics otherwise unchanged (I, Fig. S2).

To investigate the reasons behind the poor OC responsiveness, we studied protein levels of SSTR2, 3 and 5 in HEK293 and BON1 cells. Contrary to the expected, FC analysis revealed generally low abundance of the studied receptors (I, Fig. 2). BON1 harboured low levels of SSTR5, whilst SSTR3 expression was very low and SSTR2 was virtually absent. HEK293 had similar SSTR profile, but with even lower levels of SSTR5 and 3. Importantly, SSTR2, 3 and 5 levels in HEK-GS and BON-GS matched the ones of the maternal WT cells, which allows to exclude artificial shift in SSTR profile due to GS22/cAMP introduction and selection (I, Fig. 2A).

The described SSTR profiles, specifically the extremely low abundance of SSTR2 – the main OC target[354,358], explain the modest amplitude of cAMP response to OC in HEK-GS and BON-GS (I, Fig. S2). In effect, this precludes utilization of HEK-GS and BON-GS for sensitive quantitative analyses of SSTR-targeted nanoparticles. This notion is further supported by the theoretically achievable levels of OC in the assay's medium with MSN treatment, calculated from the peptide loads of MSN (I, Table 3), which appear to be in the range of 10–200 nM of OC (calculated as if all the MSN-bound peptides were in a free state) across the expected treatment window, 1–50 μg of MSN per 1 ml of medium.

In an attempt to improve the assay's sensitivity, we cloned and overexpressed human *SSTR2, 3* and *5* in HEK-GS and BON-GS cells.

5.1.2 Cells with elevated SSTR levels demonstrate superior responsiveness to targeting ligands (I)

To procure cultures with stable co-expression of GS22/cAMP probe and human *SSTR2, 3* or *5*, we cloned the respective receptor subtypes into plasmid vectors, transfected these into HEK-GS and BON-GS and selected stable clones. Of note, the generated SSTR plasmids enabled stoichiometric expression of a given SSTR subtype and mCherry fluorescent protein by means of the P2A linker[341], which facilitated isolation of the positive SSTR clones via fluorescence-activated cell sorting (FACS), utilizing mCherry fluorescence for gating signal. Furthermore, CDS of *SSTR2, 3* and *5* were N-tagged (HA, Myc and Flag, respectively) to facilitate SSTR immunolabelling with the robust anti-tag Abs (I, Fig. S3A,B).

Attempts to isolate BON-GS with stable *SSTR2* overexpression were not successful, for the transgene appeared to be poorly tolerated by the cells (presumably, via inducing apoptosis in positive transfects – data not shown). Similar effects, yet less pronounced were also observed in BON-GS with SSTR5. HEK-GS cells, on the contrary, tolerated and successfully maintained high levels of SSTR2, 3 or 5 without apparent effects on cellular well-being (I, Fig. 2A,B). The procured oligoclonal double-stable populations were denoted as HEK-GS/SSTR2_HA, HEK-GS/SSTR3_Myc and HEK-GS/SSTR5_Flag and used in subsequent experiments.

When provoked with OC, HEK-GS/SSTR2_HA and HEK-GS/SSTR5_Flag cells exhibited starkly enhanced cAMP responses as compared to the maternal HEK-GS with endogenous SSTR expression (I, Fig. 3 and Fig. S2A,B). Profound cAMP drop in HEK-GS/SSTR2_HA cells was achieved at 1 nM of OC, with the effect rising further with OC dose and reaching near-maximum at already 10–100 nM of the peptide. In HEK-GS/SSTR5_Flag, significant decrease in intracellular cAMP emerged at 50 nM of OC, with the inhibitory effect increasing dose-dependently till the highest OC dose tested, 5 μM (I, Fig. 3A-E). Differential nature of cAMP responses to OC in HEK-GS/SSTR2_HA and HEK-GS/SSTR5_Flag cells is likely to be related to higher OC affinity to SSTR2 (I, Table S1), which is in agreement with the earlier evidence[358]. Of note, SSTR2 levels in HEK-GS/SSTR2_HA were comparable to endogenous SSTR2 levels in several non-modified cell lines, which signifies physiological relevance of the bioassay (I, Fig. S4A,B).

Ultimately, as HEK-GS/SSTR2_HA cells demonstrated the highest OC sensitivity (OC IC_{50} = 0.3 nM; I, Fig. 3E) and provided the optimal resolving window for the low nanomolar range of ligand concentrations, this strain was used in the majority of targetability experiments in subsequent work.

5.1.3 The targetability bioassay robustly measures intracellular cAMP levels in living cells (I)

To ensure that the signal from GS22/cAMP sensor is truly reflective of intracellular cAMP levels, we subjected HEK-GS/SSTR2_HA cells to a different test for cAMP, AlphaScreen cAMP assay. AlphaScreen is a homogeneous antibody-based end-point competition assay with a luminescent readout[359]. Expectedly, OC response in AlphaScreen closely followed the earlier observed response in GS22/cAMP assay – cAMP levels started to decrease and the near-maximum cAMP inhibition were observed with 10 pM and 10 nM of OC, respectively (I, Fig. S5). With this, the luminescent signal from the GS22/cAMP–harbouring cells reflects the actual changes in intracellular cAMP levels and as such could provide a robust measure of cAMP signaling potency of various SSTR ligands.

5.1.4 The targetability bioassay is sensitive to solvents, which underscores the importance of the matched experimental design (I, II)

High sensitivity of the bioassay to ethanol (EtOH) was already noted in the pilot targetability experiments with the first MSN batches, for these were prepared in absolute EtOH (discussed in section 5.2.1), which lead to EtOH carry-over to the sensor cells and affected the luminescent readout. Indeed, comparative studies of MSN_{250}-PEI, injected to HEK-GS/SSTR2_HA cells with or without prior buffer exchange (the latter case involved EtOH carry-over, whilst in the former case the MSN were cleared of EtOH), supplemented with dose-effect EtOH experiments in HEK-GS, HEK-GS/SSTR2_HA and BON-GS cells, depicted EtOH as a non-linear modifier of FSK response. Specifically, EtOH potentiated positive effects of FSK on cAMP at low levels [0.0001–0.01 % (v/v)], but dose-dependently inhibited cAMP response at higher concentrations (from ≥ 0.1 %; I, Fig. 5, Fig. S7 and Supplementary Information 1). Most importantly, however, despite modifying effects of EtOH on FSK-evoked cAMP generation in the sensor cells, the general pattern and dose-dependency of cAMP response upon SSTR activation with ligands in the presence of EtOH stayed grossly unchanged, which allowed to efficiently expose and measure the extent of specific ligand-induced SSTR signaling (I, Fig. S8).

Subsequent works confirmed sensitivity of the bioassays, utilizing living cells with GS22/cAMP probe, to certain levels of other organic solvents, such as DMF (II, Fig. S2) and DMSO (unpublished data). Other complex solutions without expected pronounced inherent biological activity (such as glycerol-rich buffer of pertussis toxin preparations, characterized in ref [360]) were also found to affect response in the sensor cells. The molecular nature of the described solvent effects remains poorly understood presently. However, a functional alteration of

membranous AC isoforms is likely to be implicated here, for there is mounting evidence that plasma membrane-intercalating chemicals (such as alcohols) could affect conformation and activity of plasma membrane-dwelling proteins by altering plasma membrane fluidity and re-distribution of intramembranous lateral pressure (also discussed in SI 1 of paper I).

In practical terms, any hitherto uncharacterized component of a complex experimental sample should be treated as a possible response modifier in the targetability bioassay, and thus proper measures have to be implemented to keep this in check. With this, we strictly adhered to the dose-matched parallel design in our targetability studies (*i.e.,* every dose of non-targeted MSN was compared head-to-head to the corresponding dose of targeted MSN), and any solvent effects on the luminescent response were accounted for via pair-wise comparisons, allowing us to expose the genuine effects of experimental samples on SSTR signaling. The validity of this approach was further confirmed in the studies of MSN with the preformed protein corona (II, Fig. S6).

5.2 Proof-of-principle: the targetability bioassay is a robust method for *in vitro* evaluation of targeted nanoparticles (I)

5.2.1 MSN design, preparation and functionalization (I)

To evaluate if the bioassay could be used for targetability validation of nanocarriers, we prepared two series of SSTR-targeted MSN, based on similar maternal nanoparticles of different size, MSN_{70} and MSN_{250} (average diameters in a dry state of *ca* 60–70 and 250–300 nm, respectively)[i]. For targeting ligands, we selected three short high affinity SSTR peptides – a natural hormone somatostatin-14 (Sst14) and two synthetic peptide ligands, OC and Cyn-154806. While Sst14 exhibits low-nanomolar affinity to all five SSTR subtypes and thus is considered SSTR pan-agonist, OC preferentially binds SSTR2, and, to a lesser degree, SSTR5. Cyn-154806 has been reported to act as SSTR2-selective antagonist, *i.e.,* the peptide can avidly bind SSTR2 but does not elicit receptor activation (I, Table S1)[361–363].

MSN_{70} and MSN_{250} were further functionalized with poly(ethylenimine) (PEI), which conferred strong positive surface charge to the nanoparticles. MSN_{70} and MSN_{70}-PEI were covalently capped via a *bis*-NHS-PEG linker with Cyn-154806 or

[i] The abbreviation “MeSi” was used in referral to mesoporous silica nanoparticles throughout research paper I; however, in view of the subsequently modified terminology, and for consistency with papers II and III, the abbreviation “MSN” is used to denote mesoporous silica nanoparticles in the thesis.

OC, yielding Cyn-MSN_{70} or OC-MSN_{70}-PEI, respectively. MSN_{250}-PEI were either functionalized with OC in an identical manner (OC-MSN_{250}-PEI), or conjugated with Sst14 with the help of NH_2-PEG-COOH linker in either MES buffer or dimethylformamide (DMF; Sst14-MSN_{250}-PEI/MES or Sst14-MSN_{250}-PEI/DMF, respectively).

Targeting peptide loads varied from 5.6 μg peptide/mg dry MSN weight for Cyn-MSN_{70} to around 20 μg/mg for OC and Sst14-functionalized MSN_{70}-PEI and MSN_{250}-PEI (I, Table 2). Of note, the conjugation with *bis*-NHS-PEG linker was expected to yield a "mixed" capping of MSN, *i.e.,* some OC/Cyn-154806 moieties anchored to MSN via their terminal amines and others via Lys5 of the respective pharmacophores. Only the anchoring in the former position left the peptides' pharmacophores exposed and available for SSTR binding (I, Fig. 4). To increase the fraction of correctly-oriented peptides on MSN surface, OC linking was performed at acidic environment, taking advantage of different pKa values of the terminal amine and the amine group of Lys5[364,365]. Sst14 was selectively coupled to MSN_{250}-PEI via its carboxyl group, ensuring the correct ligand orientation.

The final formulations of MSN_{70} and MSN_{250} came as stock suspensions in absolute EtOH. EtOH ensured extended MSN stability upon refrigerated storage (I, Fig. S6) and safeguarded against microbial contamination. Physicochemical characterization of the nanoparticles is provided in Table 2 of research paper I. Further information on the MSN design, targeting peptide sequences and linking chemistry can be found in the Experimental section and Fig. 4 of the same article.

5.2.2 The targetability bioassay confirms specific SSTR engagement with targeted MSN (I)

The described MSN were assessed for targetability in HEK-GS/SSTR2_HA cells. The MSN working suspensions were prepared directly from the master MSN stocks in absolute EtOH, which resulted to MSN dose-proportional EtOH carry-over, with EtOH final levels in the assay medium generally remaining < 0.5 % (v/v). The effects of EtOH on the bioassay's readout were efficiently accounted for through the parallel matched experimental design (discussed in 5.1.4). The resulting experimental pairs for targetability assessment were: 1) MSN_{70}-PEI *vs.* OC-MSN_{70}-PEI, and MSN_{250}-PEI *vs.* OC-MSN_{250}-PEI, 2) MSN_{250}-PEI/MES *vs.* Sst14-MSN_{250}-PEI/MES, and MSN_{250}-PEI/DMF *vs.* Sst14-MSN_{250}-PEI/DMF and 3) Cyn-MSN_{70} *vs.* MSN_{70}, for OC, Sst14 and Cyn-154806 as targeting ligands, respectively.

Dose-matched comparisons within the listed MSN pairs readily exposed the enhanced ability of all the targeting peptide-functionalized MSN to inhibit FSK-induced cAMP response (I, Fig. 6). This, with all the other factors possibly affecting luminescence fully matched, could only be explained by specific SSTR2 activation

in the sensor cells by the targeting peptides. As the MSN were subjected to targetability assay within 72 h after synthesis, involving several rounds of ample MSN washing, and in view of the excellent ability of MSN to maintain targeting peptide shell upon extended storage under standard conditions (I, Fig. 7), the characterized MSN were very unlikely to be contaminated with the targeting peptides in a free form (*i.e.,* detached from the MSN). The latter aspect in effect allows to attribute the observed cAMP responses to the targeting peptides on the surface of MSN, thus validating their targetability.

Apart from confirming specific SSTR2 engagement with the targeting peptides on MSN, targetability bioassay also yielded several other important observations. Firstly, the experiments exposed varying cAMP response patterns to non-targeted MSN of different sizes and of different surface functionalization (PEI *vs.* non-PEI). More specifically, MSN_{70}-PEI and MSN_{250}-PEI differentially affected cAMP levels in the sensor cells across the same dose-range: MSN_{70} species generally potentiated FSK response, whilst MSN_{250} evoked mild and dose-dependent signal inhibition (I, Fig. 7A/D/C-F).

Furthermore, cAMP response to MSN was clearly affected by PEI functionalization. MSN_{70}-PEI appeared to induce more potent cAMP inhibition as compared to bare MSN_{70} at the same dose (I, Fig. 6A/B *vs.* 6E/G, respectively). In the absence of specific effects on SSTRs, the described cAMP responses could be explained through differential surface charge (MSN_{70} *vs.* MSN_{70}-PEI; I, Table 2) and dissimilar MSN kinetics in solution (MSN-PEI *vs.* non-PEI MSN, and MSN_{70} *vs.* MSN_{250}), with both these aspects affecting MSN-plasma membrane interactions. The described effects of MSN size and surface chemistry on signal in the bioassay further underline the vitality of the matched parallel design for proper targetability evaluation.

Secondly, and contrary to the expected, studies with Cyn-MSN_{70} *vs.* MSN_{70} demonstrated specific SSTR2 activation with Cyn-MSN_{70} (I, Fig. 6E-G). As mentioned earlier, Cyn-154806 had been originally characterized as a SSTR2 antagonist, capable of high-affinity receptor binding, but unable to activate SSTR2. Notwithstanding this, dose-effect studies with free Cyn-154806 in HEK-GS/SSTR2_HA cells further confirmed the ability of the peptide to activate SSTR2 (I, Fig. S9), supporting the observations with Cyn-MSN_{70}. And though Cyn-154806 was clearly less potent in terms of cAMP response as compared to the full SSTR agonists Sst14 and OC, our results collectively depict Cyn-154806 as a weak (partial) SSTR2 agonist rather than a SSTR2 antagonist. Our data is also in agreement with other reports of Cyn-154806 agonistic activity[366,367], which collectively calls for careful re-evaluation of the evidence from earlier studies, utilizing Cyn-154806 as SSTR2 antagonist.

A graphic abstract of research paper I (design & *in vitro* targetability evaluation of MNS) is presented in Fig. 6.

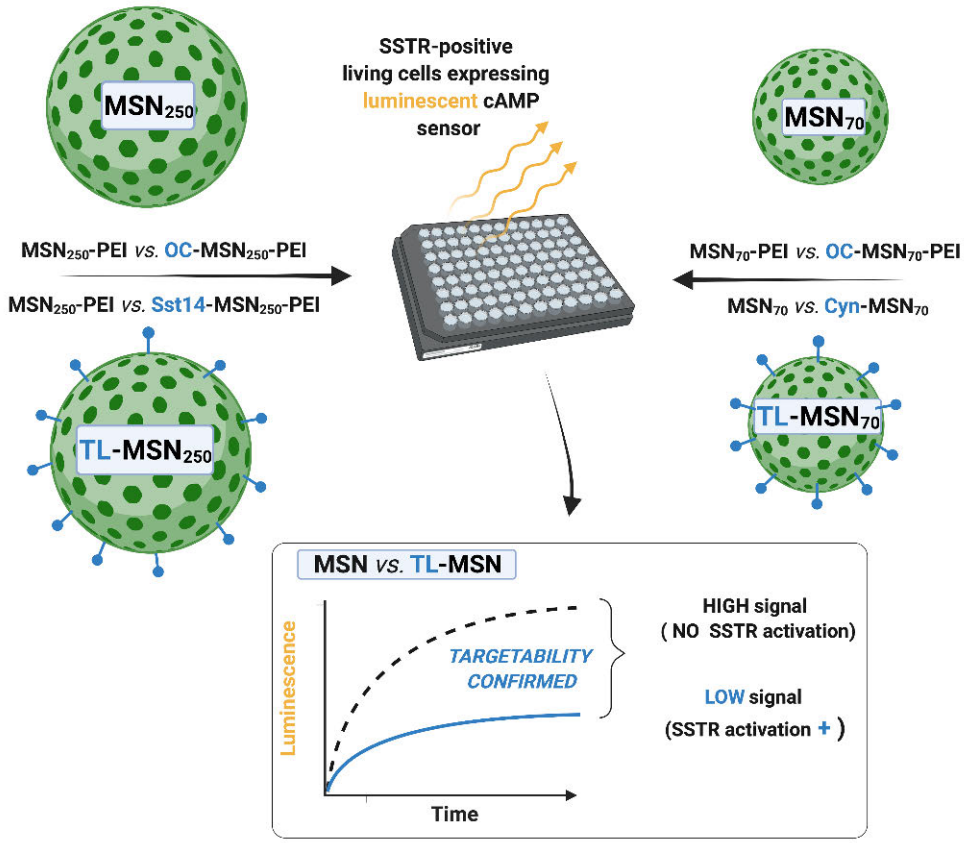

Figure 6. Schematic representation of the MSN design and *in vitro* targetability evaluation in project I. MSN_{250} and MSN_{70} – maternal nanoparticles of mean diameters of *ca* 250 and 70 nm, respectively. Targeting ligands (TL, blue clubs) utilized for MSN functionalization – octreotide, somatostatin-14, or Cyn-154806 (OC, Sst14, or Cyn, respectively). PEI – poly(ethylenimine), SSTR – somatostatin receptors. Further details – in sections 5.2.1-5.2.2 and the Experimental section of the thesis, as well as in research paper I.

5.3 *In vitro* targetability validation of octreotide-functionalized MSN in the presence of serum proteins (II)

After the pilot targetability studies with the MSN_{70} and MSN_{250} discussed in section 5.2.2, we proceeded with MSN targetability evaluation under more biologically-relevant conditions, by administering MSN to the sensor cells in serum-enriched medium. With this, we aimed to characterize the effects of adsorbed proteins (protein

corona) on the ability of targeted MSN to bind and activate SSTRs. The selected experimental design closely mimicked a scenario with *in vivo* systemic administration of MSN, when nanoparticles typically arrive at targeted sites after extended retention in blood circulation and thus almost inevitably carry biocoronas.

In this extension study, we utilized similar nanoparticles (MSN_{180} with a mean diameter of ≈ 180 nm in a dry state)[j] and OC for the active targeting ligand.

Apart from MSN targetability evaluation in the context of protein corona, the extension study pursued several secondary aims. Firstly, acknowledging importance of functional surface for performance of nanoparticles in biotic systems (also corroborated by our own data – refer to the effects of PEI layer and MSN size on cAMP response in the sensor cells, section 5.2.2), we took special steps to prepare a robust negative control for the targeted MSN. To this end, we designed a structurally similar yet expectedly inactive peptide (a.k.a scrambled peptide, SP) to serve as a *silent* counterpart of OC, validated it and used for functionalization of control MSN. The surfaces of the resulting non-targeted MSN_{SP} and actively-targeted MSN_{OC} were thus similarly decorated with small peptides, which accounted for possible non SSTR-specific effects of protein functionalization inherent to comparison of bare MSN with the derived MSN_{OC} (also discussed in 2.1.3.3).

Secondly, acknowledging the limitation of the earlier utilized OC linking protocol, characterized by suboptimal control over directionality of peptide anchoring to MSN surface (section 5.2.1), we evaluated three alternative methods for OC coupling, utilizing protective group chemistry during the peptide synthesis and attachment, in order to ensure correct peptide orientation.

Finally, in view of the inability of the bioassay to reliably discriminate between MSN-bound and free peptide species, which might provide a source of false-positive conclusions, we specifically evaluated targeted MSN for possible peptide shedding under the utilized experimental conditions. With this, a possible input of the liberated peptides in SSTR activation was carefully accounted for, which allowed us to expose the actual input of MSN-bound peptides in the evoked SSTR signaling.

5.3.1 Synthesis and characterization of peptide ligands (II)

To obtain a structurally close, yet targeting-incapable control for the active ligand OC ($_{1D}$Phe-[Cys-Phe-$_{D}$Trp-Lys-Thr-Cys]-$_{8}$Threoninol), we (1) substituted D-Trp4 and Lys5 of the OC sequence with Ala moieties and (2) kept the resulting peptide linear by preventing Cys2–Cys7 bond formation ($_{1D}$Phe-Cys-Phe-Ala-Ala-Thr-Cys-$_{8}$Threoninol; SP). Phe3, D-Trp4, Lys5 and Thr6 were earlier shown to be the

[j] As only these MSN_{180} species were used in papers II and III, for brevity MSN_{180} are referred to as simply "MSN" in this and subsequent sections of thesis.

essential residues, comprising the pharmacophore of OC when stabilized by the mentioned disulfide bond[331,368,369]. Thereby, the derived SP was expected to lose specific affinity to SSTR while maintaining close structural resemblance to OC.

OC and SP were prepared via solid phase peptide synthesis with keeping the side chains of the peptides protected. Purity of the products was confirmed by matrix assisted laser desorption ionization–time of flight mass spectrometry (MALDI-TOF MS; II, Fig. S1). Further details on peptide synthesis can be found in the Experimental section of article II.

To ensure that SP was indeed unable to bind SSTRs, we evaluated the peptide in targetability bioassay with HEK293 cells, overexpressing *SSTR2, 3* or *5*. Dose-matched studies of SP *vs.* its solvent, dimethylformamide (DMF), confirmed that SP evoked no specific cAMP response and thus could not activate SSTR2, 3 or 5 across the dose range of 100 pM–10 μM (II, Fig. S2A-F). The lack of SP agonistic activity towards SSTR2, 3 and 5 did not however preclude the possibility of a silent receptor binding (*i.e.,* SSTR engagement without receptor activation). To address this, we further evaluated SP with the same battery of sensor cells in a competition assay with Sst14, a high-affinity agonist of all five SSTR subtypes (I, Table S1). High SP dose (1 μM) did not alter the pattern and potency of Sst14 response (II, Fig. S3A-G). The latter evidence, collectively with the demonstrated inability of SP to activate SSTRs, in effect verifies that SP does not have significant specific affinity towards SSTR2, 3 or 5.

As the last step, to exclude SP toxicity, we evaluated SP in a mitochondrial respiration–based *in vitro* assay (CCK-8). SP did not affect viability of two unrelated cell lines, HEK-GS/SSTR2_HA (one of the sensor cell lines) and MCF7 (a human breast carcinoma cell line), at concentrations up to 10 μM even after 48 h of treatment (II, Fig. S4A-B). Collectively, the procured evidence depicts SP as a valid negative control ligand for MSN functionalization.

5.3.2 MSN design, preparation and functionalization (II, III)

All the nanoparticles utilized in projects II and III were based on the same maternal MSN with a mean diameter of ≈ 180 nm and were prepared in-house via the established methodology (II, Fig. 1; the Experimental sections of II–III). Peptide functionalization (SP or OC) of the MSN was carried out via three alternative linking protocols: silane coupling or EDC/NHS coupling from two different solvents, methanol (MetOH) or DMF. The derived MSN were denoted as MSN_{OC1}/MSN_{SP1}, MSN_{OC2}/MSN_{SP2} or MSN_{OC3}/MSN_{SP3}, respectively (II, Fig. 2). To enable imaging, all the nanoparticles were covalently labelled with a far-red fluorophore ATTO647N (II, Table S1). The final MSN formulations came lyophilized as single-use pre-

weighted aliquots, which were kept refrigerated (-20 °C) and resuspended in a desired solvent immediately before use.

The peptide loads of MSN, inferred indirectly from the comparative UV/Vis spectroscopy measurements of the stock peptide solutions and the supernatants after the conjugation, are specified in (II, Fig. 3C-D). Of note, the spectroscopy could not discriminate between covalent attachment and physisorption of the peptides to MSN. MSN_{OC1}/MSN_{SP1} and MSN_{OC2} evidently had less of the peptides attached as compared to MSN_{SP2} and MSN_{OC3}/ MSN_{SP3}, indicating that silane coupling was not very efficient under the utilized conditions. Discrepant attachment efficiencies of SP and OC with EDC/NHS linking might be related to differential solubility of the peptides. While OC and SP have excellent solubility in DMF, OC is less soluble in MetOH.

Peptide functionalization did not affect the dispersibility of the nanoparticles, as is evident from the identical hydrodynamic diameters of the MSN in 1 mM KCl (pH=5.0) (II, Fig. 3A). All the MSN types had comparable negative surface charge, which suggest a minor role of charge-related effects in potentially discrepant interactions of different MSN with cells (II, Fig. 3A). Further information on MSN preparation and physicochemical characterization can be found in the Experimental section and the Results section of article II.

5.3.3 MSN do not shed targeting peptides upon reconstitution in aqueous buffer (II)

As pointed out earlier, the targetability bioassay might not be able to discriminate between nanoparticle-bound and free ligand species. With this, for a robust targetability evaluation, a sample prep has to be assessed for possible presence of contaminating free targeting ligands, and if the latter are found in the MSN sample, their input in the net receptor activation has to be estimated.

To evaluate fresh aqueous suspensions of MSN (in 25 mM HEPES, pH 7.4), prepared from the lyophilized MSN stocks, for free targeting peptides, we collected supernatants (SNs) of the MSN preps by centrifugation and subjected them to the targetability bioassay with HEK-GS/SSTR2_HA cells. For all the MSN pairs under comparison, the SNs of MSN_{OC1-3} and MSN_{SP1-3} evoked the same signal in the sensor cells, which excludes the presence of measurable OC levels in the freshly prepared HEPES suspensions of the nanoparticles (II, Fig. 4A-B).

Interestingly, the SNs of both the maternal MSN and of all the SP- and OC-functionalized MSN induced a similar mild drop in intracellular cAMP as revealed through comparison to FSK response (II, Fig. 4B). This effect clearly cannot be attributed to the liberated ligands, for the non-functionalized maternal MSN (*a fortiori* devoid of any targeting peptides) triggered the identical response. The

described phenomenon was highly reproducible and could be speculatively attributed to some dissolution products of the MSN, which could affect the sensor cells and/or their responsiveness to FSK. This further underlines the importance of the matched assay design, which allows for control for possible confounders and safeguards against misinterpretation of the experimental data.

5.3.4 MSN start shedding targeting peptides upon entry to culture medium with 0.1% BSA (II)

With having ensured that fresh aqueous suspensions of MSN do not have significant levels of free targeting peptides, we proceeded with targetability evaluation of $MSN_{SP/OC1}$, $MSN_{SP/OC2}$ and $MSN_{SP/OC3}$ under simplistic conditions, by spiking fresh MSN suspensions in HEPES to HEK-GS/SSTR2_HA sensor cells, bathing in medium with 0.1 % BSA ($Med_{0.1\%BSA}$). As such experimental setup involved a passage of MSN from a monocomponent HEPES buffer to a more complex medium, we initially tested MSN for possible peptide shedding upon their entry to $Med_{0.1\%BSA}$. To address this, we collected the SNs after incubating MSN in $Med_{0.1\%BSA}$ for 5 min at RT and studied the SNs in the targetability bioassay.

Interestingly, all the OC-functionalized MSN shed some quantity of the targeting peptide in $Med_{0.1\%BSA}$, with the amount of the liberated OC being proportional to MSN dose and varying between MSN species (II, Fig. 5C-D). Specifically, MSN_{OC2} shed enough of OC to activate SSTR2 at 20–50 μg/ml, as is evident from the comparisons with the matched SNs of the maternal MSN and MSN_{SP2}. MSN_{OC1} released less of OC under the same conditions, with significant SSTR2 activation by the SN of MSN_{OC1} only observed at 50 μg/ml. MSN_{OC3} clearly demonstrated the least propensity for peptide shedding: at 20 μg/ml, the SNs of MSN_{OC3} and MSN_{SP3} evoked the same response; at 50 μg/ml, the SN of MSN_{OC3} appeared to inhibit cAMP, but the comparison with the respective SN of MSN_{SP3} did not reach significance.

The registered peptide shedding from the MSN surface in $Med_{0.1\%BSA}$ is likely to be explained by the competitive BSA adsorption to the MSN, leading to displacement and liberation of the pre-adsorbed (*i.e.,* non-covalently linked) OC moieties. This observation is in line with the recent study, reporting enhanced release of a viral peptide from MSN in the presence of serum proteins as compared to protein-free buffer[370]. Together with the discussed aspects of differential peptide solubility during MSN peptide functionalization and the related differences in the extent of peptide physisorption, this evidence highlights the importance of pre-evaluating the peptide conjugation stability under complex conditions (presence of proteins).

5.3.5 MSN_{OC1} and MSN_{OC3} demonstrate targetability in the medium with 0.1% BSA (II)

Next, we studied the non-fractionated MSN preps for targetability in $Med_{0.1\%BSA}$ (Fig. 7). Here, MSN_{OC2} and MSN_{OC3} clearly activated SSTR2 as compared to the matched doses of respective non-capped MSN and MSN_{SP}, with the effect becoming significant at 20 μg/ml of MSN and rising further with dose. MSN_{OC1} dose-dependently activated SSTR2 already from 5 μg/ml onwards (II, Fig. 5C-D, 5E-F and 5A-B, respectively). MSN_{SP1}, MSN_{SP2}, MSN_{SP3} and the non-capped MSN evoked the same response in HEK-GS/SSTR2_HA sensor cells, confirming the absence of significant SSTR2 activation with SP-decorated MSN (II, Fig. 5B/D/F).

With accounting for the input of free OC in SSTR2 activation, measured in the SNs experiments (section 5.3.4), the results with the non-fractionated MSN confirm targetability of MSN_{OC1} and MSN_{OC3} in $Med_{0.1\%BSA}$, for neither of these MSN species shed significant OC quantities when suspended in either HEPES (at doses ≤ 50 μg/ml; II, Fig. 4B) or $Med_{0.1\%BSA}$ (at doses ≤20 μg/ml and up to at least 50 μg/ml, respectively; II, Fig. 4D), while retaining ability to activate SSTR2. Taken together, the reviewed evidence attributes the observed cAMP inhibitory effects of MSN_{OC1} and MSN_{OC3} (at doses of 5–20 and 20–50 μg/ml, respectively) to MSN-bound OC, thus validating active SSTR2 targeting with MSN_{OC1} and MSN_{OC3} in $Med_{0.1\%BSA}$.

MSN_{OC2} shed significant amounts of free OC in $Med_{0.1\%BSA}$ already at 20 μg/ml, which was also the lowest dose at which the non-fractionated MSN_{OC2} could clearly activate SSTR2 (II, Fig. 5D). This hindered the deduction of the input of MSN-anchored OC into the net achieved SSTR signaling, precluding targetability claim for MSN_{OC2} in $Med_{0.1\%BSA}$.

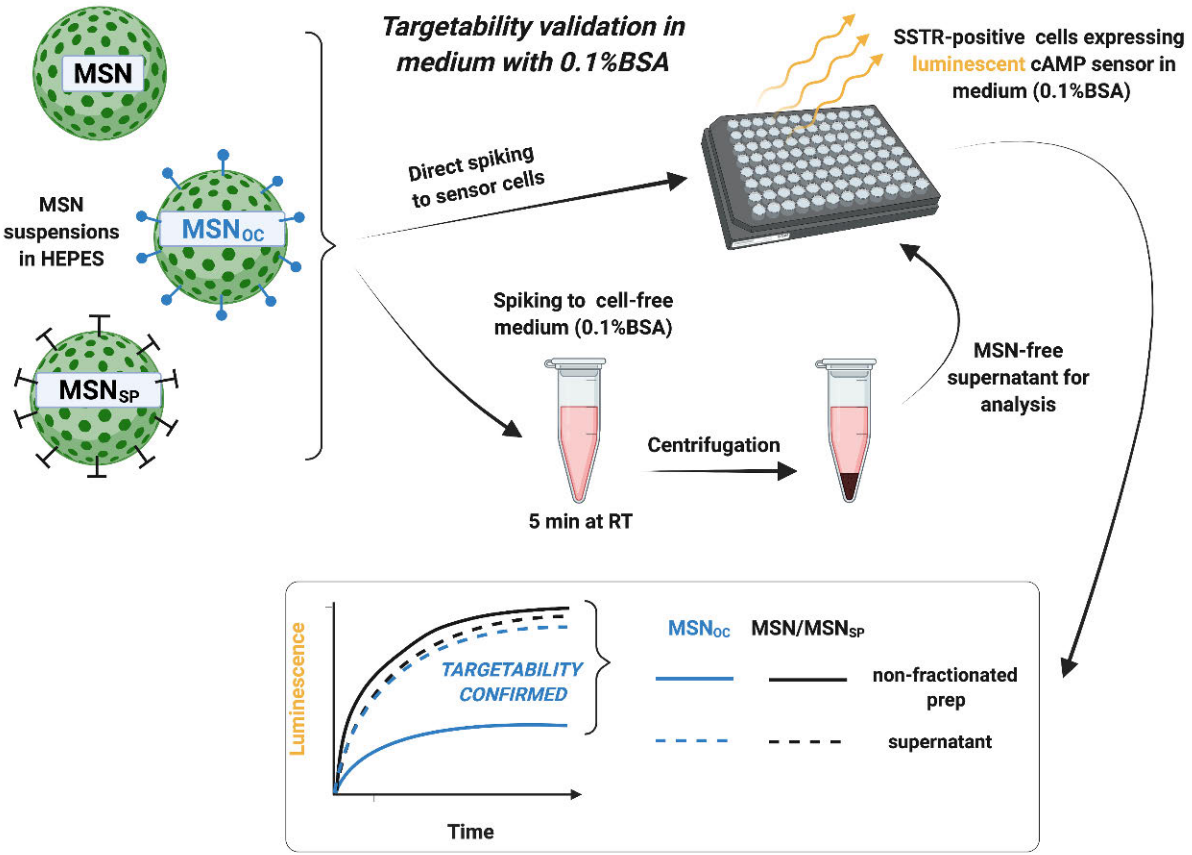

Figure 7. (the legend is on the next page)

5.3.6 MSN_{OC3} retain targetability in the presence of serum proteins (II)

To evaluate the effects of serum proteins and the derived protein corona on MSN ability to engage SSTR, we pre-incubated nanoparticles in serum-enriched medium to allow for protein build-up on MSN surface and subjected the resulting *coronated* MSN to the targetability bioassay with HEK-GS/SSTR2_HA cells, cultured in the same medium that was utilized for MSN corona formation (Fig. 8). We selected $MSN_{OC3/SP3}$ for the experiments, as these nanoparticles shed the least amount of targeting peptides in $Med_{0.1\%BSA}$, which minimized the likelihood of false-negatives due to the liberated ligands in corona studies. Technically, for corona formation, we spiked the freshly prepared MSN suspensions (5 mg/ml in HEPES) into $Med_{10\%iFBS}$ (yielding 1.5 mg/ml of MSN at 7 % w/v iFBS) and incubated the resulting samples for 60 min at +37 °C with agitation, before the final analyses.

SDS-PAGE of the acquired coronas revealed that MSN_{OC3} and MSN_{SP3} had similar corona compositions, with both nanoparticle species adsorbing less serum protein as compared to the non-functionalized maternal MSN (II, Fig. S5). Before targetability studies of the coronated MSN, we ensured that (1) during the corona build-up (1 h at +37 °C in serum-supplemented medium), free OC retains stability and signaling competence, and that (2) aqueous HEPES suspensions of MSN_{OC3} do not shed significant amounts of targeting peptides under similar conditions (1 h at +37 °C) (II, Fig. S6A-B and S6C, respectively). These experiments (1) allowed us to exclude the possibility of OC degradation during the pre-incubation phase as a possible cause of false-negative results and (2) eliminated temperature and time factors as driving forces for MSN disintegration.

Despite some technical challenges (serum affected the performance of the sensor cells, narrowing dynamic range and increasing noise in the assay), partially ameliorated by increasing MSN dose, targetability studies unambiguously demonstrated that the coronated MSN_{OC3} could still engage the targeted receptors. Specifically, MSN_{OC3} activated SSTR2 in the sensor cells at 50 μg/ml, which in the absence of significant free OC shedding, verified by probing the matched SNs, confirmed targetability of MSN_{OC3} even in the presence of protein corona (II, Fig. 6A-C). Targetability validation at higher MSN_{OC3} doses (75 μg/ml) was hindered by significant OC shedding (II, Fig. 6C).

◄ **Figure 7.** Schematic representation of MSN targetability evaluation in medium with 0.1 % BSA *in vitro*. The active targeting peptide octreotide (OC) and the inactive scrambled peptide (SP) depicted as blue clubs and black Ts, respectively. Further details – in sections 5.3.4–5.3.5 and the Experimental section of the thesis, as well as in research paper II.

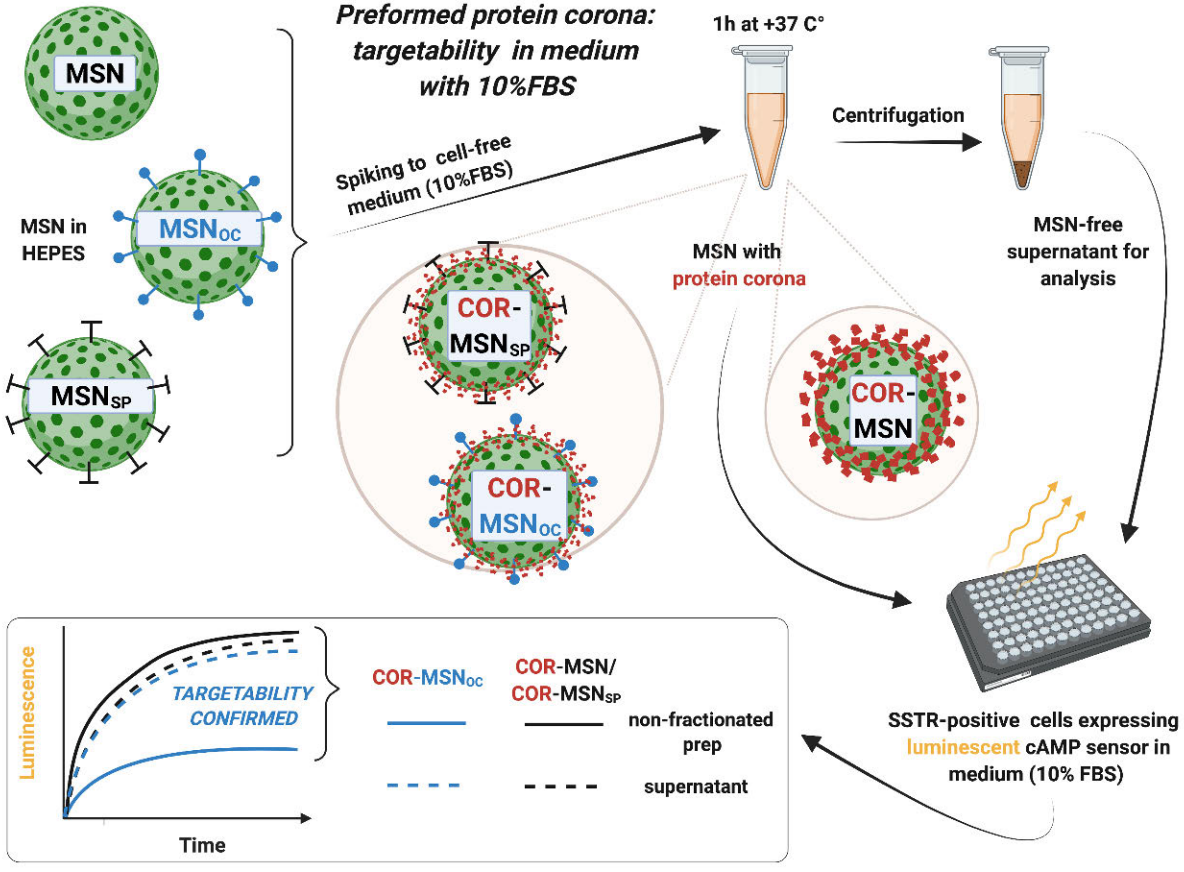

Figure 8. (the legend is on the next page)

5.4 SSTR5/2 targeting downregulates *in vitro* cellular uptake of MSN with protein corona (III)

5.4.1 Rationale for MSN internalization studies and generation of cells with varying expression of *SSTR5* and *2* (III)

In project II (section 5.3), we demonstrated that a particular MSN subtype (MSN_{OC3}, peptide-functionalized via EDC/NHS in DMF) could specifically bind and activate SSTR in the living cells both in serum-depleted and serum-enriched media. The latter case involved preincubation of nanoparticles in $Med_{10\%iFBS}$ for 1 h at +37 °C before treatment, thus MSN_{OC3} already carried the layer of adsorbed proteins on their surface (the preformed protein corona, COR-MSN_{OC3}) by the moment of initial contact with the cells, which closely resembles the scenario with *in vivo* systemic MSN administration.

In the follow-up project (III), we proceed with the preformed corona setup and evaluate whether SSTR targeting with COR-MSN_{OC3} affects cellular uptake of the targeted nanoparticles. We compare *in vitro* accumulation of the targeted and non-targeted nanoparticles in two unrelated cell lines, HEK293 and BON1, and in the derived strains, genetically modified for differential SSTR5 and SSTR2 expression (III, Table 1). This experimental setup should not only test the hypothesis of a positive link between SSTR targeting and cellular accumulation for a given targeted nanocarrier, but also expose the role of specific SSTR subtypes in the possible targetability-associated effects.

The targeting peptide OC predominantly binds SSTR2 and, less avidly, SSTR5 and 3 (the relative OC affinity for SSTR2 >> SSTR5 > SSTR3), but has no significant affinity for the remaining two receptors in the family, SSTR1 and SSTR4[4,354,371]. Earlier SSTR profiling depicted SSTR5 as the main OC target in the wild-type BON1 (BON/$SSTR_{WT}$) and HEK293 (HEK/$SSTR_{WT}$), with both the cell lines harbouring extremely low levels of SSTR2 and only BON1 being positive (weakly) for SSTR3[354]. Thus, to enable studies of SSTR5-specific effects on MSN internalization, we developed both the *SSTR5*-null and *SSTR5*-stably overexpressing

◄ **Figure 8.** *In vitro* targetability evaluation of MSN with protein coronas. The active targeting peptide octreotide (OC) and the inactive scrambled peptide (SP) depicted as blue clubs and black Ts, respectively. Coronas of serum proteins (COR), acquired with MSN incubation in $Med_{10\%iFBS}$, depicted as red patchy halos around the nanoparticles (MSN adsorbed more of protein as compared to MSN_{OC3}/MSN_{SP3}, and thus the respective COR is *thicker* on the picture). Further details – in section 5.3.6 and the Experimental section of the thesis, as well as in research paper II.

strains from the maternal WT cultures (BON/SSTR5$_{KO}$, HEK/SSTR5$_{KO}$ and BON/SSTR5$_{OE}$, HEK/SSTR5$_{OE}$, respectively). Each of the resulting *SSTR5 query triplets* of BON1 and HEK293 strains encompassed the broad SSTR5 expression range (from SSTR5 absence in SSTR5$_{KO}$ cells to weak/moderate levels in SSTR$_{WT}$ to high receptor abundance in SSTR5$_{OE}$ cultures), collectively devised to expose SSTR5 role within the context of MSN$_{OC3}$ targeting.

In a similar manner, we also combined HEK293 cells with stable SSTR2 overexpression (HEK/SSTR2$_{OE}$) with the maternal HEK/SSTR$_{WT}$ culture, obtaining a *SSTR2 query pair* (virtually no SSTR2 in SSTR$_{WT}$ cells *vs.* high SSTR2 abundance in SSTR2$_{OE}$ cells) to study SSTR2-specific effects on MSN uptake. Overview of the cell lines, utilized in the uptake studies of MSN, is presented in Table 1 (III).

HEK/SSTR2$_{OE}$ and HEK/SSTR5$_{OE}$ cells were earlier established and characterized in-house (projects I–II). BON/SSTR5$_{OE}$ were established from BON1 cells, stably-overexpressing GS22/cAMP, by means of *SSTR5* transfection (a plasmid, allowing for balanced expression of human *SSTR5* and *mCherry* fluorescent protein via P2A linker) and iterative FACS-aided enrichment of the *SSTR5*-stable clones, based on mCherry signal, as described in section 4.2.2.5. *SSTR5* expression in the procured oligoclonal culture of BON/SSTR5$_{OE}$ was validated by immunolabelling (III, Fig. S2I-K).

SSTR5-null strains were established by means of CRISPR/Cas9 editing in the WT BON1 background and in HEK293 with stable overexpression of GS22/cAMP, as detailed in the Experimental section and Table S1 of III. The selected SSTR5 knockout clones, BON/SSTR5$_{KO}$ (A11) and HEK/SSTR5$_{KO}$ (B8), were found to harbour the identical rearrangement of *SSTR5*, represented by a homozygous loss of 983 nts, in effect signifying deletion of *ca* 90 % of the CDS (III, Fig. S1). The loss of SSTR5 on a protein level in both of the clones was also validated by immunolabelling (III, Fig. S2A-H).

5.4.2 Dissimilar protein coronas translate into differential cellular accumulation of MSN and MSN$_{SP3}$ (III)

Before the actual endocytosis experiments with the targeted MSN$_{OC3}$, we evaluated uptake rates of both the candidate non-targeted controls, the maternal MSN and the derived MSN$_{SP3}$. As discussed in section 5.3.1, MSN$_{SP3}$ were functionalized with SP, which structurally resembles the active ligand OC but cannot engage SSTR. Thereby, MSN$_{SP3}$ were devised to make a structurally more relevant non-targeted pair for MSN$_{OC3}$ as compared to the maternal MSN, devoid of any peptide moieties on the surface.

MSN and MSN$_{SP3}$ were incubated in Med$_{10\%iFBS}$ for 1 h at +37 °C to acquire protein coronas (yielding COR-MSN and COR-MSN$_{SP3}$, respectively) and then

administered to BON/$SSTR_{WT}$ and HEK/$SSTR_{WT}$, equilibrated in 10% iFBS-supplemented media. FC studies revealed a uniformly elevated uptake of COR-MSN_{SP3} in both cell types, exceeding uptake of COR-MSN at 20 μg/ml dose in BON/$SSTR_{WT}$ and HEK/$SSTR_{WT}$ up to *ca* 4-fold and 5-fold, respectively (III, Fig. 1C-D). Importantly, the enhanced COR-MSN_{SP3} uptake was observed after both 2 h and 24 h of treatment and persisted at different doses of nanoparticles (5-50 μg/ml; III, Fig. 1). Fluorescence microscopy further confirmed the results of FC uptake experiments, with COR-MSN_{SP3} clearly achieving higher accumulation rates in both BON/$SSTR_{WT}$ and HEK/$SSTR_{WT}$ at 5 μg/ml after 24 h of treatment (III, Fig. 2A-I and Fig. 2J-R).

Such a profound and consistent difference in uptake of the coronated MSN_{SP3} and MSN in two unrelated cell lines was very intriguing. The elevated cellular accumulation of COR-MSN_{SP3} is unlikely to be explained with inherent biological activity of SP, for SP was earlier confirmed to be unable to bind SSTR2, 3 or 5 and induced no *in vitro* toxicity even at low-μM concentrations (section 5.3.1). Neither could the enhanced COR-MSN_{SP3} uptake be attributed to toxicity of the SP-functionalized nanoparticles, for MSN_{SP3}, just like as MSN, exerted no pronounced effects on HEK/$SSTR_{WT}$ or BON/$SSTR_{WT}$ in either mitochondrial respiration–based toxicity assay (III, Fig. S3A-B) or live cell microscopy–based toxicity screen (III, Fig. S4A/E-H).

MSN and MSN_{SP3} have very similar physicochemical characteristics (*i.e.,* hydrodynamic diameter and surface charge) in aqueous solution (II, Fig.3). However, SDS-PAGE studies of protein coronas, acquired in $Med_{10\%iFBS}$, revealed that MSN_{SP3}, just like as MSN_{OC3}, adsorbed up to 50 % less of protein as compared to MSN, which could be related to steric effects of SP/OC moieties on the surface of peptide-functionalized nanoparticles (section 5.3.6). With the experimental conditions for COR-MSN *vs.* COR-MSN_{SP3} in uptake studies fully matched otherwise, the reviewed evidence strongly implies differential protein coronas as the major factor behind discrepant internalization of the coronated MSN and MSN_{SP3}.

To further evaluate the effects of the protein corona on endocytosis of nanoparticles, we directly administered fresh aqueous suspensions of MSN and MSN_{SP3} to BON/$SSTR_{WT}$ and HEK/$SSTR_{WT}$ cells, whilst keeping the other experimental conditions unchanged. Here, neither of nanoparticles carried pre-adsorbed protein on the surface at the moment of treatment initiation, in contrast to the COR-MSN and COR-MSN_{SP3} in the preformed corona experiment. FC analysis demonstrated that COR-MSN_{SP3} were internalized more avidly by both the cell lines after 24 h as compared to MSN_{SP3} administered as HEPES suspension (III, Fig. S5A/B). MSN without the preformed corona showed a trend towards decreased uptake at 5 and 20 μg/ml dose levels in BON/$SSTR_{WT,}$ yet the comparisons with COR-MSN did not reach significance. In HEK/$SSTR_{WT}$, COR-MSN and MSN

without the preformed corona had similar uptake rates. Most importantly though, the profound uptake difference, observed between MSN_{SP3} *vs.* MSN under the preformed corona setup, was absent when the nanoparticles had no preformed corona (compare Fig. S5C and Fig. 1C (both – III), respectively). In effect, these results highlight protein corona as an important regulator of MSN internalization in the utilized experimental setup and leave very little doubt that the observed enhanced uptake of COR-MSN_{SP3} is predominantly mediated by the protein corona.

Another ramification of MSN *vs.* MSN_{SP3} studies is that the maternal non-functionalized MSN would make an invalid negative control for uptake experiments with targeted MSN_{OC3} under the preformed corona setup. Indeed, MSN and MSN_{OC3} obtain distinct coronas in serum-enriched medium as a consequence of differential surface functionalization, which does not allow for control over the corona effects. It is MSN_{SP3} that should be used as a proper non-targeted control for MSN_{OC3} instead, for MSN_{SP3} and MSN_{OC3} maintain very close surface properties after functionalization with structurally similar peptides, which translates into similar coronas in $Med_{10\%iFBS}$, thus keeping corona effects on cellular uptake in check.

5.4.3 SSTR5/2 targeting is associated with decreased *in vitro* uptake of MSN_{OC3} with the protein corona (III)

Next, we evaluated cellular accumulation of COR-MSN_{SP3} *vs.* COR-MSN_{OC3} in the SSTR5 query triplets ($SSTR_{WT}$ *vs.* $SSTR5_{OE}$ *vs.* $SSTR5_{KO}$) of BON1 and HEK293, and in the SSTR2 query pair ($SSTR_{WT}$ *vs.* $SSTR2_{OE}$) of HEK293 cells (III, Table 1). COR-MSN_{SP3} and COR-MSN_{OC3} share nearly identical physicochemical features and similar coronas, with the only functional difference between the nanoparticles being the targeting moiety (SP *vs.* OC). Thus, the selected experimental design was expected to reveal SSTR5/2 targeting–specific effects on cellular accumulation of COR-MSN_{OC3}.

FC studies revealed quite unexpected and intriguing relation between SSTR5/2 expression and relative cellular accumulation of the coronated MSN_{SP3} and MSN_{OC3} (III, Fig. 3). The cardinal features were: 1) uniformly and profoundly decreased uptake of COR-MSN_{OC3} as compared to COR-MSN_{SP3} in all of the cell types, positive for SSTR5 or 2 (both endogenous expression and overexpression), and 2) loss of the above difference, *i.e.,* almost equal uptake of COR-MSN_{OC3} and COR-MSN_{SP3} in SSTR5-null cells. Already perceivable upon visual evaluation of median fluorescence intensities (FI) of the nanoparticle-treated cells (III, Fig. 3A/D), the described uptake patterns become even better defined with quantitative comparisons by means of COR-MSN_{SP3}/COR-MSN_{OC3} *relative flux*, estimated as a ratio of median FI values in a given cell strain after respective treatments (III, Fig. 3B-C/E-F). Assuming that COR-MSN_{SP3} uptake reflects accumulation capacity for COR-

MSN_{OC3} in the absence of any SSTR activation in a given cell type, the MSN_{SP3}/MSN_{OC3} flux index should provide a robust quantitative estimate of how SSTR targeting affects cellular uptake of nanoparticles.

The evaluation of COR-MSN_{SP3}/COR-MSN_{OC3} fluxes in BON1 cells established that COR-MSN_{OC3} accumulated up to 4-5 time less than COR-MSN_{SP3} in the cells with endogenous SSTR5 expression, whilst SSTR5 overexpression decreased the uptake difference to *ca* 2–3-fold. Paradoxically, SSTR5 loss almost equalized the uptakes of COR-MSN_{OC3} and COR-MSN_{SP3} (relative flux of *ca* 1–1.5), rather than increasing the difference further from the flux level of $BON/SSTR_{WT}$. Such a relation between STTR5 abundance and the uptake COR-MSN_{SP3}/COR-MSN_{OC3} in BON1 cells was observed both after 2 h and 24 h of treatment (III, Fig. 3B-C).

Very similar relation between COR-MSN_{SP3}/COR-MSN_{OC3} flux and SSTR5 expression was also registered in HEK293 cells, yet with somewhat less pronounced differences in flux values between the cell types after 24 h. HEK293 with SSTR2 overexpression had comparable COR-MSN_{SP3}/COR-MSN_{OC3} flux to $HEK/SSTR5_{OE}$ (COR-MSN_{SP3}/COR-MSN_{OC3} flux for $HEK/SSTR_{WT}$ > $HEK/SSTR5_{OE}$ ≈ $HEK/SSTR2_{OE}$ > $HEK/SSTR5_{KO}$; III, Fig. 3F-G).

Apart from the similar dependence of COR-MSN_{SP3}/COR-MSN_{OC3} flux on SSTR5/2 expression, BON1 and HEK293 cells exhibited otherwise distinct kinetics of MSN accumulation. The uptake of coronated MSN_{SP3} and MSN_{OC3} generally diminished with treatment time in BON1 strains, yet just the reverse was observed in HEK293 (compare FI values within the BON1 and HEK293 query sets after 2 h and 24 h of treatment; III, Fig. 3A/D). This discrepancy most likely reflects inherent differences in endocytosis and/or exocytosis in the utilized cell lines.

Fluorescence microscopy confirmed the FC findings in both BON1 and HEK293 query sets (III, Fig. 4 and Fig. 5). Microscopy also demonstrated that majority of nanoparticles were confined to cytoplasmic compartment of the cells, which indicates that the bulk of fluorescence signal in FC studies was indeed coming from the internalized nanoparticles.

Importantly, with the exclusion of $HEK/SSTR2_{OE}$ that selectively responded with moderate growth inhibition to MSN_{OC3} at doses of 20 μg/ml or higher (III, Fig. S3B and Fig. S4B/G-L), neither cell type in the BON1 or HEK293 query sets exhibited signs of overt toxicity or altered proliferation upon extended treatment (up to 48 h) even with the high doses of MSN_{SP3} or MSN_{OC3} (up to 50 μg/ml in live cell microscopy–based toxicity screen or up to 100 μg/ml in CCK-8 proliferation assay; III, Fig. S4A/C-D/F-H and Fig. S3A/C-G, respectively). This in effect allows to exclude nanoparticles-induced toxicity as a possible reason for the observed differential uptake of MSN_{SP3} and MSN_{OC3}.

Taken together, internalization studies of the coronated MSN_{SP3} and MSN_{OC3} with FC and fluorescence microscopy establish that the targeted nanoparticles

accumulate much less than their non-targeted counterparts in cells expressing SSTR5 or SSTR5+2, but this uptake difference is almost negated upon SSTR5 loss. Such an uptake pattern was independently registered in the two unrelated cell lines with varying SSTR expression, featuring otherwise distinct kinetics of nanoparticle accumulation. Also, the described SSTR dependence of COR-MSN_{SP3}/COR-MSN_{OC3} flux persisted across a range of MSN doses (5–50 μg/ml) and treatment times (2–24 h) and could not be explained with toxicity of the nanoparticles. The reviewed evidence confirms SSTR5/2 involvement in uptake regulation of the COR-MSN_{OC3} and urges to reconsider the applicability of the conventional active targeting concept for nanoparticles in case of somatostatin receptors.

5.4.4 SSTR5/2 as bidirectional regulators of MSN endocytosis: a putative model and outlook (III)

The established relation between SSTR5/2 expression and *in vitro* uptake of the coronated MSN_{SP3} and MSN_{OC3} in BON1 and HEK293 cells does not comply with the conventional model of receptor targeting (the ART model, section 2.1.3), which in its simplified form implies a positive linear correlation between targeted receptor abundance and endocytosis of targeted nanoparticles. In fact, the procured evidence suggests a much more complex link between SSTR expression and uptake of the targeted MSN. In an attempt to explain the observations from our endocytosis experiments, we propose *an alternative targeting model*, which assumes a dual role of SSTR5/2 as of high-affinity binding sites and negative regulators of endocytosis (Fig. 9). This alternative model, which in simple words could be also described as a model of *a positive anchor with a negative loop*, suggests that both these SSTR subtypes: 1) facilitate adherence of targeted nanoparticles to plasma membranes of SSTR-expressing cells by virtue of high affinity ligand-receptor interactions (a positive anchoring), yet simultaneously 2) inhibit nanoparticle internalization–relevant cellular machinery via ligand-provoked downstream SSTR signaling (a negative loop). Hereby, the model stipulates that the resulting uptake rate of a SSTR-targeted nanocarrier would reflect the net sum of the above heterodromous (oppositely directed) processes with mutual dependence on SSTR5/2 abundance. The renowned function of SSTRs as of negative regulators of cell proliferation, secretion and motility ("cellular brakes"; discussed in 2.1.6) is thus recognized in the alternative model, as contrasted to the ART model, which predominantly considers targeted receptors for "passive anchors" and tends to disregard a possible influence of targeting ligand–evoked receptor signaling on endocytosis.

Under the assumption that the only difference between COR-MSN_{SP3} and COR-MSN_{OC3} is the targeting moiety, the alternative model predicts: 1) an equal uptake of COR-MSN_{OC3} and COR-MSN_{SP3} (MSN_{SP3}/MSN_{OC3} flux tending 1.0) in SSTR5/2-

devoid cells and 2) a specific MSN_{SP3}/MSN_{OC3} flux in a given cell type at a given SSTR5/2 expression, which might take values above, below or near 1.0, depending on whether (and to which degree) the negative SSTR signaling prevails over the positive SSTR anchoring or *vice versa*. MSN_{SP3}/MSN_{OC3} fluxes, registered in the BON1 and HEK293 query sets, show a reasonably good fit with the above predictions. Specifically, flux values in the cells with virtually no receptors for OC (BON/$SSTR5_{KO}$ and HEK/$SSTR5_{KO}$) revealed about equal uptakes of COR-MSN_{OC3} and COR-MSN_{SP3} (the relative flux tending 1.0). In the cells with endogenous SSTR5 expression (BON/$SSTR_{WT}$ and HEK/$SSTR_{WT}$) COR-MSN_{OC3} were accumulating up to several fold less as compared to COR-MSN_{SP3}, which could be explained by the dominance of inhibitory SSTR5 effects on endocytosis over a relatively minor promotion of MSN_{OC3} uptake by anchoring at the modest SSTR abundance.

The cells with overexpression of SSTR5 or SSTR2 (BON/$SSTR5_{OE}$, HEK/$SSTR5_{OE}$ or HEK/$SSTR2_{OE}$) featured some decrease in MSN_{SP3}/MSN_{OC3} flux as compared to the cells with endogenous SSTR levels. This effect could be understood in terms of a relatively higher increment in positive anchoring *vs.* negative signaling, but with the remaining dominance of the latter mechanism upon SSTR overexpression. In other words, SSTR5/2 signaling capacity rises with SSTR expression but reaches saturation at some receptor level due to the limited availability of second messengers or other mediators of signal transduction. However, the anchoring effect faces no such a limit, and the cumulative cellular affinity for MSN_{OC3} continues to expand proportionally to SSTR abundance in the plasma membrane of the cells.

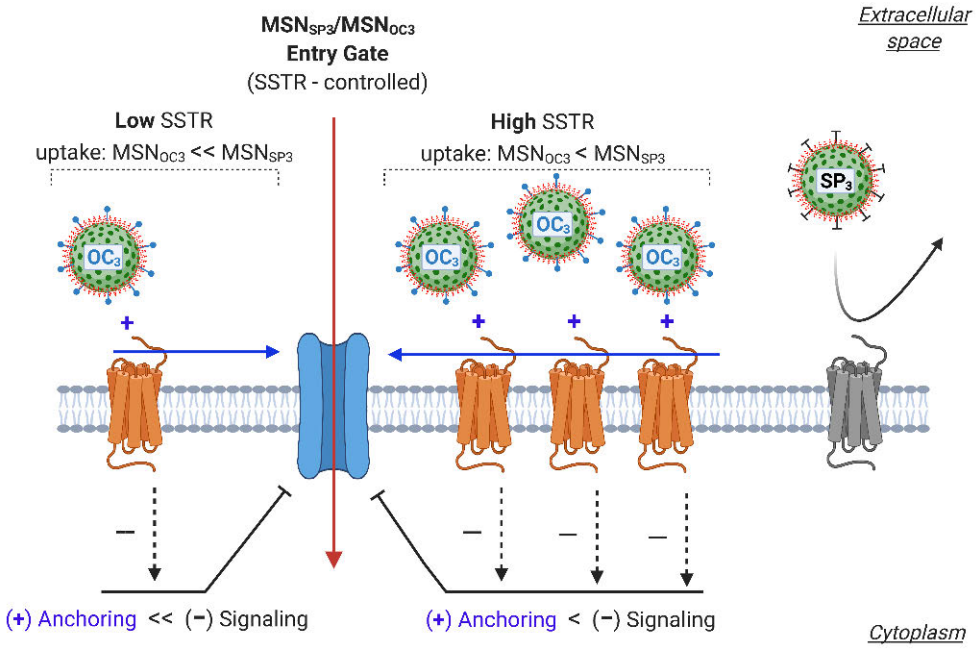

Figure 9. SSTR5/2 as bidirectional regulators of endocytosis of coronated MSN: a putative model. The proposed model of *a positive anchor with a negative loop* implies that SSTR5 and SSTR2 not only promote internalization of targeted nanoparticles by providing high affinity binding sites on plasma membranes (positive anchoring; blue arrows and *plus* signs), but also simultaneously inhibit (black dashed lines with *minus* signs) cellular internalization machinery for nanoparticles (entry gate). Thus, the resulting uptake of a targeted nanocarrier would be determined by the net effect of competing forces (positive anchoring *vs.* negative signaling), both emerging upon interaction of SSTRs with targeting ligands. The model allows for SSTR5/2 positioning both within the entry gate (as an immediate component of the internalization complex) and outside of it (as a remote direct or indirect gate regulator).

Events to the left and to the right side of the entry gate on the schematics – scenarios for COR-MSN_{OC3} internalization in cells with low SSTR5/2 abundance (*e.g.,* endogenous expression, as in BON/$SSTR_{WT}$ and HEK/$SSTR_{WT}$) or elevated SSTR5/2 expression (*e.g.,* BON/$SSTR5_{OE}$ and HEK/$SSTR5_{OE}$), respectively. In the former case, inhibition of the entry gate by SSTRs exceeds the internalization-promoting anchoring effect, which translates into a decreased uptake of COR-MSN_{OC3} *vs.* the non-targeted COR-MSN_{SP3}. In the latter case, the anchoring effect increases along with SSTR abundance, yet the inhibitory SSTR signaling continues to prevail, but its dominance over the anchoring is not that pronounced any more. This leads to a moderate increment in COR-MSN_{OC3} uptake, manifested as a decreased MSN_{SP3}/MSN_{OC3} flux in cells with SSTR overexpression. Importantly, MSN_{SP3} and MSN_{OC3} are assumed to have identical coronas and thus to utilize the same entry gate. Coronated MSN_{SP3} can neither bind nor activate SSTR5 or 2, and thus COR-MSN_{SP3} uptake reflects the capacity of the entry gate in a given cell type to internalize COR-MSN_{OC3} *without* SSTR activation. As a consequence, the model also predicts equal uptakes of COR-MSN_{OC3} and COR-MSN_{SP3} in SSTR5- and SSTR2-null cells. Refer also to the main text.

Ligand-activated and inactive (quiescent) SSTRs, dwelling in a plasma membrane (lipid bilayer) are colored orange and grey, respectively. Coronated MSN_{OC3} and MSN_{SP3} are depicted as green spheres, carrying either the active ligand (OC; blue clubs) or its inactive counterpart (SP; black Ts). Red halo around the spheres depicts protein corona.

Despite a good fit with the experimental data, the alternative model admittedly remains rather speculative at the current stage and warrants further scrutiny. Confirmative (or refuting) evidence might follow from uptake experiments involving competition with free targeting ligands[k]. More specifically, demonstration of down-regulation of COR-MSN_{SP3} uptake with co-administration of free OC selectively in SSTR5 and SSTR2-positive cells would in effect confirm regulatory function of these receptor subtypes in MSN endocytosis. Further decrease of COR-MSN_{OC3} uptake in the same cell types upon competition with OC would also support the alternative model. In the latter case, the free ligands should activate and internalize SSTRs, leading to receptor depletion in plasma membranes, thus promoting the negative signaling over the positive anchoring.

Alternatively, failure of free ligands to affect internalization of COR-MSN_{SP3} and COR-MSN_{OC3} in SSTR5 or SSTR2-expressing cells would directly contradict the alternative model and thus render it highly implausible. If this happens to be the case, it would be very difficult to explain the observed discrepant uptake of COR-MSN_{SP3} and COR-MSN_{OC3} by other factors than a different nanobiointerface (*i.e.,* minor yet functionally significant differences between coronas), putatively stemming from subtle structural difference between SP and OC (and respective surface functionalizations) and ultimately affecting interactions of nanoparticles with cells (refer also to 2.1.3.3). However, the very similar SSTR dependence of COR-MSN_{SP3}/COR-MSN_{OC3} flux in the two unrelated series of cell lines makes the latter hypothesis *apriori* less likely, in effect rendering it the hypothesis of exclusion.

The alternative model stipulates that both SSTR5 and SSTR2 act similarly as bidirectional regulators of endocytosis. Though this assumption is based on general concordance of COR-MSN_{SP3}/COR-MSN_{OC3} flux patterns in the SSTR2 query set *vs.* the SSTR5 sets, the relative uptake of the targeted and non-targeted nanoparticles was not evaluated in a combination *SSTR2*-null *vs.* SSTR2-positive, for both HEK/$SSTR_{WT}$ and HEK/$SSTR2_{OE}$ also express SSTR5 (III, Table 1). With this, diminished uptake of COR-MSN_{OC3} *vs.* COR-MSN_{SP3} in a pure SSTR2-positive background, confirming functional convergence of SSTR2 and SSTR5, awaits prospective validation.

As a last note, the proposed SSTR5/2-specific alternative model assumes that both MSN_{OC3} and the non-targeted MSN_{SP3} utilize the same endocytosis machinery, with the assumption being based on size, surface properties and protein corona similarities of nanocarriers in question. However, it could be also envisioned that targeting ligands on MSN_{OC3} may engage different machinery for MSN_{OC3}

[k] Currently restricted to SSTR agonists, due to paucity and limited availability of potent SSTR subtype–specific antagonists.

internalization via SSTR5/2 coupling, resulting in MSN_{OC3} and MSN_{SP3} utilizing dissimilar endocytosis routes. The latter may impinge on intracellular trafficking, sorting and exocytosis of nanoparticles, underlying the observed dissimilar *in vitro* cellular accumulation of COR-MSN_{OC3} and COR-MSN_{SP3}. However, the shortage of relevant experimental data as of now and the increased number of variables preclude modelling of the scenario implying distinct endocytosis routes for coronated MSN_{SP3} and MSN_{OC3}. Further studies (specifically, time-resolved evaluation of MSN endocytosis, trafficking and exocytosis, supplemented with spatial mapping and use of pathway-specific inhibitors) should better delineate the molecular machinery, underpinning cellular accumulation of COR-MSN_{SP3} and COR-MSN_{OC3} *in vitro* and particular role(s) of SSTR5/2 in this regard.

6 Summary and Concluding Remarks

In pursuit of the major objective of the thesis, *i.e.,* to estimate how SSTR targeting affects internalization of MSN under biologically-relevant conditions *in vitro*, we sequentially progressed through the following steps:

- We designed and synthesized an array of SSTR-targeted and control (non-targeted) MSN. This included evaluation of nanoparticles of different sizes and surface functionalization, as well as testing of several targeting peptides and varying conditions for peptide linking.
- We developed and validated *in vitro* bioassay able to sensitively measure SSTR activation in living cells with targeting ligands and utilized it to evaluate the prepared MSN for targetability both in protein-depleted and serum-enriched media. Thereby, we identified the particular MSN subtype (MSN_{OC3}) that retains targetability despite adsorption of serum proteins onto its surface (protein corona). The latter was particularly important, for nanoparticles inevitably acquire coronas upon *in vivo* administration, which in turn shape their functional surface and affect interaction with cells.
- We generated a series of cell lines of varying SSTR5/2 abundance (*i.e.,* from complete SSTR absence to overexpression) and utilized these for *in vitro* internalization experiments in serum-enriched medium with MSN_{OC3} and its non-targeted counterpart, MSN_{SP3}. This allowed us to expose the functional roles of SSTR5/2 in the context of cellular uptake of MSN bearing protein corona, eventually bringing us to the main objective of the study.

The thesis clearly resides at the interface of nanoscience, inorganic chemistry and molecular cell biology and as such contributes to all of these fields.

The most important chemical aspects, addressed in the thesis, concern surface functionalization of MSN with short peptides. We evaluated several approaches for peptide conjugation, utilizing different linkers and coupling conditions and yielding

varying MSN peptide loads. By combining physicochemical methods with the targetability bioassay, we studied how peptide linking chemistry affects MSN targetability in the absence or presence of serum proteins.

Specifically, we identified that different linking protocols produce MSN featuring distinct propensity for peptide shedding upon contact with protein-containing media. The phenomenon of peptide shedding appears to originate from the pool of loosely-adhered peptides, which *non-specifically stick* to MSN during the initial peptide functionalization by virtue of physisorption and later get displaced from the surface once MSN enter more complex media (possibly, due to competition with other proteins/molecules in solution). This finding suggests that the utilized linking methods frequently lead to the mixed MSN capping of both covalently bound and loosely adsorbed peptides. As a consequence of the shedding, the liberated peptides start competing with nanoparticle-anchored peptides for targeted receptors, which is not only expected to decrease efficiency of MSN targeting but could also provide a source of false-positive results if proper measures to account for this are not taken (such as separate evaluation of MSN supernatants in this work). Collectively, these findings highlight the importance of being aware of a possible peptide shedding by MSN (specifically, when MSN enter complex media) and urge to seek for improved approaches to MSN functionalization.

Another important observation was the intriguing discrepancy between the amount of MSN-associated peptides and the evoked SSTR response for MSN_{OC1} and MSN_{OC3}. As discussed in section 5.3.5, in the absence of the preformed protein corona, MSN_{OC1} activated targeted receptors more potently then MSN_{OC3} at the same dose, despite carrying *ca* 3.5-fold less of OC on the surface. Evidently, proper understanding of the relation between conjugation protocol, peptide load and ultimate capacity of MSN to bind targeted receptors is of high practical relevance. Further research should better delineate the basis for the described phenomenon, emerging upon ligand presentation from a surface at nanoscale. Altered MSN propensity to activate receptors due to peptide crowding (steric hindrance) at certain peptide loads and anchoring conditions, as well as peptide functionalization effects on how MSN interact with cellular membranes are among the possible underlying mechanisms here.

Perhaps even more important was the identification of the particular linking chemistry that yields MSN that retain targetability despite the protein corona (MSN_{OC3}, derived via EDC/NHS conjugation in DMF). This finding in effect enabled *in vitro* MSN uptake studies, allowing us to experimentally address the hypothesis of SSTR targeting for the selected MSN type. Indeed, *in vivo*, nanocarriers quickly become covered with biological macromolecules (proteins, carbohydrates, lipids, and the derivates of thereof), and the resulting biocoronas by and large instruct cellular interactions of nanoparticles. Thereby, with knowing that

MSN_{OC3} could engage SSTR even in the presence of adsorbed proteins on their surface, we could proceed with the *in vitro* MSN uptake experiments under biologically-meaningful conditions, *i.e.,* allowing for protein corona build-up on MSN and having the acceptor cells in serum-enriched media, ensuring adequate operation of endocytosis machinery (the latter is never the case with nanoparticle uptake experiments under *rectified* conditions, for serum starvation, as well as nutrient depletion grossly alter cellular physiology). With this, we mimicked the scenario for systemic MSN administration when nanoparticles reach targeted sites after extended retention in blood and thus already carry biocoronas by the moment of interaction with targeted receptors.

Our experiments not only further highlighted the importance of biocoronas for MSN interaction with cells, but confirmed the functional significance of SSTR5/2 for endocytosis of targeted COR-MSN_{OC3}. We observed a striking discrepancy in uptake between the maternal non-functionalized MSN and the derived SP-decorated MSN_{SP3} under the preformed corona setup, which could only be attributed to dissimilar coronas of the nanoparticles in question. Dissimilarities in corona compositions of MSN and MSN_{SP3} stemmed from distinct surface functionalization, *i.e.,* the absence or presence of a layer of peptide moieties. Thus, a seemingly minor structural alteration of a functional surface had tremendous impact on the interaction of MSN with cells under biologically-relevant conditions. The experiments with the coronated MSN and MSN_{SP3} compellingly demonstrated that bare MSN would make an invalid negative control for internalization studies with targeted COR-MSN_{OC3}, allowing no control for corona effects. This fully confirmed our initial rationale and *apriori* expectations, justifying the efforts invested in design, development and characterization of SP and MSN_{SP3}. In practical terms, MSN_{SP3}, a valid negative counterpart for MSN_{OC3}, safeguarded us against erroneous conclusions in the internalization studies that were likely to follow had we utilized the maternal MSN for control purposes.

To evaluate how SSTR targeting affects *in vitro* uptake of the MSN with the protein corona, we purposely established two batteries of cell lines, genetically modified for differential expression of SSTR5 and 2, and used these for experiments with COR-MSN_{SP3} and COR-$MSN_{OC3.}$ The actual effect of SSTR targeting on endocytosis was estimated as relative uptake of COR-MSN_{SP3} to COR-MSN_{OC3} (which reflected the *uptake in the absence of SSTR targeting* divided to the *uptake with SSTR targeting*). Our studies exposed quite unexpected dependence of COR-MSN_{SP3}/COR-MSN_{OC3} ratio on SSTR5 and SSTR2 expression. Specifically, COR-MSN_{OC3} accumulated much less than the non-targeted COR-MSN_{SP3} in cells with endogenous SSTR5 or SSTR2 levels, however this uptake difference tended to decrease upon SSTR5 or SSTR2 overexpression. Furthermore, COR-MSN_{SP3} and COR-MSN_{OC3} demonstrated about similar uptake rates in cells with absence or very

low levels of both the targeted receptors. The described relation between COR-MSN_{SP3}/COR-MSN_{OC3} ratio and SSTR5/2 expression was independently registered in two unrelated arrays of cells with varying levels of the targeted receptors and generally persisted across a range of MSN doses and exposures (both 2 h and 24 h of treatment). In effect, our experiments confirm that SSTR5/2 are indeed involved in uptake regulation of the coronated MSN *in vitro*.

However, the established SSTR5/2 dependence of COR-MSN_{OC3} uptake did not comply with the conventional model of active receptor targeting (ART), which, as discussed earlier, assumes a positive correlation between targeted receptor abundance and uptake of targeted nanocarriers. Our results suggest a more complex link between SSTR5/2 expression and cellular accumulation of protein corona–bearing MSN, which urged us to come up with an alternative model for SSTR5/2 targeting with nanoparticles. The proposed alternative model of *a positive anchor with a negative loop* assumes a dual functionality for SSTR5 and SSTR2 in regulation of endocytosis, implying that both these SSTR subtypes not only promote internalization of targeted nanoparticles by facilitating MSN binding to plasma membranes (a positive anchoring) but also simultaneously inhibit the relevant endocytosis machinery via targeting ligand–evoked receptor signaling (a negative loop). Thus, the resulting endocytosis rate for a given SSTR-targeted nanocarrier would be determined by the net effect of competing forces (positive anchoring *vs.* negative signaling), both emerging upon interaction of SSTR5/2 with targeting ligands. In other words, by paying homage to receptor signaling, globally overlooked by the conventional ART model, the alternative model better recapitulates complexity of SSTR biology, thus allowing to understand SSTR targeting in a more physiologically-relevant context.

Despite good fit with the evidence, the alternative model for SSTR5/2 targeting remains speculative and clearly requires further experimental corroboration. I elaborate on the latter aspect and discuss other possible explanations for our MSN internalization data in the respective section of the thesis.

Now, to the main objective of the present work. Did we succeed in answering the question of whether SSTR5/2 binding with high affinity ligands on MSN leads to enhanced cellular accumulation of nanoparticles *in vitro*? I believe that the selected experimental approach was adequate and the derived evidence is sufficient for this. However, the answer to the question is “NO”, which is to say that the conventional ART model does not appear to apply to particular receptor types (SSTR5 and SSTR2) and the selected nanocarrier (MSN with a mean diameter of *ca* 180 nm, functionalized with octreotide) under the utilized conditions *in vitro* (culture medium with 10% serum).

As discussed, our evidence rather suggests a more complex role for SSTR5 and SSTR2 in uptake regulation of the MSN bearing protein corona, depicting these receptors as predominantly negative regulators of MSN endocytosis. In other words, it may also be stated that *in vitro* targeting of SSTR5/2 is associated with a decreased uptake of MSN with the corona of serum proteins. Importantly, the latter conclusion is hypothesis-free and thus should stay valid irrespectively of whether the alternative model for SSTR5/2 role in MSN endocytosis finds further support or gets refuted.

From a translational standpoint, our *in vitro* results would rather disfavour subsequent development of MSN_{OC3} for SSTR5/2 targeting *in vivo*. However, assuming the enormous complexity of *in vivo* conditions and the inherent problems with predictive power of *in vitro* studies (including the likely differences between biocoronas *in vitro* and *in vivo*), the actual effects of SSTR5/2 targeting on uptake of MSN_{OC3} *in vivo* could only be exposed in rigorous animal experiments.

In a broader context, we expect that our results with COR-MSN_{OC3} and SSTR5/2 should be also applicable to nanocarriers of similar size, geometry and surface features under similar conditions *in vitro*. Yet, in view of the multitude of aspects, affecting behaviour of nanoparticles in complex environments, and objective difficulties in predicting how a change in one parameter of a nanocarrier (*e.g.,* particle size, surface charge or surface functionalization with a chemical moiety) would affect the others and the resulting nanobiointerface, the interpolation has to be done with caution and proper experimental backing. Functional roles of SSTR5 and SSTR2 within the context of targeted delivery with other, structurally different nanocarriers require separate experimental evaluation.

Finally, we believe that our work represents a good example of a structured approach to *in vitro* targetability evaluation of a synthetic nanocarrier. With this, we express hope that our experience with SSTR-targeted MSN, summarized herein (refer also to Fig. 10), as well as the developed technical tools (specifically, the *in vitro* targetability bioassay, which could be also applied to other receptors that signal via cAMP), would be of use for other receptor targeting endeavours, towards better understanding of how nanoparticles interact with the living matter.

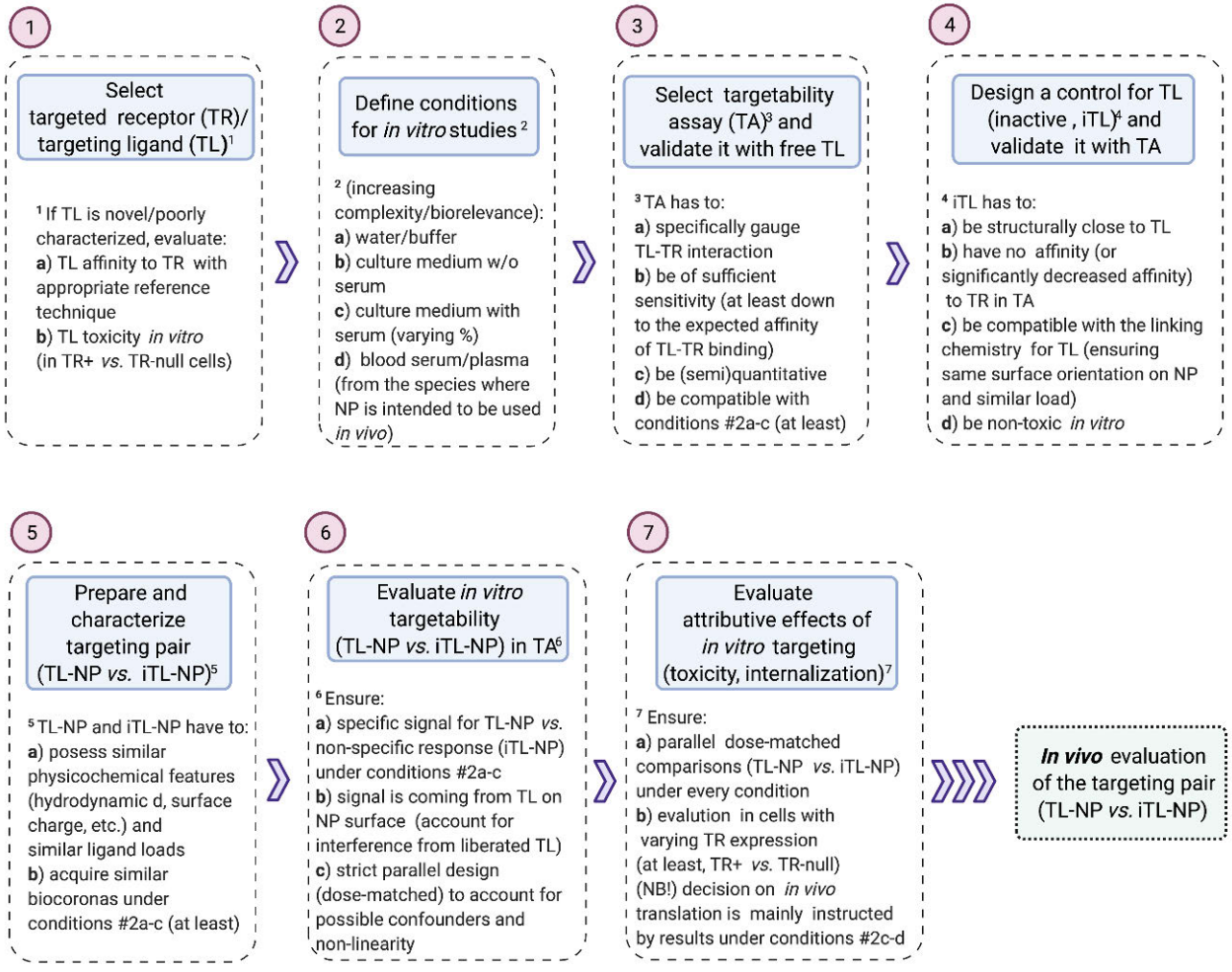

Figure 10. *In vitro* targetability evaluation of a synthetic nanocarrier: design considerations and experimental approach. Abbreviations: d – diameter; NP – nanoparticle; TA – targetability assay; (i)TL – (inactive) targeting ligand; TR – targeted receptor.

Acknowledgements

This work spans the period of 2013 – 2021 and was performed at the Medical Faculty of the University of Turku (Physiology Department; Turku Doctoral Programme of Molecular Medicine), Turku Bioscience (formerly Turku Centre for Biotechnology), and the Cell Biology department of Åbo Akademi University, Turku.

The efforts were highly collaborative and the people who significantly contributed and helped out on the way are many – with this, the author feels concerned that he might have forgotten to acknowledge someone. If this happens to be the case, the author pleads for forgiveness – this could have only happened inadvertently, merely for the inability of memory to bring to life all the nuanced moments of the past years.

Foremost, my deepest gratitude goes to my supervisors – Adolfo, Cecilia, and Veronika. None of this would have been possible had I not been extremely lucky to meet all of you in the early days and had I not received your full support and guidance over the period of my PhD studies.

Adolfo, a big thank you for picking me up during my first weeks in Turku (Cecilia and Veronika were both engaged abroad at that time, in the Netherlands and Norway, respectively). I knew next to nothing in terms of the actual lab work and was feeling quite at a loss on the campus, having no experience to tackle the mounting and constantly changing tasks. If not for your practical guidance from the early days onwards, who knows how events might have unfolded… Your invariably positive, bold, open-minded and slightly jocose attitude to experimental work and problem-solving profoundly shaped the development of my lab skills, and I can clearly see your footprints in my current *modus operandi* in the lab. Whenever trouble arose, whether in the lab or beyond, I always knew where to seek advice, for you were near, always offering your helping hand.

Cecilia, I can hardly thank you enough for the rock-solid support you have given me over all these years. Your backing was absolutely instrumental for both the material aspects of my research, and the mental and emotional sides of my performance, enabling me to consistently move forward. Your deep involvement and personal touch, analytical grasp and perspective, and readiness to take bold decisions

in daring moments are all behind the vital turns on the road-maps of our projects. I want to specifically praise you for not putting excessively rigorous restrictions on experimental flow and letting me explore novel domains – the ensuing feeling of *trust*, combined with my mounting experimental skill-set made it possible for me to bear fruit through my work. Now, thinking back, I am convinced that our joint achievements and my personal development as a researcher were both critically dependent on fostering such a milieu.

Veronika… It all started in 2011 when we met in Moscow for the first time. You were looking for someone enthusiastic to embark on the processing of archival materials and I was just lucky enough to be there. This encounter changed everything – it took me out of clinical medicine, patient wards and my home country, and plunged me into south-western Finland, Turku (a town of which, I must confess, I had not even heard before), in Cecilia's molecular biology lab, with an outline of a research project on nano-oncology on my hands. Apart from the wet-lab work guidance, I acquired a lot of common wisdom and walk of life–related experience from you; with time, our relations went beyond the conventional student-mentor framework, with me growing to think of you rather as a close senior friend. Your passing away was a tremendous loss. Hardly a day goes by without the picture of you surfacing in my memory and I still miss you dearly. This work, which you were at the very origins of, is devoted to the cherished memory of you.

Matthias, a constant member of the thesis steering committee – thank you for being with us all these years, aiding in the projects' flow well beyond the formally stipulated limits! Your advice was of genuine benefit a number of times; same goes for your shrewd reasoning regarding lab work, publishing and other aspects within the field.

As stated, the thesis works were highly multidisciplinary and collaborative. Indeed, the nanotechnology pipeline was enabled by the versatile contribution of our partner chemists, the research teams of Prof Jessica Rosenholm at ÅAU (with Diti Desai, and, at later phases, Helene Kettiger, performing nanoparticles synthesis) and Prof Mika Lindén at the University of Ulm (with Melanie Gerstenberg covering nanoparticle preparation). The highly-interactive cooperation between our labs laid the cornerstone for our joint success. I also learned a great deal within the nanotechnology domain through our team work. Thank you all so much for your ideas, vigor and contribution!

Now, to the actual environment where the thesis research was performed. The author was privileged to work in the labs of Medisiina C (Physiology Department of UTU) and Biocity Campus (Turku Bioscience and Cell Biology Department of ÅAU), which provided an excellent milieu for the projects in question. I express my deep gratitude to all the persons keeping the lab routines going and making the labs truly great and user-friendly facilities. From Physiology, I would like to

acknowledge the department's head Prof Jorma Toppari and the lab manager Tuula Hämäläinen, as well as the staff members Minna Lindroth, Mona Niiranen, and Jonna Palmu. Thomas Bymark and Gunilla Henriksson are gratefully acknowledged from Cell Biology at ÅAU. From Turku Bioscience and other facilities on the local campus, I want to specifically thank Jouko Sandholm, Markku Saari, Ketlin Adel, Inna Starskaya, Pasi Viljakainen, and Markus Peurla. I bothered you all a number of times with diverse questions over the years and always got either immediate help or sensible advice on how to tackle a problem!

I want to thank all the current and former MSc students, doctoral candidates and post-docs of Physiology Department with whom I have been working side-by-side over the years. Special thanks go to Sofia Akko, Tiina Lehtiniemi, Christoffer Löf, Sheyla Cisneros Montalvo, Opeyemi Olotu, Konrad Patyra, Ashutosh Trehan, and Ram Prakash Yadav. I am very grateful to Marcin Chrusciel for the continuous help, specifically for the tremendous aid with animal experimentation. Also, the great fishing sessions with Marcin out in the Baltic are vividly remembered!

Likewise, on the side of Cell Biology at ÅAU, I wish to acknowledge all the members of Cecilia's team (both the alumni and the current ones) who collectively contributed to the wonderful spirits and environment of the Cell Fate lab. My gratitude comes in particular to the "oldies" Christian Antila, Daniel Antfolk, Sebastian Landor, Martina Lerche, and Marika Sjöqvist, with whom I not only shared benches and offices with but also had quite a number of memorable moments outside of the lab. I also want to thank "the more recent" members of the lab Kati Kemppainen and Ezgi Özliseli, as well as Marjaana Parikainen, Amandine Schmit and Kalen Lin. I am genuinely grateful to Iida Laiho, my long-standing bench partner within the endocrine oncology project – your help was absolutely instrumental – just to think of all the experimental runs and re-runs of ours over the years! I am also thankful to Elenaé Vásquez-Ulloa for significantly contributing to the above tumour project (specifically, *in vivo* work). Warm thanks to William Eccleshall – I did enjoy our team work within Notch4 project (still hope the project will re-emerge one day) and grateful for all the help. Last, but not least, my deepest gratitude goes to my time-honored office mate and friend Rasmus Niemi. Your shoulder was always there in times of need, and this is something I will always bear in mind. Same applies to the bright moments which we've had together, especially the long nature walks and beer sessions with a distinct linguistic focus.

Apart from the studies with nanoparticles, the period of my PhD studies also involved several other projects, which I actively partook in. Some of these have already been finalized, the others are still ongoing and will hopefully yield tangible products one day. Though none of these endeavors are properly highlighted in the thesis, they were all essential for my professional maturation and thus contributed to the thesis. With this, taking the opportunity, I want to heartily thank the people who

aided over the years, specifically Larisa K Dzeranova (Research Centre for Endocrinology, Moscow), Pauliina Kronqvist and Sinikka Collanus (UTU; pathology), and Arto Pulliainen (UTU; microbiology).

The actual doctoral dissertation owes its final shape to the meticulous editing by Prof Hélder A. Santos (University of Helsinki) and Prof Paweł Piotr Jagodziński (Poznan University of Medical Sciences), to whom the author expresses deep gratitude. Also, the author is sincerely thankful to Prof Arto Urtti (University of Helsinki), who will be taking the trouble of acting in the capacity of the opponent at the upcoming thesis defense.

The financial support of the thesis-related works is generously acknowledged: European Community Mobility Programme EMA2 (#372117-1-2012-1-FI-ERAMUNDUS-EMA21), K. Albin Johanssons stiftelse, Ida Montinin Säätiö, Pentti and Tyyni Ekbom Foundation, Instrumentariumin Tiedesäätiö. The author also wants to thank Turku Doctoral Programme of Molecular Medicine for supporting his travelling to multiple courses abroad (which the author had his share of!).

Ultimately, I want to thank my dear parents – your gentle guidance, care and unwavering support from my very green years (which I appreciate more deeply now, as a father myself) made the genuine basis for the present achievement. Please, forgive me for staying so far away for such a long time! I love you both.

June 2021, Turku, Finland
Valeriy M Paramonov

Valeriy M Paramonov

Born 1986, Moscow, USSR. 2009 – graduated from I.M. Sechenov Moscow Medical Academy, Russia (M.D., diploma *summa cum laude* in general medicine). 2009/2011 – residency in clinical endocrinology & metabolism, Research Centre for Endocrinology, Moscow, Russia. 2013/2021 – doctoral candidate at the Medical Faculty of the University of Turku (Turku Doctoral Programme of Molecular Medicine, TuDMM), Finland.

References

1. Allen, T. M. Ligand-targeted therapeutics in anticancer therapy. *Nat. Rev. Cancer* **2**, 750–763 (2002).
2. Large, D. E., Soucy, J. R., Hebert, J. & Auguste, D. T. Advances in Receptor-Mediated, Tumor-Targeted Drug Delivery. *Adv. Ther.* **2**, 1800091 (2019).
3. Barbieri, F. *et al.* Peptide Receptor Targeting in Cancer: The Somatostatin Paradigm. *Int. J. Pept.* **2013**, 1–20 (2013).
4. Günther, T. *et al.* International Union of Basic and Clinical Pharmacology. CV. Somatostatin Receptors: Structure, Function, Ligands, and New Nomenclature. *Pharmacol. Rev.* **70**, 763–835 (2018).
5. Pelaz, B. *et al.* Diverse Applications of Nanomedicine. *ACS Nano* **11**, 2313–2381 (2017).
6. Shi, J., Kantoff, P. W., Wooster, R. & Farokhzad, O. C. Cancer nanomedicine: progress, challenges and opportunities. *Nat. Rev. Cancer* **17**, 20–37 (2017).
7. Kakkar, A., Traverso, G., Farokhzad, O. C., Weissleder, R. & Langer, R. Evolution of macromolecular complexity in drug delivery systems. *Nat. Rev. Chem.* **1**, 1–18 (2017).
8. Ghosh, A., Xu, W., Gupta, N. & Gracias, D. H. Active matter therapeutics. *Nano Today* **31**, 100836 (2020).
9. Kim, B. Y. S., Rutka, J. T. & Chan, W. C. W. Nanomedicine. *N. Engl. J. Med.* **363**, 2434–2443 (2010).
10. Björnmalm, M., Thurecht, K. J., Michael, M., Scott, A. M. & Caruso, F. Bridging Bio-Nano Science and Cancer Nanomedicine. *ACS Nano* **11**, 9594–9613 (2017).
11. Youn, Y. S. & Bae, Y. H. Perspectives on the past, present, and future of cancer nanomedicine. *Adv. Drug Deliv. Rev.* **130**, 3–11 (2018).
12. Almeida, J. P. M., Chen, A. L., Foster, A. & Drezek, R. In vivo biodistribution of nanoparticles. *Nanomedicine (Lond).* **6**, 815–835 (2011).
13. Bertrand, N. & Leroux, J.-C. The journey of a drug-carrier in the body: An anatomo-physiological perspective. *J. Control. Release* **161**, 152–163 (2012).
14. Dai, Q. *et al.* Particle Targeting in Complex Biological Media. *Adv. Healthc. Mater.* **7**, 1700575 (2018).
15. Ke, P. C., Lin, S., Parak, W. J., Davis, T. P. & Caruso, F. A Decade of the Protein Corona. *ACS Nano* **11**, 11773–11776 (2017).
16. Zhao, Z., Ukidve, A., Krishnan, V. & Mitragotri, S. Effect of physicochemical and surface properties on in vivo fate of drug nanocarriers. *Adv. Drug Deliv. Rev.* **143**, 3–21 (2019).
17. Pan, D. C. *et al.* Nanoparticle Properties Modulate Their Attachment and Effect on Carrier Red Blood Cells. *Sci. Rep.* **8**, 1615 (2018).
18. Betker, J. L. *et al.* Nanoparticle uptake by circulating leukocytes: A major barrier to tumor delivery. *J. Control. Release* **286**, 85–93 (2018).

19. Giulimondi, F. *et al.* Interplay of protein corona and immune cells controls blood residency of liposomes. *Nat. Commun.* **10**, 3686 (2019).
20. Semple, S. C., Chonn, A. & Cullis, P. R. Interactions of liposomes and lipid-based carrier systems with blood proteins: Relation to clearance behaviour in vivo. *Adv. Drug Deliv. Rev.* **32**, 3–17 (1998).
21. OWENSIII, D. & PEPPAS, N. Opsonization, biodistribution, and pharmacokinetics of polymeric nanoparticles. *Int. J. Pharm.* **307**, 93–102 (2006).
22. Fadeel, B. Hide and Seek: Nanomaterial Interactions With the Immune System. *Front. Immunol.* **10**, 133 (2019).
23. Bertrand, N., Wu, J., Xu, X., Kamaly, N. & Farokhzad, O. C. Cancer nanotechnology: The impact of passive and active targeting in the era of modern cancer biology. *Adv. Drug Deliv. Rev.* **66**, 2–25 (2014).
24. Maeda, H., Tsukigawa, K. & Fang, J. A Retrospective 30 Years After Discovery of the Enhanced Permeability and Retention Effect of Solid Tumors: Next-Generation Chemotherapeutics and Photodynamic Therapy—Problems, Solutions, and Prospects. *Microcirculation* **23**, 173–182 (2016).
25. Wolfram, J. & Ferrari, M. Clinical cancer nanomedicine. *Nano Today* **25**, 85–98 (2019).
26. Haraldsson, B., Nyström, J. & Deen, W. M. Properties of the Glomerular Barrier and Mechanisms of Proteinuria. *Physiol. Rev.* **88**, 451–487 (2008).
27. Soo Choi, H. *et al.* Renal clearance of quantum dots. *Nat. Biotechnol.* **25**, 1165–1170 (2007).
28. Burns, A. A. *et al.* Fluorescent Silica Nanoparticles with Efficient Urinary Excretion for Nanomedicine. *Nano Lett.* **9**, 442–448 (2009).
29. Varma, M. V. S. *et al.* Physicochemical determinants of human renal clearance. *J. Med. Chem.* **52**, 4844–4852 (2009).
30. Feng, B., LaPerle, J. L., Chang, G. & Varma, M. V. Renal clearance in drug discovery and development: Molecular descriptors, drug transporters and disease state. *Expert Opin. Drug Metab. Toxicol.* **6**, 939–952 (2010).
31. Jain, R. K. Delivery of Molecular and Cellular Medicine to Solid Tumors. *Microcirculation* **4**, 1–23 (1997).
32. Dewhirst, M. W. & Secomb, T. W. Transport of drugs from blood vessels to tumour tissue. *Nat. Rev. Cancer* **17**, 738–750 (2017).
33. Ernsting, M. J., Murakami, M., Roy, A. & Li, S.-D. Factors controlling the pharmacokinetics, biodistribution and intratumoral penetration of nanoparticles. *J. Control. Release* **172**, 782–794 (2013).
34. Poon, W. *et al.* Elimination Pathways of Nanoparticles. *ACS Nano* **13**, 5785–5798 (2019).
35. Sørensen, K. K. *et al.* The scavenger endothelial cell: a new player in homeostasis and immunity. *Am. J. Physiol. Integr. Comp. Physiol.* **303**, R1217–R1230 (2012).
36. Anderson, C. L. The liver sinusoidal endothelium reappears after being eclipsed by the Kupffer cell: a 20th century biological delusion corrected. *J. Leukoc. Biol.* **98**, 875–876 (2015).
37. Noguchi, Y. *et al.* Early Phase Tumor Accumulation of Macromolecules: A Great Difference in Clearance Rate between Tumor and Normal Tissues. *Japanese J. Cancer Res.* **89**, 307–314 (1998).
38. Leu, A. J., Berk, D. A., Lymboussaki, A., Alitalo, K. & Jain, R. K. Absence of functional lymphatics within a murine sarcoma: A molecular and functional evaluation. *Cancer Res.* **60**, 4324–4327 (2000).
39. Dreher, M. R. *et al.* Tumor Vascular Permeability, Accumulation, and Penetration of Macromolecular Drug Carriers. *JNCI J. Natl. Cancer Inst.* **98**, 335–344 (2006).

40. Huang, S. K., Papahadjopoulos, D., Berk, D. A. & Jain, R. K. Microvascular Permeability and Interstitial Penetration of Sterically Stabilized (Stealth) Liposomes in a Human Tumor Xenograft. *Cancer Res.* **54**, 3352–3356 (1994).
41. Popović, Z. *et al.* A nanoparticle size series for invivo fluorescence imaging. *Angew. Chemie - Int. Ed.* **49**, 8649–8652 (2010).
42. Anchordoquy, T. J. *et al.* Mechanisms and Barriers in Cancer Nanomedicine: Addressing Challenges, Looking for Solutions. *ACS Nano* **11**, 12–18 (2017).
43. Nel, A., Ruoslahti, E. & Meng, H. New Insights into "Permeability" as in the Enhanced Permeability and Retention Effect of Cancer Nanotherapeutics. *ACS Nano* **11**, 9567–9569 (2017).
44. Moghimi, S. M. & Simberg, D. Nanoparticle transport pathways into tumors. *J. Nanoparticle Res.* **20**, 169 (2018).
45. Baxter, L. T. & Jain, R. K. Transport of fluid and macromolecules in tumors. I. Role of interstitial pressure and convection. *Microvasc. Res.* **37**, 77–104 (1989).
46. Yuan, F. Transvascular drug delivery in solid tumors. *Semin. Radiat. Oncol.* **8**, 164–175 (1998).
47. Yuan, F. *et al.* Vascular Permeability in a Human Tumor Xenograft: Molecular Size Dependence and Cutoff Size. *Cancer Res.* **55**, 3752–3756 (1995).
48. Padera, T. P. *et al.* Lymphatic metastasis in the absence of functional intratumor lymphatics. *Science (80-.).* **296**, 1883–1886 (2002).
49. Golombek, S. K. *et al.* Tumor targeting via EPR: Strategies to enhance patient responses. *Adv. Drug Deliv. Rev.* **130**, 17–38 (2018).
50. Danhier, F. To exploit the tumor microenvironment: Since the EPR effect fails in the clinic, what is the future of nanomedicine? *J. Control. Release* **244**, 108–121 (2016).
51. Scott, A. M., Wolchok, J. D. & Old, L. J. Antibody therapy of cancer. *Nat. Rev. Cancer* **12**, 278–287 (2012).
52. Rosenblum, D., Joshi, N., Tao, W., Karp, J. M. & Peer, D. Progress and challenges towards targeted delivery of cancer therapeutics. *Nat. Commun.* **9**, 1410 (2018).
53. Ruoslahti, E., Bhatia, S. N. & Sailor, M. J. Targeting of drugs and nanoparticles to tumors. *J. Cell Biol.* **188**, 759–768 (2010).
54. Howard, M. *et al.* Vascular Targeting of Nanocarriers: Perplexing Aspects of the Seemingly Straightforward Paradigm. *ACS Nano* **8**, 4100–4132 (2014).
55. Fröhlich, E. Cellular elimination of nanoparticles. *Environ. Toxicol. Pharmacol.* **46**, 90–94 (2016).
56. Duncan, R. & Richardson, S. C. W. Endocytosis and Intracellular Trafficking as Gateways for Nanomedicine Delivery: Opportunities and Challenges. *Mol. Pharm.* **9**, 2380–2402 (2012).
57. Patel, S. *et al.* Brief update on endocytosis of nanomedicines. *Adv. Drug Deliv. Rev.* **144**, 90–111 (2019).
58. Ngoune, R., Peters, A., von Elverfeldt, D., Winkler, K. & Pütz, G. Accumulating nanoparticles by EPR: A route of no return. *J. Control. Release* **238**, 58–70 (2016).
59. Li, S.-D. & Huang, L. Pharmacokinetics and Biodistribution of Nanoparticles. *Mol. Pharm.* **5**, 496–504 (2008).
60. Moghimi, S. M. Mechanisms of splenic clearance of blood cells and particles: towards development of new splenotropic agents. *Adv. Drug Deliv. Rev.* **17**, 103–115 (1995).
61. Demoy, M. *et al.* Spleen capture of nanoparticles: influence of animal species and surface characteristics. *Pharm. Res.* **16**, 37–41 (1999).

62. Zhang, Y.-N., Poon, W., Tavares, A. J., McGilvray, I. D. & Chan, W. C. W. Nanoparticle–liver interactions: Cellular uptake and hepatobiliary elimination. *J. Control. Release* **240**, 332–348 (2016).
63. Du, B., Yu, M. & Zheng, J. Transport and interactions of nanoparticles in the kidneys. *Nat. Rev. Mater.* **3**, 358–374 (2018).
64. Dobrovolskaia, M. A. & McNeil, S. E. Immunological properties of engineered nanomaterials. *Nat. Nanotechnol.* **2**, 469–478 (2007).
65. Parhiz, H. *et al.* Unintended effects of drug carriers: Big issues of small particles. *Adv. Drug Deliv. Rev.* **130**, 90–112 (2018).
66. Baxter, L. T. & Jain, R. K. Transport of fluid and macromolecules in tumors. IV. A microscopic model of the perivascular distribution. *Microvasc. Res.* **41**, 252–272 (1991).
67. Stylianopoulos, T., Munn, L. L. & Jain, R. K. Reengineering the Physical Microenvironment of Tumors to Improve Drug Delivery and Efficacy: From Mathematical Modeling to Bench to Bedside. *Trends in Cancer* **4**, 292–319 (2018).
68. Swartz, M. A. & Lund, A. W. Lymphatic and interstitial flow in the tumour microenvironment: Linking mechanobiology with immunity. *Nat. Rev. Cancer* **12**, 210–219 (2012).
69. Stacker, S. A. *et al.* Lymphangiogenesis and lymphatic vessel remodelling in cancer. *Nat. Rev. Cancer* **14**, 159–172 (2014).
70. Padera, T. P., Meijer, E. F. J. & Munn, L. L. The Lymphatic System in Disease Processes and Cancer Progression. *Annu. Rev. Biomed. Eng.* **18**, 125–158 (2016).
71. Gerlowski, L. E. & Jain, R. K. Microvascular permeability of normal and neoplastic tissues. *Microvasc. Res.* **31**, 288–305 (1986).
72. Matsumura, Y. & Maeda, H. A New Concept for Macromolecular Therapeutics in Cancer Chemotherapy: Mechanism of Tumoritropic Accumulation of Proteins and the Antitumor Agent Smancs. *Cancer Res.* **46**, 6387–6392 (1986).
73. Bae, Y. H. & Park, K. Targeted drug delivery to tumors: Myths, reality and possibility. *J. Control. Release* **153**, 198–205 (2011).
74. Less, J. R., Skalak, T. C., Sevick, E. M. & Jain, R. K. Microvascular architecture in a mammary carcinoma: branching patterns and vessel dimensions. *Cancer Res.* **51**, 265–73 (1991).
75. Carmeliet, P. & Jain, R. K. Angiogenesis in cancer and other diseases. *Nature* **407**, 249–257 (2000).
76. Nagy, J. A., Chang, S. H., Shih, S. C., Dvorak, A. M. & Dvorak, H. F. Heterogeneity of the tumor vasculature. *Semin. Thromb. Hemost.* **36**, 321–331 (2010).
77. Dvorak, H. F. Tumors: Wounds that do not heal-redux. *Cancer Immunol. Res.* **3**, 1–11 (2015).
78. Heldin, C. H., Rubin, K., Pietras, K. & Östman, A. High interstitial fluid pressure - An obstacle in cancer therapy. *Nat. Rev. Cancer* **4**, 806–813 (2004).
79. Dvorak, H. F., Nagy, J. A., Dvorak, J. T. & Dvorak, A. M. Identification and characterization of the blood vessels of solid tumors that are leaky to circulating macromolecules. *Am. J. Pathol.* **133**, 95–109 (1988).
80. Morikawa, S. *et al.* Abnormalities in Pericytes on Blood Vessels and Endothelial Sprouts in Tumors. *Am. J. Pathol.* **160**, 985–1000 (2002).
81. Baluk, P., Morikawa, S., Haskell, A., Mancuso, M. & McDonald, D. M. Abnormalities of Basement Membrane on Blood Vessels and Endothelial Sprouts in Tumors. *Am. J. Pathol.* **163**, 1801–1815 (2003).
82. Dudley, A. C. Tumor endothelial cells. *Cold Spring Harb. Perspect. Med.* **2**, (2012).
83. Hobbs, S. K. *et al.* Regulation of transport pathways in tumor vessels: Role of tumor type and microenvironment. *Proc. Natl. Acad. Sci. U. S. A.* **95**, 4607–4612 (1998).

84. Hashizume, H. *et al.* Openings between Defective Endothelial Cells Explain Tumor Vessel Leakiness. *Am. J. Pathol.* **156**, 1363–1380 (2000).
85. Padera, T. P. *et al.* Cancer cells compress intratumour vessels. *Nature* **427**, 695–695 (2004).
86. Gabizon, A. & Papahadjopoulos, D. Liposome formulations with prolonged circulation time in blood and enhanced uptake by tumors. *Proc. Natl. Acad. Sci. U. S. A.* **85**, 6949–6953 (1988).
87. Dreher, M. R. *et al.* Tumor vascular permeability, accumulation, and penetration of macromolecular drug carriers. *J. Natl. Cancer Inst.* **98**, 335–344 (2006).
88. Milton Harris, J., Martin, N. E. & Modi, M. Pegylation: A novel process for modifying pharmacokinetics. *Clin. Pharmacokinet.* **40**, 539–551 (2001).
89. Milla, P., Dosio, F. & Cattel, L. PEGylation of Proteins and Liposomes: a Powerful and Flexible Strategy to Improve the Drug Delivery. *Curr. Drug Metab.* **13**, 105–119 (2011).
90. Suk, J. S., Xu, Q., Kim, N., Hanes, J. & Ensign, L. M. PEGylation as a strategy for improving nanoparticle-based drug and gene delivery. *Adv. Drug Deliv. Rev.* **99**, 28–51 (2016).
91. Venditto, V. J. & Szoka, F. C. Cancer nanomedicines: So many papers and so few drugs! *Adv. Drug Deliv. Rev.* **65**, 80–88 (2013).
92. Weissig, V., Pettinger, T. K. & Murdock, N. Nanopharmaceuticals (part 1): products on the market. *Int. J. Nanomedicine* **9**, 4357–4373 (2014).
93. Bobo, D., Robinson, K. J., Islam, J., Thurecht, K. J. & Corrie, S. R. Nanoparticle-Based Medicines: A Review of FDA-Approved Materials and Clinical Trials to Date. *Pharm. Res.* **33**, 2373–2387 (2016).
94. Wilhelm, S. *et al.* Analysis of nanoparticle delivery to tumours. *Nat. Rev. Mater.* **1**, (2016).
95. Choi, Y. H. & Han, H. K. Nanomedicines: current status and future perspectives in aspect of drug delivery and pharmacokinetics. *J. Pharm. Investig.* **48**, 43–60 (2018).
96. Salvioni, L. *et al.* Thirty years of cancer nanomedicine: Success, frustration, and hope. *Cancers (Basel).* **11**, (2019).
97. Nichols, J. W. & Bae, Y. H. EPR: Evidence and fallacy. *J. Control. Release* **190**, 451–464 (2014).
98. Park, K. Facing the truth about nanotechnology in drug delivery. *ACS Nano* **7**, 7442–7447 (2013).
99. Stirland, D. L., Nichols, J. W., Miura, S. & Bae, Y. H. Mind the gap: A survey of how cancer drug carriers are susceptible to the gap between research and practice. *Journal of Controlled Release* **172**, 1045–1064 (2013).
100. Kamb, A. What's wrong with our cancer models? *Nat. Rev. Drug Discov.* **4**, 161–165 (2005).
101. Ruggeri, B. A., Camp, F. & Miknyoczki, S. Animal models of disease: Pre-clinical animal models of cancer and their applications and utility in drug discovery. *Biochem. Pharmacol.* **87**, 150–161 (2014).
102. Hobson, B. & Denekamp, J. Endothelial proliferation in tumours and normal tissues: Continuous labelling studies. *Br. J. Cancer* **49**, 405–413 (1984).
103. di Tomaso, E. *et al.* Mosaic Tumor Vessels: Cellular Basis and Ultrastructure of Focal Regions Lacking Endothelial Cell Markers. *Cancer Res.* **65**, 5740–5749 (2005).
104. Sindhwani, S. *et al.* The entry of nanoparticles into solid tumours. *Nat. Mater.* **19**, 566–575 (2020).
105. Nagy, J. A., Benjamin, L., Zeng, H., Dvorak, A. M. & Dvorak, H. F. Vascular permeability, vascular hyperpermeability and angiogenesis. *Angiogenesis* **11**, 109–119 (2008).
106. Dvorak, A. M. & Feng, D. The vesiculo-vacuolar organelle (VVO): A new endothelial cell permeability organelle. *J. Histochem. Cytochem.* **49**, 419–431 (2001).
107. Kim, S. M., Faix, P. H. & Schnitzer, J. E. Overcoming key biological barriers to cancer drug delivery and efficacy. *J. Control. Release* **267**, 15–30 (2017).
108. Alitalo, K. The lymphatic vasculature in disease. *Nat. Med.* **17**, 1371–1380 (2011).

109. van der Meel, R., Vehmeijer, L. J. C., Kok, R. J., Storm, G. & van Gaal, E. V. B. Ligand-targeted particulate nanomedicines undergoing clinical evaluation: Current status. *Adv. Drug Deliv. Rev.* **65**, 1284–1298 (2013).
110. Strebhardt, K. & Ullrich, A. Paul Ehrlich's magic bullet concept: 100 years of progress. *Nat. Rev. Cancer* **8**, 473–480 (2008).
111. Sikorski, A. F., Toporkiewicz, M., Meissner, J., Matusewicz, L. & Czogalla, A. Toward a magic or imaginary bullet? Ligands for drug targeting to cancer cells: principles, hopes, and challenges. *Int. J. Nanomedicine* 1399 (2015). doi:10.2147/IJN.S74514
112. Diamantis, N. & Banerji, U. Antibody-drug conjugates - An emerging class of cancer treatment. *Br. J. Cancer* **114**, 362–367 (2016).
113. Joubert, N., Beck, A., Dumontet, C. & Denevault-Sabourin, C. Antibody–Drug Conjugates: The Last Decade. *Pharmaceuticals* **13**, 245 (2020).
114. Velikyan, I. *Theranostics, Gallium-68, and Other Radionuclides*. **194**, (Springer Berlin Heidelberg, 2013).
115. Werner, R. A. *et al.* The theranostic promise for Neuroendocrine Tumors in the late 2010s – Where do we stand, where do we go? *Theranostics* **8**, 6088–6100 (2018).
116. Lammers, T., Kiessling, F., Hennink, W. E. & Storm, G. Drug targeting to tumors: Principles, pitfalls and (pre-) clinical progress. *J. Control. Release* **161**, 175–187 (2012).
117. Ray, P., Viles, K. D., Soule, E. E. & Woodruff, R. S. Application of aptamers for targeted therapeutics. *Arch. Immunol. Ther. Exp. (Warsz).* **61**, 255–271 (2013).
118. Yoo, J., Park, C., Yi, G., Lee, D. & Koo, H. Active targeting strategies using biological ligands for nanoparticle drug delivery systems. *Cancers (Basel).* **11**, (2019).
119. Fay, F. & Scott, C. J. Antibody-targeted nanoparticles for cancer therapy. *Immunotherapy* **3**, 381–394 (2011).
120. Carter, T., Mulholland, P. & Chester, K. Antibody-targeted nanoparticles for cancer treatment. *Immunotherapy* **8**, 941–958 (2016).
121. Accardo, A., Aloj, L., Aurilio, M., Morelli, G. & Tesauro, D. Receptor binding peptides for target-selective delivery of nanoparticles encapsulated drugs. *Int. J. Nanomedicine* **9**, 1537–57 (2014).
122. Khan, M. *et al.* Exploiting cancer's phenotypic guise against itself: Targeting ectopically expressed peptide G-protein coupled receptors for lung cancer therapy. *Oncotarget* **8**, 104615–104637 (2017).
123. Danhier, F., Le Breton, A. & Préat, V. RGD-Based Strategies To Target Alpha(v) Beta(3) Integrin in Cancer Therapy and Diagnosis. *Mol. Pharm.* **9**, 2961–2973 (2012).
124. Garcia-Bennett, A., Nees, M. & Fadeel, B. In search of the Holy Grail: Folate-targeted nanoparticles for cancer therapy. *Biochem. Pharmacol.* **81**, 976–984 (2011).
125. Zwicke, G. L., Ali Mansoori, G. & Jeffery, C. J. Utilizing the folate receptor for active targeting of cancer nanotherapeutics. *Nano Rev.* **3**, 18496 (2012).
126. Daniels, T. R. *et al.* The transferrin receptor and the targeted delivery of therapeutic agents against cancer. *Biochim. Biophys. Acta - Gen. Subj.* **1820**, 291–317 (2012).
127. Torrice, M. Does Nanomedicine Have a Delivery Problem? *ACS Cent. Sci.* **2**, 434–437 (2016).
128. Lammers, T. *et al.* Cancer nanomedicine: Is targeting our target? *Nat. Rev. Mater.* **1**, 1–2 (2016).
129. Park, K. The beginning of the end of the nanomedicine hype. *J. Control. Release* **305**, 221–222 (2019).
130. Bobo, D., Robinson, K. J., Islam, J., Thurecht, K. J. & Corrie, S. R. Nanoparticle-Based Medicines: A Review of FDA-Approved Materials and Clinical Trials to Date. *Pharm. Res.* **33**, 2373–87 (2016).

131. Berk, D. A., Yuan, F., Leunig, M. & Jain, R. K. Direct in vivo measurement of targeted binding in a human tumor xenograft. *Proc. Natl. Acad. Sci.* **94**, 1785–1790 (1997).
132. Luker, K. E. *et al.* In vivo imaging of ligand receptor binding with Gaussia luciferase complementation. *Nat. Med.* **18**, 172–177 (2012).
133. Rudkouskaya, A. *et al.* Quantitative imaging of receptor-ligand engagement in intact live animals. *J. Control. Release* **286**, 451–459 (2018).
134. Patching, S. G. Surface plasmon resonance spectroscopy for characterisation of membrane protein–ligand interactions and its potential for drug discovery. *Biochim. Biophys. Acta - Biomembr.* **1838**, 43–55 (2014).
135. Draczkowski, P., Matosiuk, D. & Jozwiak, K. Isothermal titration calorimetry in membrane protein research. *J. Pharm. Biomed. Anal.* **87**, 313–325 (2014).
136. Correia, J. J. & Stafford, W. F. *Sedimentation Velocity: A Classical Perspective*. *Methods in Enzymology* **562**, (Elsevier Inc., 2015).
137. de Jong, L. A. A., Uges, D. R. A., Franke, J. P. & Bischoff, R. Receptor–ligand binding assays: Technologies and Applications. *J. Chromatogr. B* **829**, 1–25 (2005).
138. Pollard, T. D. A Guide to Simple and Informative Binding Assays. *Mol. Biol. Cell* **21**, 4061–4067 (2010).
139. Paramonov, V. M., Mamaeva, V., Sahlgren, C. & Rivero-Müller, A. Genetically-encoded tools for cAMP probing and modulation in living systems. *Front. Pharmacol.* **6**, 1–21 (2015).
140. Hughes, P., Marshall, D., Reid, Y., Parkes, H. & Gelber, C. The costs of using unauthenticated, over-passaged cell lines: how much more data do we need? *Biotechniques* **43**, 575–586 (2007).
141. Liu, Y. *et al.* Multi-omic measurements of heterogeneity in HeLa cells across laboratories. *Nat. Biotechnol.* **37**, 314–322 (2019).
142. Chang, C.-C. *et al.* Liposome encapsulation reduces cantharidin toxicity. *Food Chem. Toxicol.* **46**, 3116–21 (2008).
143. Li, X. *et al.* Specific targeting of breast tumor by octreotide-conjugated ultrasmall superparamagnetic iron oxide particles using a clinical 3.0-tesla magnetic resonance scanner. *Acta radiol.* **50**, 583–594 (2009).
144. Sun, M. *et al.* Octreotide-modification enhances the delivery and targeting of doxorubicin-loaded liposomes to somatostatin receptors expressing tumor in vitro and in vivo. *Nanotechnology* **21**, 475101 (2010).
145. Zhang, J. *et al.* A novel octreotide modified lipid vesicle improved the anticancer efficacy of doxorubicin in somatostatin receptor 2 positive tumor models. *Mol. Pharm.* **7**, 1159–1168 (2010).
146. Iwase, Y. & Maitani, Y. Octreotide-targeted liposomes loaded with CPT-11 enhanced cytotoxicity for the treatment of medullary thyroid carcinoma. *Mol. Pharm.* **8**, 330–7 (2011).
147. Zhang, Y., Wang, X., Wang, J., Zhang, X. & Zhang, Q. Octreotide-modified polymeric micelles as potential carriers for targeted docetaxel delivery to somatostatin receptor overexpressing tumor cells. *Pharm. Res.* **28**, 1167–1178 (2011).
148. Dai, W. *et al.* Spatiotemporally controlled co-delivery of anti-vasculature agent and cytotoxic drug by octreotide-modified stealth liposomes. *Pharm. Res.* **29**, 2902–11 (2012).
149. Petersen, A. L. *et al.* Positron emission tomography evaluation of somatostatin receptor targeted 64Cu-TATE-liposomes in a human neuroendocrine carcinoma mouse model. *J. Control. Release* **160**, 254–263 (2012).
150. Huo, M. *et al.* Somatostatin receptor-mediated tumor-targeting drug delivery using octreotide-PEG-deoxycholic acid conjugate-modified N-deoxycholic acid-O, N-hydroxyethylation chitosan micelles. *Biomaterials* **33**, 6393–6407 (2012).

151. Zou, A. *et al.* Octreotide-Modified N-Octyl-O, N-Carboxymethyl Chitosan Micelles as Potential Carriers for Targeted Antitumor Drug Delivery. *J. Pharm. Sci.* **101**, 627–640 (2012).
152. Helbok, A. *et al.* Targeting properties of peptide-modified radiolabeled liposomal nanoparticles. *Nanomedicine Nanotechnology, Biol. Med.* **8**, 112–118 (2012).
153. Xiao, Y. *et al.* Co-delivery of doxorubicin and siRNA using octreotide-conjugated gold nanorods for targeted neuroendocrine cancer therapy. *Nanoscale* **4**, 7185 (2012).
154. Abou, D. S. *et al.* 89Zr-Labeled Paramagnetic Octreotide-Liposomes for PET-MR Imaging of Cancer. *Pharm. Res.* **30**, 878–888 (2013).
155. Xu, W. *et al.* Octreotide-functionalized and resveratrol-loaded unimolecular micelles for targeted neuroendocrine cancer therapy. *Nanoscale* **5**, 9924 (2013).
156. Su, Z. *et al.* Effect of octreotide surface density on receptor-mediated endocytosis in vitro and anticancer efficacy of modified nanocarrier in vivo after optimization. *Int. J. Pharm.* **447**, 281–292 (2013).
157. Orocio-Rodríguez, E. *et al.* Two Novel Nanosized Radiolabeled Analogues of Somatostatin for Neuroendocrine Tumor Imaging. *J. Nanosci. Nanotechnol.* **15**, 4159–69 (2015).
158. Liu, T. *et al.* Development of octreotide-conjugated polymeric prodrug of bufalin for targeted delivery to somatostatin receptor 2 overexpressing breast cancer in vitro and in vivo. *Int. J. Nanomedicine* **11**, 2235–2250 (2016).
159. Abdellatif, A. A. H. *et al.* Novel gold nanoparticles coated with somatostatin as a potential delivery system for targeting somatostatin receptors. *Drug Dev. Ind. Pharm.* **42**, 1782–1791 (2016).
160. Jaskula-Sztul, R. *et al.* Thailandepsin A-loaded and octreotide-functionalized unimolecular micelles for targeted neuroendocrine cancer therapy. *Biomaterials* **91**, 1–10 (2016).
161. Banerjee, I. *et al.* Paclitaxel-loaded solid lipid nanoparticles modified with Tyr-3-octreotide for enhanced anti-angiogenic and anti-glioma therapy. *Acta Biomater.* **38**, 69–81 (2016).
162. Zhang, X., Yang, C., Zhou, J. & Huo, M. Somatostatin Receptor-Mediated Tumor-Targeting Nanocarriers Based on Octreotide-PEG Conjugated Nanographene Oxide for Combined Chemo and Photothermal Therapy. *Small* **12**, 3578–3590 (2016).
163. Chen, G. *et al.* KE108-conjugated unimolecular micelles loaded with a novel HDAC inhibitor thailandepsin-A for targeted neuroendocrine cancer therapy. *Biomaterials* **97**, 22–33 (2016).
164. Benito, A. B. *et al.* Functional Single-Chain Polymer Nanoparticles: Targeting and Imaging Pancreatic Tumors in Vivo. *Biomacromolecules* **17**, 3213–3221 (2016).
165. Kim, I. *et al.* One-Dimensional Supramolecular Nanoplatforms for Theranostics Based on Co-Assembly of Peptide Amphiphiles. *Biomacromolecules* **17**, 3234–3243 (2016).
166. Li, H., Yuan, D., Sun, M. & Ping, Q. Effect of ligand density and PEG modification on octreotide-targeted liposome via somatostatin receptor in vitro and in vivo. *Drug Deliv.* **23**, 3562–3572 (2016).
167. Jackson, A. W. *et al.* Octreotide Functionalized Nano-Contrast Agent for Targeted Magnetic Resonance Imaging. *Biomacromolecules* **17**, 3902–3910 (2016).
168. Shekhter Zahavi, T. *et al.* Molecular engineering of somatostatin analogue with minimal dipeptide motif induces the formation of functional nanoparticles. *ChemNanoMat* **3**, 27–32 (2017).
169. Bharti, R. *et al.* Somatostatin receptor targeted liposomes with Diacerein inhibit IL-6 for breast cancer therapy. *Cancer Lett.* **388**, 292–302 (2017).
170. Vijayan, V. M., Shenoy, S. J. & Muthu, J. Octreotide-conjugated fluorescent PEGylated polymeric nanogel for theranostic applications. *Mater. Sci. Eng. C* **76**, 490–500 (2017).

171. Bhowmik, A. *et al.* Anti-SSTR2 peptide based targeted delivery of potent PLGA encapsulated 3,3'-diindolylmethane nanoparticles through blood brain barrier prevents glioma progression. *Oncotarget* **8**, 65339–65358 (2017).
172. Ahmadi, Y. *et al.* In vivo magnetic resonance imaging of pancreatic tumors using iron oxide nanoworms targeted with PTR86 peptide. *Colloids Surfaces B Biointerfaces* **158**, 423–430 (2017).
173. Abdellatif, A. A. H., Abdelhafez, W. A. & Sarhan, H. A. Somatostatin decorated quantum dots for targeting of somatostatin receptors. *Iran. J. Pharm. Res.* **17**, 513–524 (2018).
174. Nguyen, H. T. *et al.* Multifunctional nanoparticles as somatostatin receptor-targeting delivery system of polyaniline and methotrexate for combined chemo–photothermal therapy. *Acta Biomater.* **68**, 154–167 (2018).
175. Kuan, S. L. *et al.* Boosting Antitumor Drug Efficacy with Chemically Engineered Multidomain Proteins. *Adv. Sci.* **5**, 1–13 (2018).
176. Li, L. *et al.* Dual-targeting liposomes for enhanced anticancer effect in somatostatin receptor II-positive tumor model. *Nanomedicine (Lond).* **13**, 2155–2169 (2018).
177. Seidler, C. *et al.* Dynamic Core–Shell Bioconjugates for Targeted Protein Delivery and Release. *Chem. - An Asian J.* **13**, 3474–3479 (2018).
178. Abdellatif, A. A. H., Abou-Taleb, H. A., Abd El Ghany, A. A., Lutz, I. & Bouazzaoui, A. Targeting of somatostatin receptors expressed in blood cells using quantum dots coated with vapreotide. *Saudi Pharm. J.* **26**, 1162–1169 (2018).
179. Zhu, H. Z. *et al.* Identification and imaging of miR-155 in the early screening of lung cancer by targeted delivery of octreotide-conjugated chitosan-molecular beacon nanoparticles. *Drug Deliv.* **25**, 1974–1983 (2018).
180. Braga, T. L. *et al.* Octreotide Nanoparticles Showed Affinity for In Vivo MIA Paca-2 Inducted Pancreas Ductal Adenocarcinoma Mimicking Pancreatic Polypeptide-Secreting Tumor of the Distal Pancreas (PPoma). *Pharm. Res.* **36**, (2019).
181. Xia, L. *et al.* Multimodality imaging of naturally active melanin nanoparticles targeting somatostatin receptor subtype 2 in human small-cell lung cancer. *Nanoscale* **11**, 14400–14409 (2019).
182. Poudel, K. *et al.* Multifaceted NIR-responsive polymer-peptide-enveloped drug-loaded copper sulfide nanoplatform for chemo-phototherapy against highly tumorigenic prostate cancer. *Nanomedicine Nanotechnology, Biol. Med.* **21**, 102042 (2019).
183. Varshosaz, J., Raghami, F., Rostami, M. & Jahanian, A. PEGylated trimethylchitosan emulsomes conjugated to octreotide for targeted delivery of sorafenib to hepatocellular carcinoma cells of HepG2. *J. Liposome Res.* **29**, 383–398 (2019).
184. Abdellatif, A. A. H. *et al.* Fluorescent Nanoparticles Coated with a Somatostatin Analogue Target Blood Monocyte for Efficient Leukaemia Treatment. *Pharm. Res.* **37**, (2020).
185. Shelar, S. B. *et al.* Electrostatically bound lanreotide peptide - gold nanoparticle conjugates for enhanced uptake in SSTR2-positive cancer cells. *Mater. Sci. Eng. C* **117**, (2020).
186. Banerjee, I. *et al.* A peptide-modified solid lipid nanoparticle formulation of paclitaxel modulates immunity and outperforms dacarbazine in a murine melanoma model. *Biomater. Sci.* **7**, 1161–1178 (2019).
187. dos Santos, T., Varela, J., Lynch, I., Salvati, A. & Dawson, K. A. Effects of Transport Inhibitors on the Cellular Uptake of Carboxylated Polystyrene Nanoparticles in Different Cell Lines. *PLoS One* **6**, e24438 (2011).
188. Vercauteren, D. *et al.* The Use of Inhibitors to Study Endocytic Pathways of Gene Carriers: Optimization and Pitfalls. *Mol. Ther.* **18**, 561–569 (2010).

189. Saha, K. *et al.* Surface functionality of nanoparticles determines cellular uptake mechanisms in mammalian cells. *Small* **9**, 300–305 (2013).
190. Herd, H. *et al.* Nanoparticle Geometry and Surface Orientation Influence Mode of Cellular Uptake. *ACS Nano* **7**, 1961–1973 (2013).
191. Jiang, W., Kim, B. Y. S., Rutka, J. T. & Chan, W. C. W. Nanoparticle-mediated cellular response is size-dependent. *Nat. Nanotechnol.* **3**, 145–150 (2008).
192. Albanese, A., Tang, P. S. & Chan, W. C. W. The Effect of Nanoparticle Size, Shape, and Surface Chemistry on Biological Systems. *Annu. Rev. Biomed. Eng.* **14**, 1–16 (2012).
193. Kinnear, C., Moore, T. L., Rodriguez-Lorenzo, L., Rothen-Rutishauser, B. & Petri-Fink, A. Form Follows Function: Nanoparticle Shape and Its Implications for Nanomedicine. *Chem. Rev.* **117**, 11476–11521 (2017).
194. Walkey, C. D., Olsen, J. B., Guo, H., Emili, A. & Chan, W. C. W. Nanoparticle size and surface chemistry determine serum protein adsorption and macrophage uptake. *J. Am. Chem. Soc.* **134**, 2139–2147 (2012).
195. Zhang, H. *et al.* Ligand Size and Conformation Affect the Behavior of Nanoparticles Coated with in Vitro and in Vivo Protein Corona. *ACS Appl. Mater. Interfaces* **10**, 9094–9103 (2018).
196. Reubi, J. C. Peptide Receptors as Molecular Targets for Cancer Diagnosis and Therapy. *Endocr. Rev.* **24**, 389–427 (2003).
197. Dézsi, L. *et al.* Regional differences in nitric oxide-dependent vascular responses to somatostatin. *Physiol. Res.* **45**, 291–296 (1996).
198. Curtis, S. B. *et al.* Somatostatin receptor subtype expression and function in human vascular tissue. *Am. J. Physiol. Circ. Physiol.* **278**, H1815–H1822 (2000).
199. Smith, W. H. T. *et al.* Somatostatin receptor subtype expression in the human heart: Differential expression by myocytes and fibroblasts. *J. Endocrinol.* **187**, 379–386 (2005).
200. Badway, A. C., West, F. M., Tente, S. M. & Blake, A. D. Somatostatin regulates intracellular signaling in human carotid endothelial cells. *Biochem. Biophys. Res. Commun.* **319**, 1222–1227 (2004).
201. Florio, T. *et al.* Somatostatin inhibits tumor angiogenesis and growth via somatostatin receptor-3-mediated regulation of endothelial nitric oxide synthase and mitogen-activated protein kinase activities. *Endocrinology* **144**, 1574–1584 (2003).
202. Colombo, M. *et al.* Tumour homing and therapeutic effect of colloidal nanoparticles depend on the number of attached antibodies. *Nat. Commun.* **7**, 13818 (2016).
203. Tonigold, M. *et al.* Pre-adsorption of antibodies enables targeting of nanocarriers despite a biomolecular corona. *Nat. Nanotechnol.* **13**, 862–869 (2018).
204. Mammen, M., Choi, S. K. & Whitesides, G. M. Polyvalent interactions in biological systems: Implications for design and use of multivalent ligands and inhibitors. *Angew. Chemie - Int. Ed.* **37**, 2754–2794 (1998).
205. Weissleder, R., Kelly, K., Sun, E. Y., Shtatland, T. & Josephson, L. Cell-specific targeting of nanoparticles by multivalent attachment of small molecules. *Nat. Biotechnol.* **23**, 1418–1423 (2005).
206. Wang, J., Tian, S., Petros, R. A., Napier, M. E. & Desimone, J. M. The complex role of multivalency in nanoparticles targeting the transferrin receptor for cancer therapies. *J. Am. Chem. Soc.* **132**, 11306–11313 (2010).
207. Poon, Z. *et al.* Ligand-clustered 'patchy' nanoparticles for modulated cellular uptake and in vivo tumor targeting. *Angew. Chemie - Int. Ed.* **49**, 7266–7270 (2010).
208. Fakhari, A., Baoum, A., Siahaan, T. J., Le, K. B. & Berkland, C. Controlling Ligand Surface Density Optimizes Nanoparticle Binding to ICAM-1. *J. Pharm. Sci.* **100**, 1045–1056 (2011).

209. Elias, D. R., Poloukhtine, A., Popik, V. & Tsourkas, A. Effect of ligand density, receptor density, and nanoparticle size on cell targeting. *Nanomedicine Nanotechnology, Biol. Med.* **9**, 194–201 (2013).
210. Li, L., Zhang, Y. & Wang, J. Effects of ligand distribution on receptor-diffusion-mediated cellular uptake of nanoparticles. *R. Soc. Open Sci.* **4**, 170063 (2017).
211. Deci, M. B., Liu, M., Dinh, Q. T. & Nguyen, J. Precision engineering of targeted nanocarriers. *Wiley Interdiscip. Rev. Nanomedicine Nanobiotechnology* **10**, (2018).
212. Zhang, K., Gao, H., Deng, R. & Li, J. Emerging Applications of Nanotechnology for Controlling Cell-Surface Receptor Clustering. *Angew. Chemie - Int. Ed.* **58**, 4790–4799 (2019).
213. Zhang, Q. & Reinhard, B. M. Ligand Density and Nanoparticle Clustering Cooperate in the Multivalent Amplification of Epidermal Growth Factor Receptor Activation. *ACS Nano* **12**, 10473–10485 (2018).
214. Roberts, M. F. & Kruchten, A. E. *Receptor biology*. (Wiley -VCH Verlag, 2016).
215. Alberts, B. *et al. Molecular Biology of the Cell*. (Garland Science, Taylor & Francis Group, 2015).
216. Feng, X.-H. & Derynck, R. Ligand-independent Activation of Transforming Growth Factor (TGF) β Signaling Pathways by Heteromeric Cytoplasmic Domains of TGF-β Receptors. *J. Biol. Chem.* **271**, 13123–13129 (1996).
217. Guo, G. *et al.* Ligand-Independent EGFR Signaling. *Cancer Res.* **75**, 3436–3441 (2015).
218. Ben-Shlomo, A. *et al.* Selective regulation of somatostatin receptor subtype signaling: evidence for constitutive receptor activation. *Mol. Endocrinol.* **21**, 2565–2578 (2007).
219. Ben-Shlomo, A. *et al.* Constitutive somatostatin receptor activity determines tonic pituitary cell response. *Mol. Endocrinol.* **23**, 337–348 (2009).
220. Austin, C. D. *et al.* Death-receptor activation halts clathrin-dependent endocytosis. *Proc. Natl. Acad. Sci.* **103**, 10283–10288 (2006).
221. Sorkin, A. & Von Zastrow, M. Endocytosis and signalling: Intertwining molecular networks. *Nat. Rev. Mol. Cell Biol.* **10**, 609–622 (2009).
222. Lemmon, M. A., Freed, D. M., Schlessinger, J. & Kiyatkin, A. The Dark Side of Cell Signaling: Positive Roles for Negative Regulators. *Cell* **164**, 1172–1184 (2016).
223. Schmid, S. L. Reciprocal regulation of signaling and endocytosis: Implications for the evolving cancer cell. *J. Cell Biol.* **216**, 2623–2632 (2017).
224. Nel, A. E. *et al.* Understanding biophysicochemical interactions at the nano-bio interface. *Nat. Mater.* **8**, 543–557 (2009).
225. Treuel, L., Docter, D., Maskos, M. & Stauber, R. H. Protein corona – from molecular adsorption to physiological complexity. *Beilstein J. Nanotechnol.* **6**, 857–873 (2015).
226. Foo, K. Y. & Hameed, B. H. Insights into the modeling of adsorption isotherm systems. *Chem. Eng. J.* **156**, 2–10 (2010).
227. Vogler, E. A. Protein adsorption in three dimensions. *Biomaterials* **33**, 1201–1237 (2012).
228. Condon, J. B. *Surface Area and Porosity Determinations by Physisorption*. (Elsevier, 2020). doi:10.1016/C2018-0-00544-7
229. *Biomaterials science : an introduction to materials in medicine*. (Academic Press, 2013).
230. Cedervall, T. *et al.* Understanding the nanoparticle-protein corona using methods to quntify exchange rates and affinities of proteins for nanoparticles. *Proc. Natl. Acad. Sci. U. S. A.* **104**, 2050–2055 (2007).
231. Barrett, K. E., Barman, S. M., Brooks, H. L., Yuan, J. X.-J. & Preceded by: Ganong, W. F. *Ganong's review of medical physiology*. (McGraw-Hill Education, 2019).

232. Hau, J. & Schapiro, S. J. *Handbook of Laboratory Animal Science, Volume I*. (CRC Press, 2010). doi:10.1201/b10416
233. Tenzer, S. *et al.* Rapid formation of plasma protein corona critically affects nanoparticle pathophysiology. *Nat. Nanotechnol.* **8**, 772–781 (2013).
234. Docter, D. *et al.* The nanoparticle biomolecule corona: lessons learned – challenge accepted? *Chem. Soc. Rev.* **44**, 6094–6121 (2015).
235. Gessner, A., Lieske, A., Paulke, B. R. & Müller, R. H. Influence of surface charge density on protein adsorption on polymeric nanoparticles: analysis by two-dimensional electrophoresis. *Eur. J. Pharm. Biopharm.* **54**, 165–170 (2002).
236. Tenzer, S. *et al.* Nanoparticle Size Is a Critical Physicochemical Determinant of the Human Blood Plasma Corona: A Comprehensive Quantitative Proteomic Analysis. *ACS Nano* **5**, 7155–7167 (2011).
237. Ashby, J., Pan, S. & Zhong, W. Size and Surface Functionalization of Iron Oxide Nanoparticles Influence the Composition and Dynamic Nature of Their Protein Corona. *ACS Appl. Mater. Interfaces* **6**, 15412–15419 (2014).
238. Maffre, P. *et al.* Effects of surface functionalization on the adsorption of human serum albumin onto nanoparticles – a fluorescence correlation spectroscopy study. *Beilstein J. Nanotechnol.* **5**, 2036–2047 (2014).
239. Pozzi, D. *et al.* Surface chemistry and serum type both determine the nanoparticle–protein corona. *J. Proteomics* **119**, 209–217 (2015).
240. Vogt, C. *et al.* Proteomics Analysis Reveals Distinct Corona Composition on Magnetic Nanoparticles with Different Surface Coatings: Implications for Interactions with Primary Human Macrophages. *PLoS One* **10**, e0129008 (2015).
241. Saikia, J., Yazdimamaghani, M., Hadipour Moghaddam, S. P. & Ghandehari, H. Differential Protein Adsorption and Cellular Uptake of Silica Nanoparticles Based on Size and Porosity. *ACS Appl. Mater. Interfaces* **8**, 34820–34832 (2016).
242. Marichal, L. *et al.* Protein corona composition of silica nanoparticles in complex media: Nanoparticle size does not matter. *Nanomaterials* **10**, 1–15 (2020).
243. Madathiparambil Visalakshan, R. *et al.* The Influence of Nanoparticle Shape on Protein Corona Formation. *Small* **16**, 2000285 (2020).
244. Laurent, S., Burtea, C., Thirifays, C., Rezaee, F. & Mahmoudi, M. Significance of cell 'observer' and protein source in nanobiosciences. *J. Colloid Interface Sci.* **392**, 431–445 (2013).
245. Hadjidemetriou, M. *et al.* In Vivo Biomolecule Corona around Blood-Circulating, Clinically Used and Antibody-Targeted Lipid Bilayer Nanoscale Vesicles. *ACS Nano* **9**, 8142–8156 (2015).
246. Pozzi, D. *et al.* The biomolecular corona of nanoparticles in circulating biological media. *Nanoscale* **7**, 13958–13966 (2015).
247. Strojan, K. *et al.* Dispersion of Nanoparticles in Different Media Importantly Determines the Composition of Their Protein Corona. *PLoS One* **12**, e0169552 (2017).
248. Johnston, B. D. *et al.* Colloidal Stability and Surface Chemistry Are Key Factors for the Composition of the Protein Corona of Inorganic Gold Nanoparticles. *Adv. Funct. Mater.* **27**, 1–9 (2017).
249. Panzuto Capurso, G., Della Fave, G., F. Medical treatment of gastro-entero-pancreatic endocrine tumors. in *A Century of Advances in Neuroendocrine Tumor Biology and Treatment* (ed. Modlin Oberg, K, I. M.) (Felsenstein C.C.C.P., 2007).
250. Lundqvist, M. *et al.* The evolution of the protein corona around nanoparticles: a test study. *ACS Nano* **5**, 7503–9 (2011).

251. Barrán-Berdón, A. L. *et al.* Time evolution of nanoparticle-protein corona in human plasma: Relevance for targeted drug delivery. *Langmuir* **29**, 6485–6494 (2013).
252. Bertoli, F., Garry, D., Monopoli, M. P., Salvati, A. & Dawson, K. A. The Intracellular Destiny of the Protein Corona: A Study on its Cellular Internalization and Evolution. *ACS Nano* **10**, 10471–10479 (2016).
253. Hadjidemetriou, M., Al-Ahmady, Z. & Kostarelos, K. Time-evolution of in vivo protein corona onto blood-circulating PEGylated liposomal doxorubicin (DOXIL) nanoparticles. *Nanoscale* **8**, 6948–6957 (2016).
254. Kittler, S. *et al.* The influence of proteins on the dispersability and cell-biological activity of silver nanoparticles. *J. Mater. Chem.* **20**, 512–518 (2010).
255. Gebauer, J. S. *et al.* Impact of the Nanoparticle–Protein Corona on Colloidal Stability and Protein Structure. *Langmuir* **28**, 9673–9679 (2012).
256. Miclăuş, T. *et al.* Dynamic protein coronas revealed as a modulator of silver nanoparticle sulphidation in vitro. *Nat. Commun.* **7**, 11770 (2016).
257. Hu, X., Li, D. & Mu, L. Biotransformation of graphene oxide nanosheets in blood plasma affects their interactions with cells. *Environ. Sci. Nano* **4**, 1569–1578 (2017).
258. Mahmoudi, M., Bertrand, N., Zope, H. & Farokhzad, O. C. Emerging understanding of the protein corona at the nano-bio interfaces. *Nano Today* **11**, 817–832 (2016).
259. Salvati, A. *et al.* Transferrin-functionalized nanoparticles lose their targeting capabilities when a biomolecule corona adsorbs on the surface. *Nat. Nanotechnol.* **8**, 137–143 (2013).
260. Mirshafiee, V., Mahmoudi, M., Lou, K., Cheng, J. & Kraft, M. L. Protein corona significantly reduces active targeting yield. *Chem. Commun.* **49**, 2557–2559 (2013).
261. Dai, Q. *et al.* Targeting Ability of Affibody-Functionalized Particles Is Enhanced by Albumin but Inhibited by Serum Coronas. *ACS Macro Lett.* **4**, 1259–1263 (2015).
262. Rybak-Smith, M. J., Tripisciano, C., Borowiak-Palen, E., Lamprecht, C. & Sim, R. B. Effect of functionalization of carbon nanotubes with psychosine on complement activation and protein adsorption. *J. Biomed. Nanotechnol.* **7**, 830–839 (2011).
263. Vlasova, I. I. *et al.* Adsorbed plasma proteins modulate the effects of single-walled carbon nanotubes on neutrophils in blood. *Nanomedicine Nanotechnology, Biol. Med.* **12**, 1615–1625 (2016).
264. Wang, Z. *et al.* Specifically Formed Corona on Silica Nanoparticles Enhances Transforming Growth Factor β1 Activity in Triggering Lung Fibrosis. *ACS Nano* **11**, 1659–1672 (2017).
265. Lara, S. *et al.* Identification of Receptor Binding to the Biomolecular Corona of Nanoparticles. *ACS Nano* **11**, 1884–1893 (2017).
266. Dal Magro, R. *et al.* Artificial apolipoprotein corona enables nanoparticle brain targeting. *Nanomedicine Nanotechnology, Biol. Med.* **14**, 429–438 (2018).
267. Deng, Z. J., Liang, M., Monteiro, M., Toth, I. & Minchin, R. F. Nanoparticle-induced unfolding of fibrinogen promotes Mac-1 receptor activation and inflammation. *Nat. Nanotechnol.* **6**, 39–44 (2011).
268. Dominguez-Medina, S. *et al.* Adsorption and Unfolding of a Single Protein Triggers Nanoparticle Aggregation. *ACS Nano* **10**, 2103–2112 (2016).
269. Monopoli, M. P., Åberg, C., Salvati, A. & Dawson, K. A. Biomolecular coronas provide the biological identity of nanosized materials. *Nat. Nanotechnol.* **7**, 779–786 (2012).
270. Chen, F. *et al.* Complement proteins bind to nanoparticle protein corona and undergo dynamic exchange in vivo. *Nat. Nanotechnol.* **12**, 387–393 (2017).
271. Simon, J. *et al.* Unraveling the In Vivo Protein Corona. *Cells* **10**, 132 (2021).
272. Mukherjee, S., Ghosh, R. N. & Maxfield, F. R. Endocytosis. *Physiol. Rev.* **77**, 759–803 (1997).

273. Conner, S. D. & Schmid, S. L. Regulated portals of entry into the cell. *Nature* **422**, 37–44 (2003).
274. Tuma, P. L. & Hubbard, A. L. Transcytosis: Crossing cellular barriers. *Physiological Reviews* **83**, 871–932 (2003).
275. Hediger, M. A., Clémençon, B., Burrier, R. E. & Bruford, E. A. The ABCs of membrane transporters in health and disease (SLC series): Introduction. *Mol. Aspects Med.* **34**, 95–107 (2013).
276. Navale, A. M. & Paranjape, A. N. Glucose transporters: physiological and pathological roles. *Biophys. Rev.* **8**, 5–9 (2016).
277. PALACÍN, M., ESTÉVEZ, R., BERTRAN, J. & ZORZANO, A. Molecular Biology of Mammalian Plasma Membrane Amino Acid Transporters. *Physiol. Rev.* **78**, 969–1054 (1998).
278. Canton, I. & Battaglia, G. Endocytosis at the nanoscale. *Chem. Soc. Rev.* **41**, 2718 (2012).
279. Donahue, N. D., Acar, H. & Wilhelm, S. Concepts of nanoparticle cellular uptake, intracellular trafficking, and kinetics in nanomedicine. *Adv. Drug Deliv. Rev.* **143**, 68–96 (2019).
280. Doherty, G. J. & McMahon, H. T. Mechanisms of endocytosis. *Annu. Rev. Biochem.* **78**, 857–902 (2009).
281. Ungewickell, E. J. & Hinrichsen, L. Endocytosis: clathrin-mediated membrane budding. *Curr. Opin. Cell Biol.* **19**, 417–25 (2007).
282. Carver, L. A. & Schnitzer, J. E. Caveolae: mining little caves for new cancer targets. *Nat. Rev. Cancer* **3**, 571–581 (2003).
283. Mayor, S. & Pagano, R. E. Pathways of clathrin-independent endocytosis. *Nat. Rev. Mol. Cell Biol.* **8**, 603–12 (2007).
284. Sandvig, K., Kavaliauskiene, S. & Skotland, T. Clathrin-independent endocytosis: an increasing degree of complexity. *Histochem. Cell Biol.* **150**, 107–118 (2018).
285. Kerr, M. C. & Teasdale, R. D. Defining macropinocytosis. *Traffic* **10**, 364–371 (2009).
286. Stuart, L. M. & Ezekowitz, R. A. B. Phagocytosis. *Immunity* **22**, 539–550 (2005).
287. Sahay, G., Alakhova, D. Y. & Kabanov, A. V. Endocytosis of nanomedicines. *J. Control. Release* **145**, 182–195 (2010).
288. Stewart, M. P., Lorenz, A., Dahlman, J. & Sahay, G. Challenges in carrier-mediated intracellular delivery: Moving beyond endosomal barriers. *Wiley Interdiscip. Rev. Nanomedicine Nanobiotechnology* **8**, 465–478 (2016).
289. Francia, V., Montizaan, D. & Salvati, A. Interactions at the cell membrane and pathways of internalization of nano-sized materials for nanomedicine. *Beilstein J. Nanotechnol.* **11**, 338–353 (2020).
290. Fung, K. Y. Y., Fairn, G. D. & Lee, W. L. Transcellular vesicular transport in epithelial and endothelial cells: Challenges and opportunities. *Traffic* **19**, 5–18 (2018).
291. Chithrani, B. D., Ghazani, A. a. & Chan, W. C. W. Determining the size and shape dependence of gold nanoparticle uptake into mammalian cells. *Nano Lett.* **6**, 662–668 (2006).
292. Chithrani, B. D. & Chan, W. C. W. Elucidating the mechanism of cellular uptake and removal of protein-coated gold nanoparticles of different sizes and shapes. *Nano Lett.* **7**, 1542–1550 (2007).
293. Gratton, S. E. A. *et al.* The effect of particle design on cellular internalization pathways. *Proc. Natl. Acad. Sci. U. S. A.* **105**, 11613–11618 (2008).
294. Lu, F., Wu, S.-H., Hung, Y. & Mou, C.-Y. Size Effect on Cell Uptake in Well-Suspended, Uniform Mesoporous Silica Nanoparticles. *Small* **5**, 1408–1413 (2009).
295. Chu, Z., Huang, Y., Tao, Q. & Li, Q. Cellular uptake, evolution, and excretion of silica nanoparticles in human cells. *Nanoscale* **3**, 3291–3299 (2011).
296. Toy, R., Peiris, P. M., Ghaghada, K. B. & Karathanasis, E. Shaping cancer nanomedicine: The effect of particle shape on the in vivo journey of nanoparticles. *Nanomedicine* **9**, 121–134 (2014).

297. Shang, L., Nienhaus, K. & Nienhaus, G. U. Engineered nanoparticles interacting with cells: size matters. *J. Nanobiotechnology* **12**, 5 (2014).
298. Guo, P. *et al.* Nanoparticle elasticity directs tumor uptake. *Nat. Commun.* **9**, 130 (2018).
299. Iversen, T. G., Skotland, T. & Sandvig, K. Endocytosis and intracellular transport of nanoparticles: Present knowledge and need for future studies. *Nano Today* **6**, 176–185 (2011).
300. Smith, S. A., Selby, L. I., Johnston, A. P. R. & Such, G. K. The Endosomal Escape of Nanoparticles: Toward More Efficient Cellular Delivery. *Bioconjug. Chem.* **30**, 263–272 (2019).
301. Rosenholm, J. M. *et al.* Targeting of Porous Hybrid Silica Nanoparticles to Cancer Cells. *ACS Nano* **3**, 197–206 (2009).
302. Rosenholm, J. M. *et al.* Cancer-Cell-Specific Induction of Apoptosis Using Mesoporous Silica Nanoparticles as Drug-Delivery Vectors. *Small* **6**, 1234–1241 (2010).
303. Mamaeva, V. *et al.* Mesoporous Silica Nanoparticles as Drug Delivery Systems for Targeted Inhibition of Notch Signaling in Cancer. *Mol. Ther.* **19**, 1538–1546 (2011).
304. Mamaeva, V. *et al.* Inhibiting notch activity in breast cancer stem cells by glucose functionalized nanoparticles carrying γ-secretase inhibitors. *Mol. Ther.* **24**, 926–936 (2016).
305. Li, Z., Barnes, J. C., Bosoy, A., Stoddart, J. F. & Zink, J. I. Mesoporous silica nanoparticles in biomedical applications. *Chem. Soc. Rev.* **41**, 2590 (2012).
306. Mamaeva, V., Sahlgren, C. & Lindén, M. Mesoporous silica nanoparticles in medicine--recent advances. *Adv. Drug Deliv. Rev.* **65**, 689–702 (2013).
307. Castillo, R. R., Lozano, D. & Vallet-Regí, M. Mesoporous Silica Nanoparticles as Carriers for Therapeutic Biomolecules. *Pharmaceutics* **12**, 432 (2020).
308. Manzano, M. & Vallet-Regí, M. Mesoporous Silica Nanoparticles for Drug Delivery. *Adv. Funct. Mater.* **30**, 1902634 (2020).
309. He, Q., Shi, J., Zhu, M., Chen, Y. & Chen, F. The three-stage in vitro degradation behavior of mesoporous silica in simulated body fluid. *Microporous Mesoporous Mater.* **131**, 314–320 (2010).
310. Lu, J., Liong, M., Li, Z., Zink, J. I. & Tamanoi, F. Biocompatibility, biodistribution, and drug-delivery efficiency of mesoporous silica nanoparticles for cancer therapy in animals. *Small* **6**, 1794–1805 (2010).
311. Liu, T. *et al.* Single and repeated dose toxicity of mesoporous hollow silica nanoparticles in intravenously exposed mice. *Biomaterials* **32**, 1657–1668 (2011).
312. He, Q., Zhang, Z., Gao, F., Li, Y. & Shi, J. In vivo biodistribution and urinary excretion of mesoporous silica nanoparticles: Effects of particle size and PEGylation. *Small* **7**, 271–280 (2011).
313. Yu, T., Greish, K., McGill, L. D., Ray, A. & Ghandehari, H. Influence of Geometry, Porosity, and Surface Characteristics of Silica Nanoparticles on Acute Toxicity: Their Vasculature Effect and Tolerance Threshold. *ACS Nano* **6**, 2289–2301 (2012).
314. Hao, N. *et al.* In Vitro Degradation Behavior of Silica Nanoparticles Under Physiological Conditions. *J. Nanosci. Nanotechnol.* **12**, 6346–6354 (2012).
315. Croissant, J. G., Fatieiev, Y. & Khashab, N. M. Degradability and Clearance of Silicon, Organosilica, Silsesquioxane, Silica Mixed Oxide, and Mesoporous Silica Nanoparticles. *Adv. Mater.* **29**, (2017).
316. Dogra, P. *et al.* Establishing the effects of mesoporous silica nanoparticle properties on in vivo disposition using imaging-based pharmacokinetics. *Nat. Commun.* **9**, 4551 (2018).
317. Hoffmann, F., Cornelius, M., Morell, J. & Fröba, M. Silica-based mesoporous organic-inorganic hybrid materials. *Angew. Chemie - Int. Ed.* **45**, 3216–3251 (2006).

318. Wu, S. H. & Lin, H. P. Synthesis of mesoporous silica nanoparticles. *Chem. Soc. Rev.* **42**, 3862–3875 (2013).
319. Knežević, N. & Durand, J. O. Large pore mesoporous silica nanomaterials for application in delivery of biomolecules. *Nanoscale* **7**, 2199–2209 (2015).
320. Rahikkala, A. *et al.* Mesoporous Silica Nanoparticles for Targeted and Stimuli-Responsive Delivery of Chemotherapeutics: A Review. *Adv. Biosyst.* **2**, 1–33 (2018).
321. Barui, S. & Cauda, V. Multimodal decorations of mesoporous silica nanoparticles for improved cancer therapy. *Pharmaceutics* **12**, 1–33 (2020).
322. Waser, B., Tamma, M.-L., Cescato, R., Maecke, H. R. & Reubi, J. C. Highly efficient in vivo agonist-induced internalization of sst2 receptors in somatostatin target tissues. *J. Nucl. Med.* **50**, 936–41 (2009).
323. Patel, Y. C. Somatostatin and its receptor family. *Front. Neuroendocrinol.* **20**, 157–98 (1999).
324. Møller, L. N., Stidsen, C. E., Hartmann, B. & Holst, J. J. Somatostatin receptors. *Biochim. Biophys. Acta - Biomembr.* **1616**, 1–84 (2003).
325. Cervia, D. & Bagnoli, P. An update on somatostatin receptor signaling in native systems and new insights on their pathophysiology. *Pharmacol. Ther.* **116**, 322–341 (2007).
326. Florio, T. Somatostatin/somatostatin receptor signalling: phosphotyrosine phosphatases. *Mol. Cell. Endocrinol.* **286**, 40–8 (2008).
327. Theodoropoulou, M. & Stalla, G. K. Somatostatin receptors: from signaling to clinical practice. *Front. Neuroendocrinol.* **34**, 228–52 (2013).
328. Csaba, Z., Peineau, S. & Dournaud, P. Molecular mechanisms of somatostatin receptor trafficking. *J. Mol. Endocrinol.* **48**, R1–R12 (2012).
329. Rocheville, M. Receptors for Dopamine and Somatostatin: Formation of Hetero-Oligomers with Enhanced Functional Activity. *Science (80-.).* **288**, 154–157 (2000).
330. Somvanshi, R. K. & Kumar, U. Pathophysiology of GPCR Homo- and Heterodimerization: Special Emphasis on Somatostatin Receptors. *Pharmaceuticals (Basel).* **5**, 417–446 (2012).
331. Janecka, A., Zubrzycka, M. & Janecki, T. Somatostatin analogs. *J. Pept. Res.* **58**, 91–107 (2001).
332. Weckbecker, G. *et al.* Opportunities in somatostatin research: biological, chemical and therapeutic aspects. *Nat. Rev. Drug Discov.* **2**, 999–1017 (2003).
333. Lamberts, S. W. J. & Hofland, L. J. ANNIVERSARY REVIEW: Octreotide, 40 years later. *Eur. J. Endocrinol.* **181**, R173–R183 (2019).
334. Zaknun, J. J. *et al.* The joint IAEA, EANM, and SNMMI practical guidance on peptide receptor radionuclide therapy (PRRNT) in neuroendocrine tumours. *Eur. J. Nucl. Med. Mol. Imaging* **40**, 800–16 (2013).
335. Brabander, T. *et al.* Best Practice & Research Clinical Endocrinology & Metabolism Peptide receptor radionuclide therapy of neuroendocrine tumours. *Best Pract. Res. Clin. Endocrinol. Metab.* **30**, 103–114 (2016).
336. Richards, B. *et al.* Multiplex PCR amplification from the CFTR gene using DNA prepared from buccal brushes/swabs. *Hum. Mol. Genet.* **2**, 159–63 (1993).
337. Potorac, I. *et al.* A vital region for human glycoprotein hormone trafficking revealed by an LHB mutation. *J. Endocrinol.* **231**, 197–207 (2016).
338. Rivero-Müller, A., Lajić, S. & Huhtaniemi, I. Assisted large fragment insertion by Red/ET-recombination (ALFIRE)--an alternative and enhanced method for large fragment recombineering. *Nucleic Acids Res.* **35**, e78 (2007).
339. Gibson, D. G. *et al.* Enzymatic assembly of DNA molecules up to several hundred kilobases. *Nat. Methods* **6**, 343–5 (2009).

340. Trehan, A., Rotgers, E., Coffey, E. T., Huhtaniemi, I. & Rivero-Müller, A. CANDLES, an assay for monitoring GPCR induced cAMP generation in cell cultures. *Cell Commun. Signal.* **12**, 1–17 (2014).
341. Szymczak-Workman, A. L., Vignali, K. M. & Vignali, D. A. A. Design and construction of 2A peptide-linked multicistronic vectors. *Cold Spring Harb. Protoc.* **7**, 199–204 (2012).
342. Cong, L. *et al.* Multiplex genome engineering using CRISPR/Cas systems. *Science* **339**, 819–23 (2013).
343. Cong, L. & Zhang, F. *Chromosomal Mutagenesis*. **1239**, (Springer New York, 2015).
344. Aach, J., Mali, P. & Church, G. CasFinder: Flexible algorithm for identifying specific Cas9 targets in genomes. *bioRxiv* 0–8 (2014).
345. Ran, F. A. *et al.* Genome engineering using the CRISPR-Cas9 system. *Nat. Protoc.* **8**, 2281–308 (2013).
346. Burden, R. L., Faires, D. J. & Burden, A. M. *Numerical Analysis*. (Brooks Cole, 2015).
347. Schindelin, J. *et al.* Fiji: An open-source platform for biological-image analysis. *Nature Methods* **9**, 676–682 (2012).
348. Binkowski, B. F. *et al.* A luminescent biosensor with increased dynamic range for intracellular cAMP. *ACS Chem. Biol.* **6**, 1193–1197 (2011).
349. Binkowski, B. F., Fan, F. & Wood, K. V. Luminescent biosensors for real-time monitoring of intracellular cAMP. *Methods Mol. Biol.* **756**, 263–71 (2011).
350. Evers, B. M. *et al.* Establishment and characterization of a human carcinoid in nude mice and effect of various agents on tumor growth. *Gastroenterology* **101**, 303–11 (1991).
351. Leu, F. P., Nandi, M. & Niu, C. The effect of transforming growth factor beta on human neuroendocrine tumor BON cell proliferation and differentiation is mediated through somatostatin signaling. *Mol. Cancer Res.* **6**, 1029–42 (2008).
352. Sun, L.-C., Mackey, L. V., Luo, J., Fuselier, J. A. & Coy, D. H. Targeted chemotherapy using a cytotoxic somatostatin conjugate to inhibit tumor growth and metastasis in nude mice. *Clin. Med. Oncol.* **2**, 491–9 (2008).
353. Taelman, V. F. *et al.* Upregulation of Key Molecules for Targeted Imaging and Therapy. *J. Nucl. Med.* **57**, 1805–1810 (2016).
354. Paramonov, V. M. *et al.* Targeting Somatostatin Receptors By Functionalized Mesoporous Silica Nanoparticles - Are We Striking Home? *Nanotheranostics* **2**, 320–346 (2018).
355. Seamon, K. B., Padgett, W. & Daly, J. W. Forskolin: unique diterpene activator of adenylate cyclase in membranes and in intact cells. *Proc. Natl. Acad. Sci. U. S. A.* **78**, 3363–7 (1981).
356. Hurley, J. H. Structure, Mechanism, and Regulation of Mammalian Adenylyl Cyclase. *J. Biol. Chem.* **274**, 7599–7602 (1999).
357. Insel, P. a. & Ostrom, R. S. Forskolin as a tool for examining adenylyl cyclase expression, regulation, and G protein signaling. *Cell. Mol. Neurobiol.* **23**, 305–14 (2003).
358. Lesche, S., Lehmann, D., Nagel, F., Schmid, H. a & Schulz, S. Differential effects of octreotide and pasireotide on somatostatin receptor internalization and trafficking in vitro. *J. Clin. Endocrinol. Metab.* **94**, 654–61 (2009).
359. Taouji, S., Dahan, S., Bosse, R. & Chevet, E. Current Screens Based on the AlphaScreen™ Technology for Deciphering Cell Signalling Pathways. *Curr. Genomics* **10**, 93–101 (2009).
360. Paramonov, V. M., Sahlgren, C., Rivero-Müller, A. & Pulliainen, A. T. iGIST—A Kinetic Bioassay for Pertussis Toxin Based on Its Effect on Inhibitory GPCR Signaling. *ACS Sensors* **5**, 3438–3448 (2020).
361. Bass, R. T. *et al.* Identification and characterization of novel somatostatin antagonists. *Mol. Pharmacol.* **50**, 709–15 (1996).

362. Ginj, M. *et al.* Radiolabeled somatostatin receptor antagonists are preferable to agonists for in vivo peptide receptor targeting of tumors. *Proc. Natl. Acad. Sci. U. S. A.* **103**, 16436–41 (2006).
363. Feniuk, W., Jarvie, E., Luo, J. & Humphrey, P. P. A. Selective somatostatin sst2 receptor blockade with the novel cyclic octapeptide, CYN-154806. *Neuropharmacology* **39**, 1443–1450 (2000).
364. Na, D. H., Murty, S. B., Lee, K. C., Thanoo, B. C. & DeLuca, P. P. Preparation and stability of poly(ethylene glycol) (PEG)ylated octreotide for application to microsphere delivery. *AAPS PharmSciTech* **4**, E72 (2003).
365. Peng, J. *et al.* Octreotide-conjugated PAMAM for targeted delivery to somatostatin receptors over-expressed tumor cells. *J. Drug Target.* **22**, 428–438 (2014).
366. Djordjijevic, D. *et al.* Effect of 17beta-estradiol on somatostatin receptor expression and inhibitory effects on growth hormone and prolactin release in rat pituitary cell cultures. *Endocrinology* **139**, 2272–7 (1998).
367. Nunn, C., Schoeffter, P., Langenegger, D. & Hoyer, D. Functional characterisation of the putative somatostatin sst2 receptor antagonist CYN 154806. *Naunyn. Schmiedebergs. Arch. Pharmacol.* **367**, 1–9 (2003).
368. Vale, W., Rivier, J., Ling, N. & Brown, M. Biologic and immunologic activities and applications of somatostatin analogs. *Metabolism* **27**, 1391–1401 (1978).
369. Bauer, W. *et al.* SMS 201-995: a very potent and selective octapeptide analogue of somatostatin with prolonged action. *Life Sci.* **31**, 1133–40 (1982).
370. Braun, K., Stürzel, C. M., Kirchhoff, F. & Lindén, M. In Vitro Evaluation of a Peptide-Mesoporous Silica Nanoparticle Drug Release System against HIV-1. *Inorganics* **8**, 42 (2020).
371. Reubi, J. C. & Schonbrunn, A. Illuminating somatostatin analog action at neuroendocrine tumor receptors. *Trends Pharmacol. Sci.* **34**, 676–88 (2013).
372. Dutta, D., Pulsipher, A., Luo, W., Mak, H. & Yousaf, M. N. Engineering Cell Surfaces via Liposome Fusion. *Bioconjug. Chem.* **22**, 2423–2433 (2011).
373. Jiang, Y. *et al.* Direct cytosolic delivery of siRNA using nanoparticle-stabilized nanocapsules. *Angew. Chemie - Int. Ed.* **54**, 506–510 (2015).
374. Kube, S. *et al.* Fusogenic Liposomes as Nanocarriers for the Delivery of Intracellular Proteins. *Langmuir* **33**, 1051–1059 (2017).
375. Atukorale, P. U. *et al.* Structure–Property Relationships of Amphiphilic Nanoparticles That Penetrate or Fuse Lipid Membranes. *Bioconjug. Chem.* **29**, 1131–1140 (2018).
376. Irannejad, R. *et al.* Conformational biosensors reveal GPCR signalling from endosomes. *Nature* **495**, 534–8 (2013).
377. Tsvetanova, N. G., Irannejad, R. & von Zastrow, M. G Protein-coupled Receptor (GPCR) Signaling via Heterotrimeric G Proteins from Endosomes. *J. Biol. Chem.* **290**, 6689–6696 (2015).

TURUN
YLIOPISTO
UNIVERSITY
OF TURKU

Painosalama Oy, Turku, Finland 2021

ISBN 978-951-29-8516-6 (PRINT)
ISBN 978-951-29-8517-3 (PDF)
ISSN 0355-9483 (Print)
ISSN 2343-3213 (Online)